UNIVERSITY OF OKLAHOMA

GRADUATE COLLEGE

THE DEVELOPMENT OF A NEW KA-BAND NEAR-FIELD PLANAR MEASUREMENT SYSTEM FOR A DIGITAL PHASED ARRAY RADAR

A THESIS

SUBMITTED TO THE GRADUATE FACULTY

in partial fulfillment of the requirements for the

Degree of

MASTER OF SCIENCE

By

Luis Felipe Moncada Calmet
Norman, Oklahoma
2024

THE DEVELOPMENT OF A NEW KA-BAND NEAR-FIELD PLANAR MEASUREMENT SYSTEM FOR A DIGITAL PHASED ARRAY RADAR

A THESIS APPROVED FOR THE
SCHOOL OF ELECTRICAL AND COMPUTER ENGINEERING

BY THE COMMITTEE CONSISTING OF

Dr. Jorge Salazar-Cerreño, Chair

Dr. Rockee Zang

Dr. Timothy Filley

Acknowledgments

First and foremost, I would like to acknowledge God's encouraging presence in my life, He is my strength and my peace.

I also want to extend my gratitude to my beloved parents, whose sacrifice is the reason for my achievements. All my gratitude to my cherished siblings, you are my team and my unconditional friends.

A special thanks to my advisor Dr. Salazar, who not only gave me the fabulous opportunity to do a master's degree at OU, but also taught me by example, initiative and hard work. In the same way, I want to express my gratitude to all my committee members, whose valuable time and insights were invested into the revision of this thesis, thank you for all your contributions.

A significant mention to my second home, the ARRC, and all those members who were part of my grow as a person and as a student, thank you for your friendship and selflessly consistent help, thank you for making my life easier, you have my everlasting gratitude.

An important acknowledgement to the team members whose participation was crucial in the design and assembly of this near-field scanner. Thank you Alexis Oblitas, Brian Stade, Carson Bolinger and Caleb Nelson, for your hard work, cooperation and willingness.

Finally, I would like to thank our sponsor, Tomorrow.io, for the opportunity and the trust placed in our team.

Table of Contents

List of Tables

List of Figures

Abstract

A near-field planar scanner is an electromechanical system whose objective is to obtain the far-field pattern of a mostly directive antenna by recording its electromagnetic fields in the near-field region by taking measurements at different points on an imaginary finite plane in front of the antenna under test; the collected data are then mathematically processed to obtain the far-field patterns.

Near-field planar scanners are an excellent solution to the various limitations involved in far-field measurement. This type of system does not require an extremely large anechoic chamber to avoid external and self-interference in a controlled environment and does not require the AUT to rotate or move in any direction, making this system ideal for measuring array antennas.

Currently the use of array antennas is proliferating, so the need for affordable systems to test and calibrate them is essential. The objective of this thesis is to provide the design and assembly steps of a low-budget, customizable, open-source near-field planar scanner.

This thesis discusses the mathematical equations and theoretical foundations of near-field planar scanners. It also explains our proposed hardware and software design, highlighting the most important considerations. This work also discusses the process to perform an antenna measurement using the present system taking advantage of all its capabilities and finally, this thesis presents the accuracy and correct operation of the proposed scanner.

Chapter 1

Introduction

1.1 Introduction

Near-field scanners were conceived as a solution to several constraints that measuring at far field ranges may imply. The distance needed between the Antenna Under Test (AUT) and probe can be impractically large, perhaps, the required amount of pattern data requires plenty of time to measure on a far-field range [1]. Near-field planar scanners are widely use antenna measurement systems that have been in development since the decade of 1950. Interest arose with the development of electrically large antennas; antennas whose rotation to be measured in the far-field was extremely difficult due to their size or structural weakness; array antennas with a considerable number of elements; antennas with complex far-field patterns; or non-reciprocal antennas [2]. Moreover, near-field measurements, in contrast with moving range antenna outdoor measurements, may provide some advantages such as control of the electromagnetic and climate conditions, fact that leads to improvements in security, accuracy and performance [3].

Different techniques to reduce the dimensions of antenna measurement systems have been proposed over the years. The scale model technique is an approach to obtain antenna information on a complex environment (aircraft, satellites, ships) by creating a scaled model, this allows a better control over the measurements and provides an accurate first design for the antenna [4]. Plane wave generators are systems which purpose is to create planes waves at the AUT location, making possible to test antennas in a considerable shorter distance that testing at far-field would have been required, this technique includes the compact ranges, dielectric lenses and metallic lenses. The antenna focusing technique consist on concentrate or focus the antenna at the desired length, this method is used mainly for antennas that allow to adjust its focus, for instance, parabolic reflector antennas or analog phased arrays [5].

The method proposed in this work is the near-field probing with mathematical transformation to indirectly obtain the far-field patterns. The setup incorporates a probe antenna located from a recommended 3 to 5 λ separation from the AUT (best tradeoff between evanescent modes, multiple reflections and correct pattern coverage) [3]. The probe system consist of a mechanical positioning structure holding an open-ended waveguide, it scans the magnitude and phase of the electromagnetic fields over a defined surface of sample points, then this data is processed by an algorithm based on the *Field Equivalence Principle*, in order to compute the far-field pattern [6].

Near-field scanners can be divided into three main configurations: planar, cylindrical and spherical. Planar scanners are especially useful for high directivity antennas or when the antenna rotation is not desired, like big phased arrays. In this system the probe performs a rasters scanning in front of the AUT, meanwhile this last stays fixed. Cylindrical configuration is suitable for fan-beam antennas or when the project is budgeted, being the least costly structure, since it only requires two axes. The procedure of measuring for this geometry consist of the AUT mounted on a rotary table and a probe which linear movement is parallel to the rotation axis of the AUT. Usually, the probe moves up and down, meanwhile the AUT rotates in the yaw axis. The spherical configuration is specially used for low gain and omnidirectional antennas, since a spherical near-field scanner is able to get a extensive number of angles of the computed far-field pattern, meanwhile with the planar, the maximum area to compute is one hemisphere of the complete radiation pattern sphere. The setup for this system is a fixed upward facing AUT and a structure that allows the probe to rotate in azimuth and elevation always facing the AUT.

Now, it is important to mention that the system proposed in this thesis follows the rectangular configuration, this is necessary to remark since there are three different layouts for planar measurements, polar, bipolar and rectangular [7]. Regarding the polar and bipolar layouts, they were conceived as a simplified and inexpensive near-field methods, in terms of mechanical implementation, to conduct planar near-field scanning, at the expense of a more complex mathematical far-field calculation process, the necessity to rotate the AUT, and the use of interpolation algorithms to achieve the accuracy of the rectangular planar configuration, that slow-down the scan time [8].

In the subsequent sections to avoid excessive use of words identifying the proposed system as rectangular near-field planar scanner, the reader is kindly asked to understand that the presented system is now pointed out as near-field planar scanner.

1.2 Motivation

Near-field planar scanners have been improved over the years, they started as simple systems that did not perform a near-field to far-field transformation, to a complex systems that include capabilities as probe correction, different scanning configurations, hologram projection calculation, and further additional functions. One aspect that is now well addressed by latest research is the accuracy required for systems that are intended to work at high frequencies (>30 GHz). mm-Wave frequencies require high precision linear mechanical positioning with high repeatability. The suggested accuracy range for a near-field scanner is $\frac{\lambda}{100}$ to $\frac{\lambda}{50}$ [3]; therefore, a Ka-band positioning system should have an accuracy of at least 150 μm.

Near-field planar scanners have a limited scan area, this area is given by the largest dimension of the AUT and probe aperture, the desired maximum far-field pattern angle, and the distance between the AUT and probe. The factor with stronger contribution to the scan area is usually the AUT size. Given that the proposed system aims to measure a large phased array radar from Tomorrow.io, the required scanning dimensions in x and y-axis are 2.5 by 1.2 m, respectively. To achieve that area a system 3.57 m long and 2.16 m tall was designed.

The accuracy and size are conditions that are opposed and compromise themselves. This situation generates a number of challenges. An end-to-end position error in z-axis, or planarity of less than 150 μm must be maintained. Due to the size and weight of the mechanical parts, micro vibrations will also occur, specially right after a movement has finished; moreover, given the separation between the rotary table and the probe tip, micro misalignments will be present during the change of polarization, fact that must be taken into account, especially knowing that the alignment between the AUT and the probe is critical for high cross-polarization isolation. In addition, given the changing and heavy nature of the structure it is necessary to evaluate the behavior for, at least, the more stressed positions, for example, when the probe is moved all the way forward, the torque increment produced by the enlargement in z-axis will cause the probe to be more prone to vibrations and even to get bended down some microns. Another important feature is the speed, acceleration and deceleration of mainly the x-axis and y-axis, considering the regular movement is the half lambda scanning step (for the point-by-point method), the maximum travel during a scan should be 5.7 mm for 26.5 GHz (considering Ka-band); for such small step, the speed of the scan will be given by the speed of the axes, but also by the acceleration and deceleration of the axes; therefore, the correct configurations should be set in the motor controllers to maximize the overall scan speed, without compromising the lifespan of the positioners by over stressing them or without compromising stability.

To the aforementioned challenges it is necessary to include the importance of a friendly user graphical interface (GUI), which guides the user through the process of measurement, allowing the easy result acquisition and analysis. In addition, extra requests from Tomorrow.io had to be fulfilled, such as, a communication system to allow computers in the same Local Area Network (LAN) to control the scanner and to make the hardware and software able to receive fast modifications, in other words, a versatile open source system.

The purpose of this thesis is to address these challenges through the carefully design and assembly of a fast, accurate, user-friendly and reconfigurable planar near-field scanner for Ka-band.

1.3 Literature Review

Given the substantial amount of research in the area of near-field probing with far-field mathematical transformation, the content of this review is exclusively for rectangular planar near-field to far-field transformation. The purpose of this review is to identify the existing problems on this field, and in that way clearly show where is the contribution of this work.

For planar near-field scanning, the recommended sample point spacing is half lambda or less, this is to avoid aliasing errors. If we consider a large antenna array (1 m x 1 m) that works at 40 GHz, and the spacing between the AUT and probe is 3λ, the number of required sample points for an angle truncation of $\pm 60^o$ is roughly 84000, hence if the system takes half a second to move from one point to another and make a measurement, the time the system would have needed to perform a single polarization scan would have been almost 12 hours and for both polarizations a whole day, even when this time can be reduced by minimizing the distance AUT to probe, stronger reflections will occur [9], so it is not the best solution. For this reason, an effort has been made in recent years to reduce this scanning time. One of the solutions several companies offer (NSI-MI, MVG, ASYSOL) is the continuous scan mode, here, the probe no longer stops in each sample point to take a measurement, but takes the measurements in the course of the movement from edge to edge of the scanning window, so the stepped movement is relegated to just one dimension of the plane. This method reduces the scan time exponentially, however, at the expense of accuracy, specially when the frequency sweep is large (more than 40 frequencies), and an increased system complexity, given the demanded knowledge of the exact velocity, acceleration and deceleration of the positioner to track the probe by time, or demands a probe tracking sensor, such us encoders or laser trackers.

Another approach to reduce the scan time is the multi-probe strategy, this method proposes the use an array of open-ended waveguides, where each element in the array is compressed by a vertically and horizontally polarized antennas, which are separated by a distance of 2λ to reduce the coupling between them [10]. The idea of this method is to reduce the scan time by sampling in several positions at the same time, or in a fast sequence if a switch with one receiver is utilized, so if the multi-probe array consist of X number probes for each polarization, the time needed for a scan would be X times lower. A clear example of this method is the *T-DualScan*, a planar near-field system developed by MVG that offers the capability to perform measurements with a single probe or a multi-probe linear array. This scanner has been utilized in [11] to calculate an accurate multi-probe pattern and, in [12] to determine a multi-probe pattern based on the average probe pattern technique, for post-processing multi-probe correction. It also has been employed in [13] as part of the studies of a technique to speed up the process of measuring multi-beam antennas.

Further improvement strategies have been included to the multi-probe systems. In [8] a multi-probe array was utilized to develop a spiral scanning methodology to save acquisition time, showing good results for uniform patterns of array antennas. In [14] the planar wide mesh approach, a non redundant sampling technique, is combined with a multi-probe near-field system, reducing the scanning time 100 times over the time a single probe conventional near-field antenna system takes for a measurement. Furthermore, This multi-probe strategy has been extended to a scan window fully populated of probes, one example is the *RFScanner*, developed by the company YIC Technologies, it is a compact near-field to far-field scanner that is able to provide far-field patterns in almost "real-time", it works from 300 MHz to 6 GHz for a maximum AUT size of 160 mm x 100 mm. This instrument is employed in [15] as a framework to implement an adaptive data acquisition technique to minimize the number of samples to speed up the near-field measurements.

So far this review has covered the current work on strategies to decrease the near-field scan time. However, there are other features in which these systems are being enhanced. As an effort to simplify the near-field scanner system [16] proposes a technique to perform continuous scans without the use of probe position sensors. By recording the steps sent to the stepper motors it is possible to estimate the position if there is a reference point. Additionally, if the frequency sweep for the measurements is inverted (from lower to higher, to from higher to lower) for every other row of sample points during the continuous scan, the small position deviation or shift for each frequency, due to the continuous scan, is mitigated.

Besides the strategies to improve the near-field scanner, there is also a substantial amount of research dedicated to address the correct near-field measurement practices and correct procedures for calibration [17] and alignment. Useful information such as mechanical tightness, tools and procedures for alignment and mitigation of planarity and positional errors can be find in [18]. Additional considerations must be made when the system is intended to operate at high frequencies, the studies in [19] and [20] done for sub-millimeter frequencies, show how to deal with thermal structural changes (by the means of a tracking interferometer and the use of granite for the structure), cable phase instability, planarity errors and probe translation during polarization rotation, due to mechanical misalignment and size and weight of the probe sub-system. Further information about these subjects will be provided in the subsequent chapters.

1.4 Proposed System

The system discussed in this document is a high-precision inverted "T" planar near-field scanner whose operational frequencies are between 26.5 GHz and 40 GHz, where the minimum and maximum frequencies are limited by the open-ended waveguide probe antenna, if the probe and its cable are not considered, the system would be able to work from 18 to 54 GHz (for the Ka-band), which are the frequency extender limits. In summary, the proposed scanner with no modifications can measure Ka-band antennas.

The scanner consists of two main physical parts, the 4-axis positioning structure for the probe, and the equipment rack. The probe positioner is compressed by one belt driven linear positioner (x-axis), two lead screw driven linear positioners (y and z-axis) and one rotary table (ϕ-axis). This rotary table holds the frequency extender, the probe and its absorbers . Figure 1.1 shows the entire positioning structure plus the equipment rack (absorbers are hidden in order to better illustrate the details of the structure).

Regarding the dimensions, this positioner is 3573.8 mm long in x , 2159 mm in y and 1309.9 mm in z. The maximum motion ranges for the probe are 2500 mm in x, 1200 mm in y, 125 mm in z-axis and 90^o in ϕ (the rotary table can actually rotate 360^o, but the movement was limited by software to prevent the RF cables from excessive tension or torsion and because more than 90^o rotation is no needed).

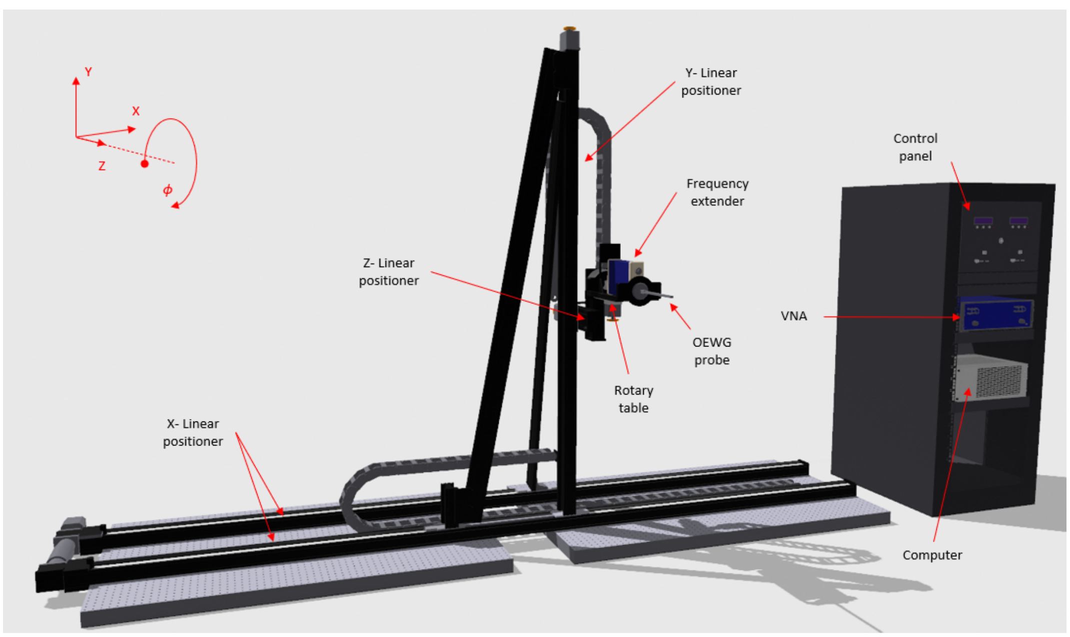

Figure 1.1: 3D rendering of proposed 4-axis NF planar system

Regarding the equipment rack, this is a piece of the system that gathers the electrical end electronic equipment to make the scanner work. This rack is divided in 5 sections, the upper one is the control panel, it comprise the motor controllers, the encoder readouts, the button to start and stop the system. An additional emergency stop push button is connected from this panel to a position close to the monitor, so the user can stop the system immediately while using the GUI. This panel allows complete control of the mechanical parts thanks to the jogging buttons and the joysticks connected to the controllers. A complete description of the functionalities of the control panel is provided in chapter three.

The VNA and a panel for the RF cables connections are in the second section of the equipment rack. Given that the VNA ports are in the front side, and the VNA needed to be installed facing the front, all the RF cables that go to the frequency extenders would have been connected from the front of the equipment rack; given that this makes the cables to be more susceptible to damages and damages the aesthetic of the rack, a extra panel was installed, so small cables go from the front of the VNA to the panel, then larger cables go from the RF panel to the back of the rack and from there to the frequency extenders. More information regarding the VNA is provided in the third chapter.

The computer can be find in the third section, it is in charge to orchestrate the scans by commanding the motor controllers, the readouts and the VNA. Given the number of USB connections required and extra internal USB card was installed, adding six extra ports to the computer. The monitor, mouse and keyboard are located in a desktop next to the equipment rack. The fourth section is a group of three drawers, the intention is to store the scanner maintenance equipment, such us the calibration tools, torque wrenches, lubricant for the mobile parts and small spare parts. Also, to store informational resources like the manuals (VNA, motor controllers, encoders and the system manual). The UPS is in the fifth and lower section, given its weight, was important to keep it closer to the floor so the rack center of mass is closer to the floor, maintaining in this way stability. The UPS was included in the system for a number of reasons, first of all is a clean source of electricity, in other words, free of harmonics. A clean source helps to extend the lifespan of the equipment. Second, the UPS provides protection against peaks of currents that can also damage the system. Finally, in case of a power outage, the user will have plenty of time to pause the scan and shut down the system in the correct manner. Figure 1.2 shows a general view of scanner parts and how are they interconnected through a block diagram.

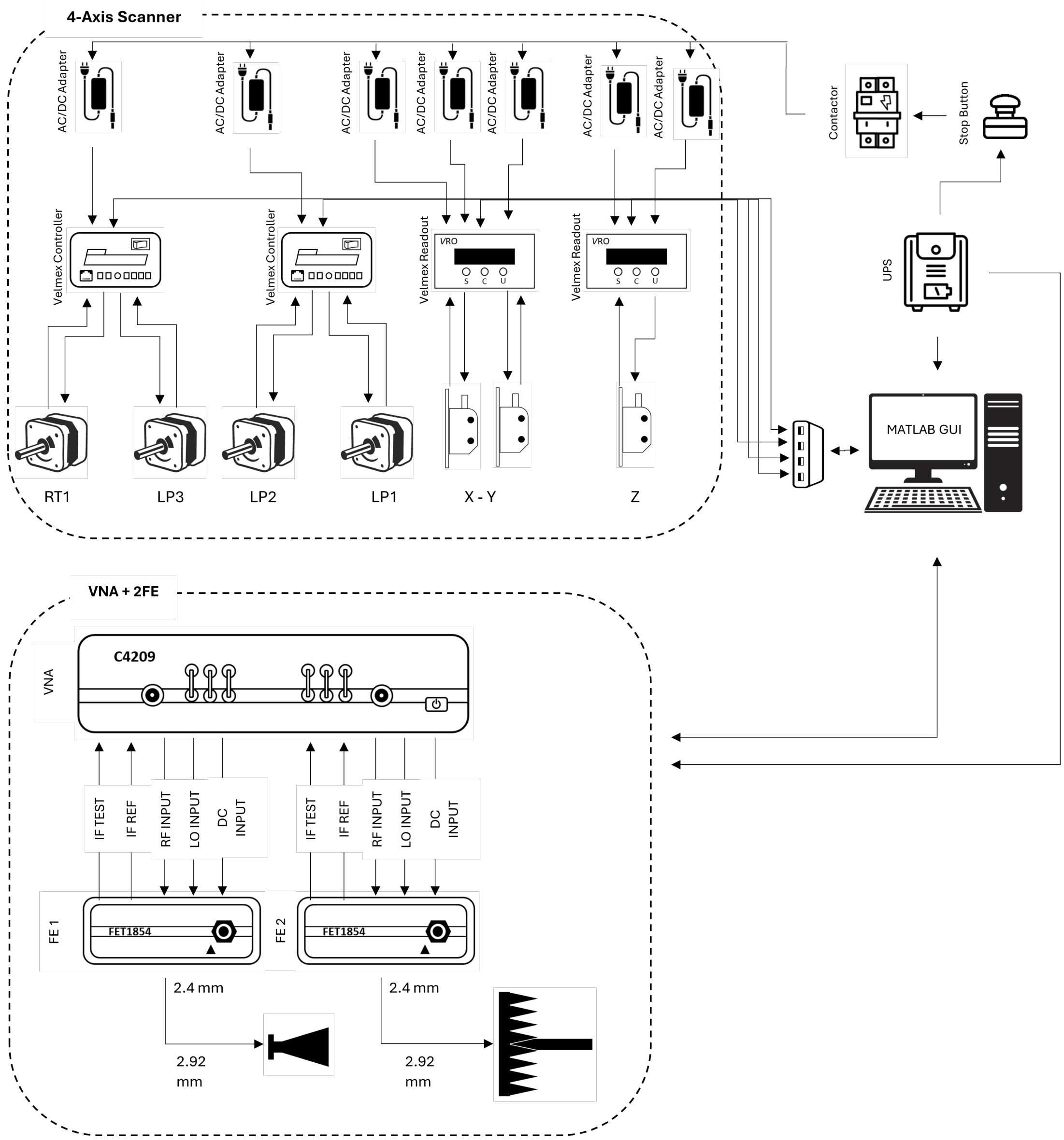

Figure 1.2: Near-field planar scanner block diagram

This block diagram was divided in two major sections, the upper one presents the parts related to the movement of the system, as we can see the stepper motors of the four axes are connected to two motor controllers, each positioner posses two cables, one for the motor itself and another for the limit switches installed on the rails, then, these controllers have special power adapters that are connected to the UPS.

The lower part of the diagram holds the RF components in the system, we can see that the VNA is connected to the computer and is powered directly buy the UPS, then the frequency extenders are connected to the VNA and powered by it as well, lastly, the probe and AUT are connected to the extenders.

The scanner specifications are summarized in the Table 1.1.

Table 1.1: Planar Near-field scanner specifications

Specifications	**Value**	**Unit**
Scan Range x-axis	2500	mm
Scan Range y-axis	1200	mm
Scan Range z-axis	125	mm
Planarity	- RMS	mm
Position repeatability x	0.1 RMS	mm
Position repeatability y	0.1 RMS	mm
Position repeatability z	0.1 RMS	mm
Scan speed x	50.8	mm/s
Scan speed y	25.4	mm/s
Scan speed z	12.7	mm/s
Maximum probe payload	5	Kg
Operational frequencies	8.2-12.4 and 26.5-40	GHZ
Dimensions	3574 x 2159 x 1309	mm

1.5 Thesis Overview

The major objective of this thesis is to provide a complete and detailed description of the design, fabrication and operation of a near-field planar scanner. In that sense, this thesis covers all the required topics through six chapters to accomplish the mentioned objective. This present first chapter is an introduction, where the reader gets a general view of the proposed system (features, specifications and conformation), the importance and motivation for its development, and an overview of the state of the art for similar systems.

The second chapter covers the fundamental theory to understand the near-field to far-field transformation for a planar rectangular scanner. It starts with a brief revision of the antenna regions, then an explanation of the *Modal expansion* and finalize with the detailed step by step mathematical procedure to transform the amplitude and phase of the rectangular near-field samples, to a spherical far-field patterns. This chapter is mostly based on chapter 17 of the book *Antenna Theory Analysis and Design* by Balanis.

The third chapter is focused on the description and explanation of the system design and assembly, through the identification of components, their function and interconnection. This chapter also covers the design of the graphical user interface, a description of the utilized software and the TCP/IP communication.

Chapter fourth delineates the process to conduct near-field antenna measurements with the proposed system, the scanner maintenance and correct power up and power down of the system.

In the fifth chapter the scanner performance is analyzed and the antenna measurements validated with measurements provided by the antenna vendors.

The sixth chapter focuses on the conclusions of the thesis and future work.

1.6 Participation and Contributions

The construction of a system as complex as a near-field planar scanner involves different fields of expertise and requires spending time on design, logistics, assembly, testing, validation, installation at the final operational site, user training, manual writing and much more. Therefore, the realization of this project includes the involvement of different people throughout the entire construction process. This section is intended to recognize the people who participated in this project and their respective tasks.

Dr. Salazar and ARRC mechanical engineers were responsible for the mechanical design. This design was based on the ARRC [21] millimeter wave multipurpose scanner system. This design was done prior to my participation.

Brian Stade and Carson Bolinger were the primary students assigned to the assembly process of the first scanner design, which also involved fabrication of additional parts, packaging and shipping. They also assisted during commissioning at the installation site. Alexis Oblitas and Caleb Nelson were the lead students assigned to the assembly of the second scanner design.

Alexis Oblitas had a special involvement in the commissioning and installation of the first system and also participated in the scanner software by adding the continuous scanning function and code debugging.

As far as the author of this thesis is concerned, my functions and participation can be summarized as follows. As can be seen, as project manager I participated in all phases of the scanner construction after design.

- Scanner secondary assembly support and assembly supervision.
- Project logistics.
- Scanner software design and implementation of graphical user interface (main task).
- Scanner testing, calibration and validation.
- Operation manual writing.
- Secondary support in packing and shipping.
- Commissioning in the installation site.
- Scanner users training.

In addition, this thesis give rise to the development of two papers. One is a review of the planar scan window formulation and its impact on co-polar and cross-polar isolation. The second one is a study of the probe collar absorber dimensions for high accurate co-polar mismatch and cross-polarization isolation.

Chapter 2

Fundamentals

2.1 Field regions

Antennas propagate electromagnetic fields which vary as a function of distance and angular coordinates, this is called the field distribution; however, at certain space from the antenna, this field distribution can be approximated to no longer be function of the distance, because of the minimum phase and amplitude variation for every point of the angular coordinates. Hence, there are two major field regions, the near-field, where the electromagnetic fields change with distance and the angular point of observation, and the far-field region, where we can simplify the distribution as just function of the angular coordinates. The most widely accepted formula which assures a maximum phase error of $\pi/8$, especially for electrically large antennas ($D > \lambda$), that divides these regions is [1].

$$R_2 = \frac{2D^2}{\lambda} \tag{2.1}$$

Where D is the largest dimension of the antenna aperture and λ the wavelength. In the closest region of the antenna in near-field, the electric and magnetic field are not in phase, this asynchronous behavior causes the system to be reactive and the fields rapidly change its orientation [22]. This reactive behavior decays exponentially and the antenna becomes a mostly radiating object. Therefore, the near-field region should be divided into reactive and radiating sub-regions, where the largely accepted formula that sets the boundary for the reactive region is.

$$R_1 = 0.62\sqrt{\frac{D^3}{\lambda}} \tag{2.2}$$

Where D is again the largest dimension of the antenna aperture and λ the wavelength. In conclusion, the antenna radiated fields structure is divided into three regions reactive near-field, radiating near-field and far-field. Refer to picture 2.1.

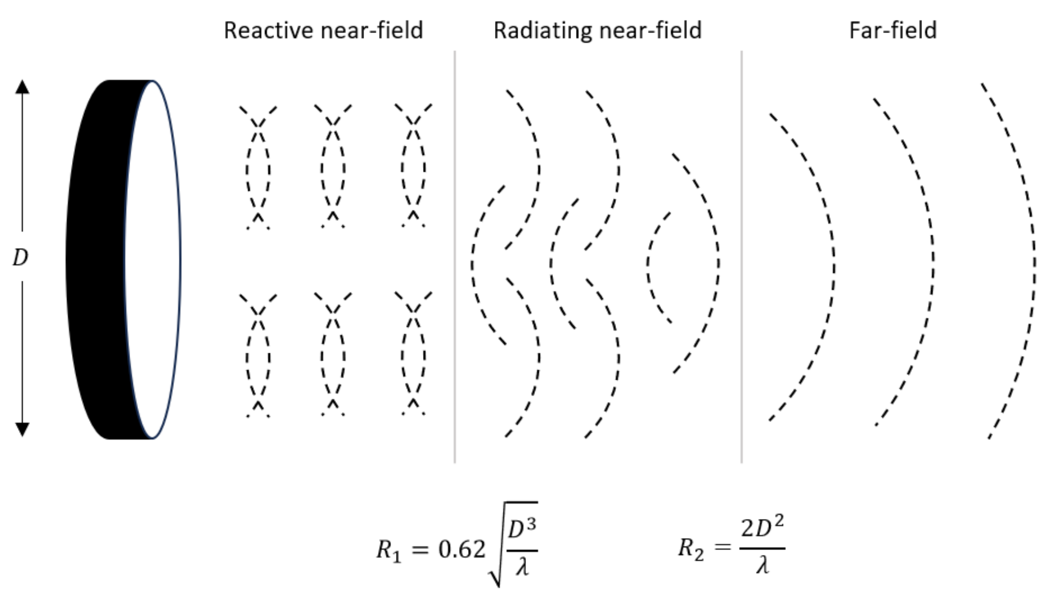

Figure 2.1: Antenna field regions

2.2 Modal expansion

The modal expansion method states that a radiated field distribution of an aperture antenna can be expressed as the summation of planar waves coming out of that aperture. Each planar wave has a different θ angle with the normal to the aperture plane.

This combination of plane waves is called *angular spectrum of plane waves*. We can think of this as a time periodic signal that can be expressed as the summation of sinusoidal signals of different frequencies applying a Fourier transform. In the same way, the radiated field can be expressed as the summation of plane waves of different angles by applying the Fourier transform.

The following pages explain this method and present a procedure for finding the angular spectrum of plane waves from measurements in the vicinity of the antenna and then using that information to obtain the far-field patterns.

Let us simplify the problem to just one plane wave being propagated at an angle θ with the normal to the aperture plane, as Figure 2.2 illustrates. The arbitrary magnetic field is tangential to the aperture plane and the electric field is in the region $x < 0$.

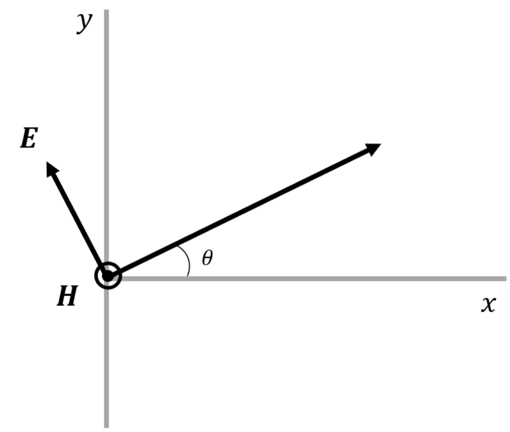

Figure 2.2: Plane wave being radiated from an aperture

The electric and magnetic fields that describe the propagated wave are shown by the Equation (2.3), and the aperture electric field distribution ($x = 0$) required to maintain this wave is described by the Equation (2.4).

$$\begin{cases} \mathbf{E}(x,y) = A(-sin\theta, cos\theta, 0)e^{-jk(cos\theta x + sin\theta y)} \\ \\ \mathbf{H}(x,y) = \eta A(0,0,1)e^{-jk(cos\theta x + sin\theta y)} \end{cases} \tag{2.3}$$

$$\boldsymbol{E_y}(0,y) = Acos\theta e^{-jkSy} \tag{2.4}$$

Any wave travelling over the aperture in the form of (2.4) produces a plane wave described by Equation (2.3). Now, if we focus in $Acos\theta$, we see that it defines the amplitude and phase of the plane wave at the origin. So, for this single case we can say that the angular spectrum of plane waves that produces $Acos\theta$ (a plane wave) in the origin, is itself. It is like wondering, what are the sine waves required to produce the signal of a sine wave; well, it is just that same sine wave. So Booker [23] defines the angular spectrum of plane waves, for this case as:

$$P(S) = \lambda A(S) cos\theta \tag{2.5}$$

Where some mathematical tricks were considered for convenience. First, λ was added, so later we can use the Fourier transform theory to go from the angular spectrum to the radiated fields. And P is a function of S, which is an abbreviation for $sin\theta$. Just θ cannot be used because the evanescent modes make θ to be complex, instead $sin\theta$ could be greater than 1, but still real. Further explanation can be found in [23].

Now, if we apply this concept for a number of plane waves being radiated each infinitesimal angle from the aperture, it is necessary to replace $Acos\theta$ from (2.5) in Equations (2.3) and (2.4), and integrate with respect to S from $-\infty$ to ∞ we will get:

$$\begin{cases} \mathbf{E}(x,y) = \frac{1}{\lambda}\int_{-\infty}^{\infty} P(S)(-sin\theta, cos\theta, 0)e^{-jk(cos\theta x + sin\theta y)}\frac{dS}{cos\theta} \\ \\ \mathbf{H}(x,y) = \frac{\eta}{\lambda}\int_{-\infty}^{\infty} P(S)(0,0,1)e^{-jk(cos\theta x + sin\theta y)}\frac{dS}{cos\theta} \end{cases} \tag{2.6}$$

$$\boldsymbol{E_y}(0,y) = \frac{1}{\lambda}\int_{-\infty}^{\infty} P(S)e^{-jkSy}dS \tag{2.7}$$

From (2.6) we can see that it is possible to obtain the electromagnetic fields at any point in the plane $x-y$ if the angular spectrum of plane waves is known. $P(S)$ can be found by applying the inverse Fourier transform to (2.7), this leads to the next equation.

$$P(S) = \int_{-\infty}^{\infty} \boldsymbol{E_y}(0,y)e^{jkSy}dy \tag{2.8}$$

In summary, it is appropriate to say that the radiated fields can be calculated from the collection of the tangential electric field in the aperture.

2.3 Asymptotic evaluation of the radiated fields

In the last section it was mentioned that in order to obtain the radiated fields at any point in the space it is necessary to apply the Fourier transform to the angular spectrum, and in order to obtain the angular spectrum it is necessary to calculate the inverse Fourier transform of the tangential electric fields in the aperture. Hence, the process to derive the far-field electric fields apparently consist of two Fourier transformations; however, this section presents an approximation that works when the distance from the aperture to the observing point is sufficiently large (far-field), using this approximation there is no need to calculate the Fourier transform of the angular spectrum, given that the electric field becomes the angular spectrum multiplied by a function that depends on r, the distance from the point to the aperture, k, the wave number and θ the elevation angle.

This analysis can be found in Balanis [6] Chapter 12, and it is described as the asymptotic evaluation of the radiated fields. That section applies a method called *Stationary Phase*, which is an approximation for complex exponential factors that change rapidly. The explanation of this method goes beyond the scope of the present thesis; therefore, just the initial and final equations are presented.

Unlike Booker, Balanis presents the spatial transformations with wavenumbers and not angles, the idea is the same, but now, instead of calling it the angular spectrum, this will be called wavenumber spectrum. Using Balanis's nomenclature and for an aperture of two dimensions, the Fourier transform of the wavenumber spectrum is:

$$\mathbf{E}(x, y, z) = \frac{1}{4\pi^2} \int_{-\infty}^{\infty} \int_{-\infty}^{\infty} f(k_x, k_y) e^{-j\boldsymbol{k}\cdot\boldsymbol{r}} dk_x dk_y \tag{2.9}$$

As it is possible to see, the wavenumber spectrum is denoted by "f" and its argument is no longer S but is the spatial frequencies or wavenumbers in x and

y. The double integral is because of the two-dimensional aperture, and it was derived by the *Parserval's theorem*.

After the application of the *Stationary Phase Method* the resultant equation for the electric field in far-field is:

$$\mathbf{E}(r,\theta,\phi) \simeq j\frac{ke^{-jkr}}{2\pi r}[cos\theta\boldsymbol{f}(ksin\theta cos\phi, ksin\theta sin\phi] \tag{2.10}$$

The electric field is now in spherical coordinates, given that the stationary points, found by the applied method, are radial to the aperture. Additionally, the spectrum is a vector whose components are x, y and z. Due to the fact that in far-field the dominant components of the electric field are just θ and ϕ, the spectrum vector is transformed to spherical coordinates and the electric field is presented just in terms of θ and ϕ.

$$\boldsymbol{E}_\theta(r,\theta,\phi) \simeq j\frac{ke^{-jkr}}{2\pi r}(\boldsymbol{f}_x cos\phi + \boldsymbol{f}_y sin\phi) \tag{2.11}$$

$$\boldsymbol{E}_\phi(r,\theta,\phi) \simeq j\frac{ke^{-jkr}}{2\pi r}cos\theta(-\boldsymbol{f}_x sin\phi + \boldsymbol{f}_y cos\phi) \tag{2.12}$$

Equation 2.11 and 2.12 describe the far-field radiation for elevation and azimuth angles. As was above stated, for far-field ranges the calculation of the radiation fields, involve an inverse Fourier transformation of the tangential electric fields in the aperture, to acquire f_x and f_y, and the application of Equations 2.11 and 2.12 to obtain the far-field radiation.

Balanis presents the equations of the inverse Fourier transformations of tangential electric field as follows:

$$\boldsymbol{f}_x = \int_{-b/2}^{b/2}\int_{-a/2}^{a/2}\boldsymbol{E}_{xa}(x',y',0)e^{jk(x'sin\theta cos\phi + y'sin\theta sin\phi)}dx'dy' \tag{2.13}$$

$$\boldsymbol{f}_y = \int_{-b/2}^{b/2} \int_{-a/2}^{a/2} \boldsymbol{E}_{ya}(x', y', 0) e^{jk(x' sin\theta cos\phi + y' sin\theta sin\phi)} dx' dy' \tag{2.14}$$

Where a and b are the dimensions of the aperture and x' and y' are the co-ordinates in the source or aperture. Figure 2.3 illustrates the two dimensional aperture and its rectangular and spherical coordinates.

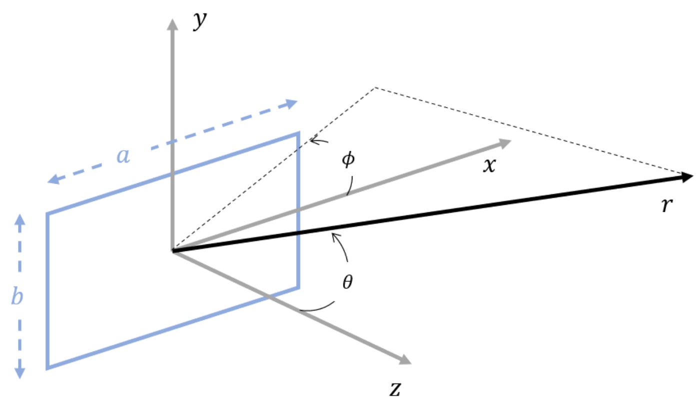

Figure 2.3: Rectangular aperture and coordinate systems

It is important to notice that in order to acquire the far-field radiation, tangential fields measurements in x and y directions are needed, in other words, co-polar and cross-polar measurements should be performed; however, for some antennas the cross-polar electric field magnitudes are considerable smaller than the co-polar magnitudes; therefore, if the co-polarization happens in y, f_x can be approximated to 0 in Equations 2.11 and 2.12, reducing, in this way, the scanning time in half. The success of this approximation depends on the scanning window angle truncation and the directivity of the antenna.

2.4 Near-field to far-field transformation computations

To start the computations some information is required about the setup of the near-field scanner. First of all, the AUT must be placed from 3λ to 5λ distance from the probe, which should not be circularly polarized and should not have nulls in the angular section facing the AUT, usually a good probe is an open-ended waveguide. Once the probe and the distance probe to AUT have been selected, the second step is to calculate the scanning window.

Also called scan area truncation, is the process to determine the area to scan based mainly on the desired angle range validity of the computed far-field radiation. The equation to calculate the dimensions of the scan area is the following.

$$L = D + P + 2Z tan\theta \tag{2.15}$$

Where L is the width and height of the scan area, D is the largest dimension of the AUT aperture, P is the largest dimension of the probe aperture, Z is the distance AUT to probe, and θ is the maximum and minimum angle of the valid computed far-field radiation data, where the 0^o angle is in the boresight direction [24]. Refer to Figure 2.4 for an illustration of the parameters on the equation.

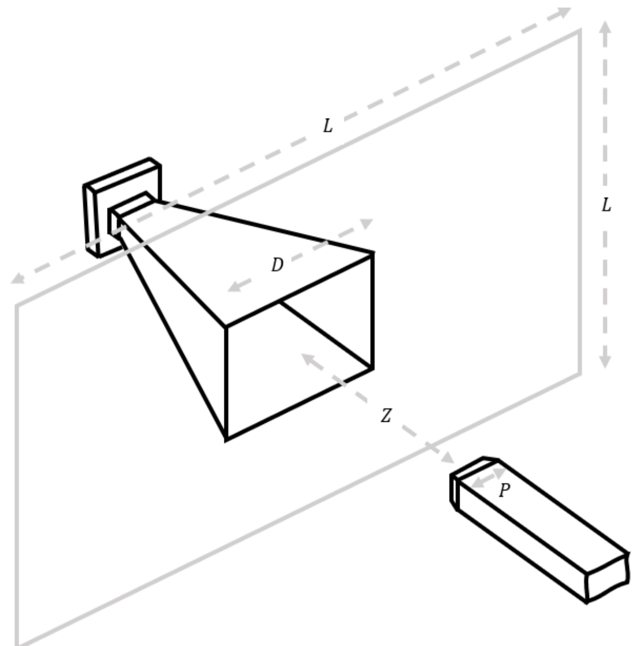

Figure 2.4: Parameters to calculate the scan area

As illustrated, the scan area is a square given that the height and the width have the same dimension. The next step is to determine the number and separation of sample points for each dimension. The procedure consists of dividing L by $\lambda/2$; we should expect a rational number, so the next step is to approximate the result to the closer higher natural number, this is going to be the number of points to sample per dimension and is denoted by N. Then, L should be divided by N and the result is the separation between sample points, denoted by Δ, whose value is slightly smaller than $\lambda/2$, fact that helps to satisfy the Nyquist sampling criterion. An important thing to consider in this step is, if the intention is to measure a list of frequencies, instead of just a single frequency, λ should be calculated with the highest frequency.

The next step is to start sampling the tangential fields for co and cross polarizations. Since the VNA will return magnitude and phase, these values should be arranged in a field form. The magnitude usually in dB should be converted to linear, and the angle should be placed in the exponential multiplying the magnitude. Therefore, if the matrix of magnitudes for a certain frequency is M and if the matrix for phases for a certain frequency is P, then the resultant matrix of tangential electric field for y polarization is calculated as follows:

$$\boldsymbol{E}_y = 10^{\frac{M}{20}} e^{jP} \tag{2.16}$$

The same calculation should be done for x polarization.

The following step is to calculate the inverse Fourier transform of the tangential fields. For a discrete two-dimensional calculation, it is possible to use the MATLAB command **ifft2** which is the inverse fast Fourier transform for two-dimensional matrices, this operation should be done for both polarizations, and results in the wavenumber spectrums for x and y polarizations. Subsequently, these wavenumber spectrums matrices must be transformed from rectangular to spherical coordinates, this process is based on an interpolation between a grid of rectangular wavenumbers and a grid of the wavenumbers transformed to spherical coordinates.

The next step in the calculation of the fields is the use of 2.11 and 2.12, where r has to be a large number, since it represents the far-field distance in meters. Also, θ and ϕ in these equations are actually matrices that were generated using **meshgrid** where θ goes from $-\pi/2$ to $\pi/2$, and ϕ goes from 0 to π.

At this point the fields are finally calculated, now it is time to present or plot the data. So, it is necessary to select a polarization definition, in order to determine the values to plot for co and cross polarizations. Ludwig [25] divides the definitions into three, where the second one is actually divided in two depending on chosen coordinate system and orientation of the pattern. We should be careful with the orientation of the antenna, in this system the antenna is always considered to be radiating in the z axis, if the orientation is changed, then different results will be obtained from the same Ludwig definitions specially for ϕ angles from 5^o to 85^o; additionally, the definition must be selected according to the type of antenna under test. For further information on this topic refer to Aboserwal paper [26].

The system implemented considers Ludwig definition 2-1, 2-2 and 3, being the third one, the one set by default. Equations 2.17 and 2.18 present the calculations to obtain co and cross polarization using Ludwig third definition, for an antenna which polarization is aligned in y according to Figure 2.5.

$$\boldsymbol{E}_{co-3} = \boldsymbol{E}_{\theta}(\theta, \phi) sin\phi + \boldsymbol{E}_{\phi}(\theta, \phi) cos\phi \tag{2.17}$$

$$\boldsymbol{E}_{cross-3} = \boldsymbol{E}_{\theta}(\theta, \phi) cos\phi - \boldsymbol{E}_{\phi}(\theta, \phi) sin\phi \tag{2.18}$$

Where E_θ and E_ϕ were acquired using the Equations 2.11 and 2.12. And, in the case of a MATLAB computation, ϕ is actually the meshed grid of ϕ and θ as stated above.

There are different ways to present the far-field radiation data; however, the most common one is by cuts. These cuts are sections of the radiation field at specific and of interest angles. There are three main cuts, E, H and D. The E cut is in the direction of the polarization of the antenna, the H cut is the cut perpendicular to E, and the D cut is the middle between E and H, in other words, rotated 45^o from E or H, in azimuth. Figure 2.5 illustrates the cuts, where if the polarization of the horn is aligned with the y axis, then the E cut is represented by the blue line ($\phi = 90^o$), the H cut by the green line ($\phi = 0^o$), and the D cut ($\phi = 45^o$) by the red line. It is worthy to indicate that even when in the figure each cut is a complete circle, we should plot just the region of the valid truncated angle θ.

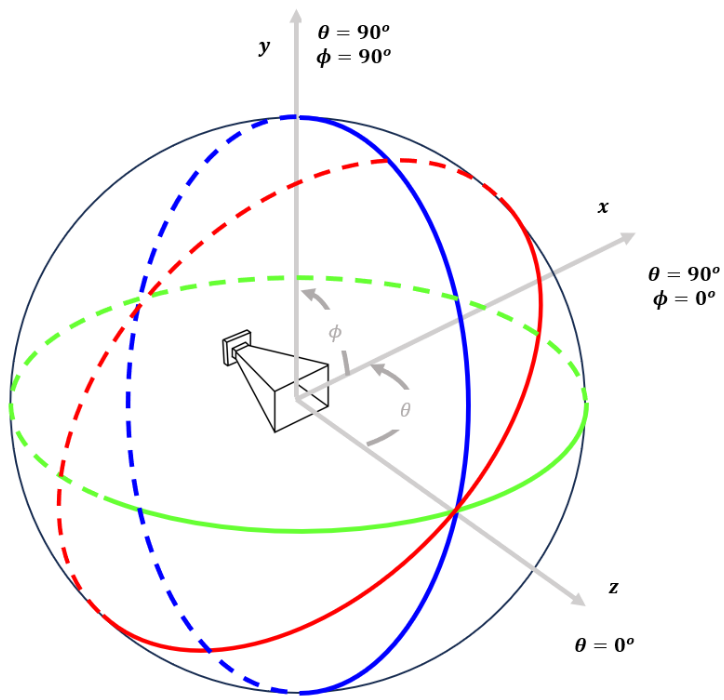

Figure 2.5: Far-field main cuts

In conclusion, the near-field to far-field process can be summarized in 8 steps.

1. Find the dimensions of the scan area using Equation 2.15.

2. Find the number and spacing of sample points.

3. Arrange the magnitude and phase measurements in the wave form.

4. Calculate the inverse Fourier transform of the tangential fields to obtain the spectrums.

5. Transform the spectrums from rectangular to spherical coordinates.

6. Use Equations 2.11 and 2.12 to calculate the far-field pattern in spherical coordinates, where r has to be a large number.

7. Select a Ludwig polarization definition to calculate the far-field co and cross-polarizations.

8. Plot the cuts of interest.

2.5 Probe Correction

We have already mentioned the steps to perform the near-field to far-field transformation; however, the result is not accurate, in fact, the acquired far-field is far from being correct, especially for the angles farther away from the AUT boresight. The issue is that the effect of the probe field has not been taken into account, so the transformation to far-field includes coupling of the probe pattern.

The process of accounting for the probe fields and removing them from the aforementioned far-field data is called *probe correction* or *probe compensation*.

A comprehensive analysis of the near-field measurements regarding to the probe effect is presented by Paris [27] where the effect of the probe is considered using the Lorentz reciprocity theorem. According to Paris, the probe is really measuring the voltage that gets excited on the probe antenna due to the existing fields at the tip of the probe, this is defined as such:

$$p_B(\boldsymbol{r_0}) = \int_{S_0} (\boldsymbol{E_a} \times \boldsymbol{H_b} - \boldsymbol{E_b} \times \boldsymbol{H_a}) \cdot \hat{\boldsymbol{n}} da \tag{2.19}$$

Where $p_B(\boldsymbol{r_0})$ is the real signal measured by the probe, $\boldsymbol{E_a}$ and $\boldsymbol{H_a}$ are the electric and magnetic fields, respectively, produced by the AUT, $\boldsymbol{E_b}$ and $\boldsymbol{H_b}$ are the electric and magnetic fields produced by the probe, and $\hat{\boldsymbol{n}}$ is the vector normal to the surface of integration which is supposed to be an infinite plane between the AUT and probe. The same definition is applied for the magnetic fields with the same subscripts. It is important to mention that this equation neglects the effects of mutual coupling between the antennas and the probe scattered fields [27].

If the fields are expressed in the terms of their wavenumber spectrums, where $\boldsymbol{F}$ is the spectrum for the AUT and $\boldsymbol{G}$ is the spectrum for the probe. Then, the signal measured by the probe can be expressed as such:

$$p_B(\boldsymbol{r_0}) = \frac{8\pi^2}{\omega\mu}\int_{-\infty}^{\infty}\int_{-\infty}^{\infty} k_z\boldsymbol{F}(k_y,k_x)\cdot\boldsymbol{G}(k_y,-k_x)\cdot e^{-j\boldsymbol{k}\cdot\boldsymbol{r_0}}dk_y dk_x \tag{2.20}$$

We can see that the argument of those integrals is the wavenumber spectrum of $p_B(\boldsymbol{r_0})$. Equation 2.20 is simplified by Taybi [28], with the statement that the multiplication of the AUT and probe spectrums is the measured signal spectrum. Additionally, Taybi presents the spectrums as functions of the AUT to probe distance and the selected frequency.

$$\boldsymbol{P_B}(k_x,k_y,d,f) = \boldsymbol{F}(k_x,k_y,d,f)\boldsymbol{G}(k_x,k_y,d,f) \tag{2.21}$$

From Equation 2.21 we can deduce that the real AUT spectrum can be found from the division of the measured signal spectrum and the probe field spectrum. However, we still need to know the probe spectrum in advance. Masters [29] proposes a technique called *probe-square-root*, it explains how to acquire the probe pattern using a near-field scanner, and states that if the probe crosspol effects are neglected, then, the real AUT field is calculated as:

$$\boldsymbol{E_p} = \frac{\boldsymbol{E_{pu}}}{\boldsymbol{E_{pp1}}} \tag{2.22}$$

$$\boldsymbol{E_c} = \frac{\boldsymbol{E_{cu}}}{\boldsymbol{E_{pp2}}} \tag{2.23}$$

Where E_p and E_c are the co and crosspolar AUT real response, respectively, E_{pu} and E_{cu} are the uncorrected co and crosspolar AUT response, and E_pp1 and E_pp2 are the co and crosspolar probe response. These two equations match with the statement of Taybi.

According to the *probe-square-method*, it is possible to obtain the probe real pattern using a near-field system if the AUT and probe are the same antenna, then, the real probe pattern is the square root of the pattern levels, if they are in a linear scale, or dividing by two, if the pattern levels are in dB.

Once the probe's real pattern is known, it is possible to remove its influence from the measured pattern and acquire the real AUT pattern.

Chapter 3

System design and assembly

3.1 Design

The first step in a design process is to understand the requirements, in this case, given by Tomorrow.io. Then, after a research, the system architecture and technology should be established according to the requirements.

3.1.1 Requirements

We can divide the requirements by software and hardware. Software specifications can be further divided into back-end, where the pieces of code that control the system are organized, and front-end, which is the interface between the user and the back-end.

Tomorrow.io, the company sponsoring this project, requested a software that enable them to send commands from different computers or systems in their local network. In other words, the system should be able to switch from manual control (performed with joysticks), to GUI control, to remote control. On top of that, security and privacy are needed; therefore, the local network is not connected to the internet; hence, the program must be independent from the internet. Furthermore, the program must be structured in a way that allow to make modifications without compromising the functioning of other code in the program, for instance, if the VNA is replaced by new technology or device (SDR), then, just the rules of communication with the new device should be adapted, making our software and system versatile and expandable.

Regarding the GUI requirements, it was very important for Tomorrow.io to be able to visualize and download the far-field processed data for the whole AUT hemisphere. In other words, the user is be able to analyze a 3D plot of the computed far-field and download the 3D pattern data for copol and crosspol, for the different frequencies programmed. Additionally, it is important for them to be able to run a scan including both orthogonal polarizations or just one polarization, this in case crosspol is negligible or not necessary for analysis purposes or they want to save time at expense of one polarization information.

Not all of the software requirements were on Tomorrow.io's side, as part of a prestigious organization like ARRC we felt a responsibility to design a high quality product. For us, the graphical user interface had to be designed with two main goals in mind: to be easy to use, meaning that even new users can take advantage of all the features of the software, and secondly, to be complete, in the sense that provides different tools so the user can customize the measurement according to his needs, this is the reason why the software includes, hologram projection, zero padding truncation, analysis comparison window, ability to plot near-field cuts, VNA monitor, and more. All the functionalities will be discussed later in this chapter.

About hardware requirements, the requested system is a near-field planar scanner aiming to work at X-band (8.2-12.4 GHz) and Ka-band (27-40 GHz) [6]. The scan dimensions should be a minimum of 2000 mm in x-axis and 1200 mm in y-axis. The minimum payload for the probe antenna has to be 5 kg. From the requested frequency band, the requirements for repeatability, accuracy and planarity are set to $\lambda/50$, then if the highest frequency provided is 40 GHz, we must ensure an accuracy of at least 150 μm for the whole system.

3.1.2 System architecture

The structure selected for the scanner is called inverted "T", like most planar rectangular near-field scanners, it consists of a horizontal x-positioner and an attached vertical y-positioner. An additional third positioner in z is considered in order to accurately vary the distance from the probe to the AUT. An actuator to rotate the probe is required to change the polarization, in this case, we decided to use a rotary table attached to the z-positioner. As for the base of the scanner, given that accuracy and stability is needed, this should be installed on a completely flat, sturdy and antivibrations surface, for this reason a couple of optical breadboards were chosen for the base of the system.

Seeking for structural stability the vertical positioner is reinforced by two diagonal flat extrusions fixed one at one side of the positioner and other behind it, forming a right triangular pyramid. This two diagonal extrusions are very important since they serve as an alignment tool for the vertical positioner, considering that this positioner could be tilted either towards the x or z-axis.

In addition, the center of mass of the structure should be located as low as possible to the floor and as close as possible to the vertical positioner to minimize vibrations. Therefore, the z-positioner was designed to be a short mechanic piece next to the y-positioner.

To protect the scanner parts and surroundings, it is necessary to install a sensor that stops motion when the probe reaches the limits of each positioner. Fortunately, all positioners come with physical limit switches for each end. Unlike the positioners, the rotary table does not includes limit switches, in this case, its movement has to be restricted by software, so we do not provide a joystick for probe rotation.

Given that this system is intended to work up to 40 GHz, long RF cables from the equipment rack to the probe are not the best solution, phase and magnitude variations for 40 GHz are around 0.5 dB and 10^o, respectively, due to the probe movement during a scan; therefore, for a more stable and reliable measurement frequency extenders (FE) are required. Each FE must be installed in the closest possible area to its antenna, probe or AUT. For this reason a plate attached to the rotary table holding the frequency extender and the probe was considered in the design, in this way the probe rotation includes the rotation of the frequency extender connected to the probe by a semi-rigid 1.85 mm RF cable.

Due to the metallic nature of the scanner, absorbers must be attached primarily to the areas facing the AUT or where diffraction could occur; hence, three main areas where covered. The first one is the vertical structure compressed by the vertical positioner and diagonal stability structures, a series of plates where installed to the vertical structure with the use of aluminum spacers, then adhesive velcro tape was sticked on the plates so the absorbers can be easily attached or removed; the second one, is the area where the horizontal positioners are, a row of absorbers was installed in front of the breadboards, these are intended to cover the horizontal positioner and part of the breadboards; the third area and most important one is surrounding the probe. Some considerations should be followed in order to do not alter the probe gain [30]. This absorber is also called "probe collar" and the idea is to cover the metallic structure holding the probe. Special 3D printed brackets to hold the probe collar were design, in this way the absorbers can be installed and uninstalled easily.

An important component of the scanner are the cables, from the vertical axis alone there are twelve coming out of the FE, encoders, motors and limit switches. It is essential to arrange them in such a way as to apply the least amount of torsion and tension to them and also to cause the least amount of interference with the scanner structure. To this end, the design took into account the cable tracks as a way to allow movement but at the same time have them organized and protected.

The final part of the system architecture design is the equipment rack, a correct organization of the devices in it is essential. The devices arranged are the computer, keyboard, mouse, monitor, VNA, UPS, motor controllers, encoder readouts, emergency stop button circuitry, start/stop button and the joysticks. The motor controllers, encoder readouts and start/stop button are planned to be at the top, in a section called control panel, from where the user will be able to manually control the scanner movement, configure some encoder parameters and start or stop the system. The idea of the front panel is that it should be at a height where the user does not need to stoop to operate the system; therefore, the rack height should be slightly lower than the average human height. Below the control panel, the VNA is located, the reason for this position is mainly because from each port there are four RF cables running to the FEs, in order to protect these connections, these cables need to be in a place away from accidental movements of the user's limbs, chair or bench that may damage the connections, This is also at a height were the user can comfortably modify the connections (When the system has to go from X-band to Ka-band or viceversa). The section below the VNA is perfect for the keyboard and mouse, as this height is ideal for a standing person to type. For the keyboard, a compact and retractable one was selected, which also comes with a mouse pad. Typically, monitors in server racks are small, so a regular 27-inch monitor was install using a retractable mounting bracket to one side of the rack. Right under the keyboard, the computer tower is installed in the rack, followed by two drawers, this are intended to store different scanner associated stuff such as tools, maintenance material, spare parts, VNA calibration kit and manual. Finally, at the lowest section, the UPS is located, which serves to lower the rack center of mass given its heavy weight. The rack has casters, in case it is necessary to turn it for maintenance.

3.1.3 Technology

This section presents and collects the specific chosen devices for the scanner.

One of the critical parts for the system are the horizontal *BiSliders*, a linear positioners that can move forwards and backwards, they should be sturdy and strong enough to move the parts over it, they should provide a large range of motion, and at he same time they should be able to work for long periods of time keeping its accuracy. The best option for this task would be a lead screw driven *BiSliders*; however, this kind of actuators have a limited range of motion; therefore, a belt-driven *BiSliders* was selected. The horizontal axis consists of two belt-driven *BiSliders* made of hard anodized aluminum extrusion, one of them has a stepper motor and transmit the movement by a shaft that connects them both. Figure 3.1 presents the *BiSliders* and its features. It is remarkable the anti-backlash technology and the stainless steel reinforced, polyurethane precision timing belt of the *Velmex BiSliders*, making them ideal for our purposes. The *BiSliders* have two cables, one six-wire cable for the stepper motor and a four-wire cable for the limit switches.

One of the special features of the *Velmex BiSliders* are the mechanical limit switches incorporated at both ends of the positioners, they work as over-travel protection and as reference for homing. These switches can be relocated. Their implementation in a *BiSliders* can be seen in Figure 3.1 (little blue lid block).

Figure 3.1: Belt Driven BiSlide (Courtesy: Velmex, inc)

For the y and z-axis we are using a lead screw-driven linear positioner, unlike the belt-driven, the screw-driven is made for heavier loads, higher precision but lower speed and range. Figure 3.2 presents the y and z-axis bislider features. The difference between the y and z, is that the screw threat for the y-axis is finer, which means higher accuracy, according to the manufacturer, the accuracy is 76 um for a travel of 25 cm. The maximum cantilevered load capacity for a dynamic load is 56.5 $N \cdot m$.

For the ϕ movement the *Velmex* B48 series rotary table was chosen. This rotary table is excellent given the high accuracy (100 arc-second $\approx 0.03^o$), repeatability (1 arc-second $\approx 0.0003^o$) and load capacity in a vertical configuration of 11.3 kg. Refer to Figure 3.3 for an illustration of the rotary table.

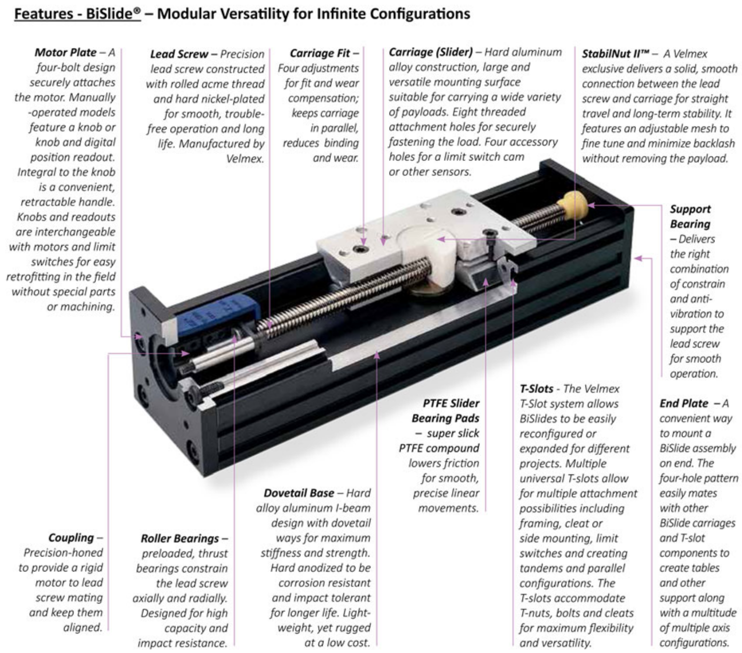

Figure 3.2: Screw Driven BiSlide (Courtesy: Velmex, inc)

Figure 3.3: Rotary table (Courtesy: Velmex, inc)

All these actuators need a special controller provided by Velmex, called *VMX*.

This controller mainly generates electric signals to drive the motors, based on a set of commands. Each controller can drive a maximum of two stepper motors. These controllers receive commands from the computer through a RS-232 to USB cable. Two special features from these controllers are their capability to store sequences of movements, and its front panel that allows manual control of the driven motors. Figure 3.4 illustrate the VMX and presents its features.

Figure 3.4: VMX controller (Courtesy: Velmex, inc)

The next items on the list are the encoders and their readouts. The functioning principle of this incremental encoders used in the system it is magnetism. Basically, there is a magnetic strip attached to the to the extrusion, with small positive and negative magnetic poles sandwiched in between. Then, the encoder is fixed on the magnetic strip on the moving plate or carrier, so, when the system moves through the aluminum extrusion, it detects the change of polarization and in this way it can measure the distance traveled with a certain resolution that is given by the size of the magnetic poles. These encoders are connected to Velmex readouts called *VRO*, their task is to process the signals coming from the encoders and convert them into distance in either inches or millimeters, the distances measured are sent to the computer by an RS-232 to USB cable.

Figure 3.5: VRO encoder readout (Courtesy: Velmex, inc)

The main RF components are the VNA and FEs. For the VNA we selected the Copper Mountain C4220, a two port VNA which works from 100 KHz up to 20

GHz, its dynamic range is 133 dB (10 Hz IF BW), the measurement time per point is less than 10 μs and it's compatible with a frequency extension system. The FEs selected are the Copper Mountain FET1854, they can extend the frequency up to 54 GHz. The dynamic range is 130 dB (10 Hz IF BW), and they take less than 10 μs to do a measurement. Figure 3.6 shows the VNA and FEs connection setup.

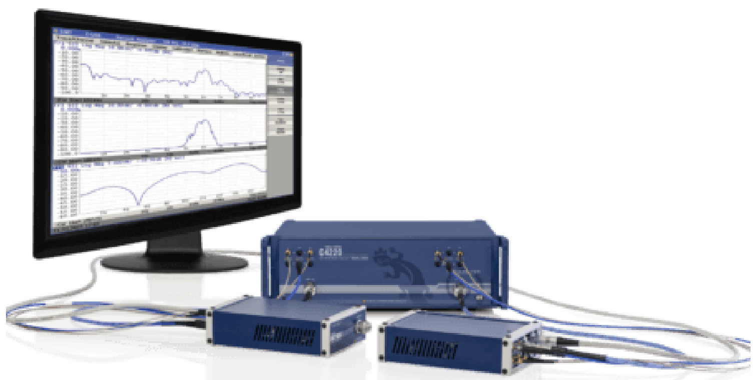

Figure 3.6: Setup of the C4220 VNA and the FET1854 extenders

The equipment rack front panel was designed to show the controllers front panels, the readouts and a button to toggle between start and stop. For the connection of the scanner start-stop button and the emergency stop button an electric circuit was designed based on a type of relay called contactor. Figure 3.7 presents the electric connections diagram for the start and stop of the scanner. When the "START" is switched the coil is energized and the K contacts close energizing the power strip. If the emergency stop is pushed, the coil is de-energized and the K contacts get open. L, N and PE terminals represent the Hot, Neutral and Ground lines, respectively.

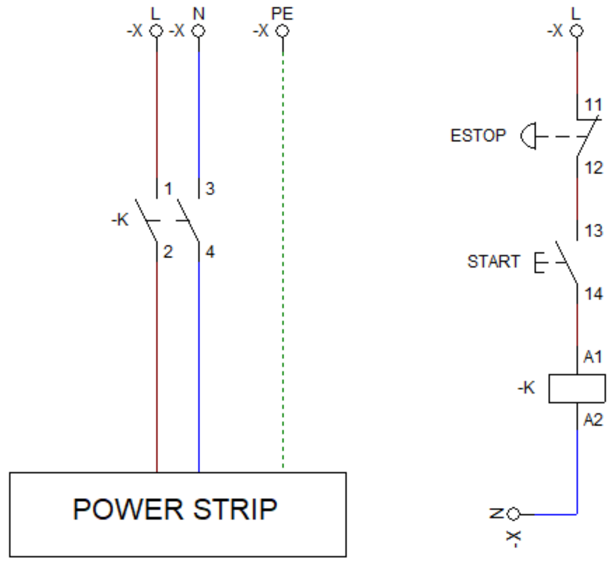

Figure 3.7: Electrical diagram for start and stop of the system

The selected probe for Ka-band is an open-ended waveguide manufactured by Microwave Vision Group. The waveguide band is WR28, so it can work in the 26.5 to 40 GHz frequency range. The probe for X-band works in the WR90 band, so it can work properly between 8.2 and 12.4 GHz

The last important piece of equipment mentioned in this chapter is the UPS. It will extend the system runtime to 5 minutes (for a system that consumes 1350 Watts) in case of a power outage . In addition, the UPS automatic voltage regulation feature helps to extend the span life of the connected devices. This UPS also comes with surge protection and its battery lasts an average of 4 years and the type is lead-acid.

3.2 Assembly

The assembly process starts by placing and aligning the optical breadboards on the floor, next to each other leaving a space of 10” between them, this is given that this gap allows the cables for the AUT system to pass through the scanner going directly from the equipment rack to the AUT fixture, this 10 inches it is also required to cover the majority of the length of the *BiSliders*. The breadboards function is to provide a solid flat stainless steel surface with threaded holes to ease further machinery installation on top. It also incorporates side panels that dampen vibrations. To make sure both breadboards are at the same level, considering the floor is not perfectly flat, four heavy-duty adjustable furniture leg levelers were attached to each corner of each optical breadboard. Then, with an I-Beam level and with a self-leveling cross line laser level, the team managed to level both optical breadboards at the same height throughout the whole surface. Figure 3.8 shows both breadboards being aligned; also, to enhance the laser visualization, the room lights were turned off.

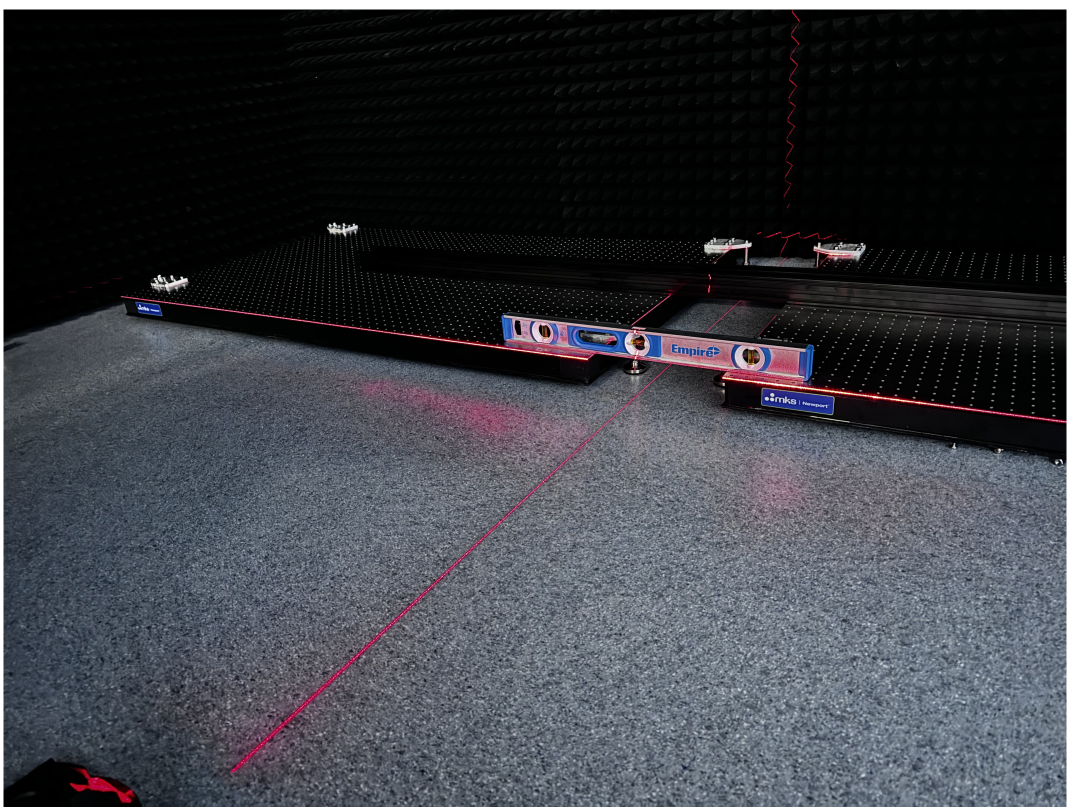

Figure 3.8: Horizontal system alignment (Courtesy: eMWave-tech)

The next step is the installation of the linear positioner belt-driven *BiSliders*, which perform the movement in the x-axis, these two belt sliders are bolted down to the breadboards by the use of special cleats whose separation is determined by the load and the travel length (more information can be found on Velmex website). These belt sliders are mounted on the middle of the optical breadboards, they are separated ten inches. Given that just one of these belt sliders has a stepper motor, the motion is transmitted to the other through a shaft . In order to measure if the *BiSliders* are as much parallel as possible, a magnetic dial indicator was mounted on the moving plate (also called carriage) and the tip of the indicator was touching the adjacent slider, the indicator was set to zero and it was moved from end to end. The registered variations were less than the maximum allowable error of 150 μm. Figure 3.9 illustrates the first stage of the scanner assembly.

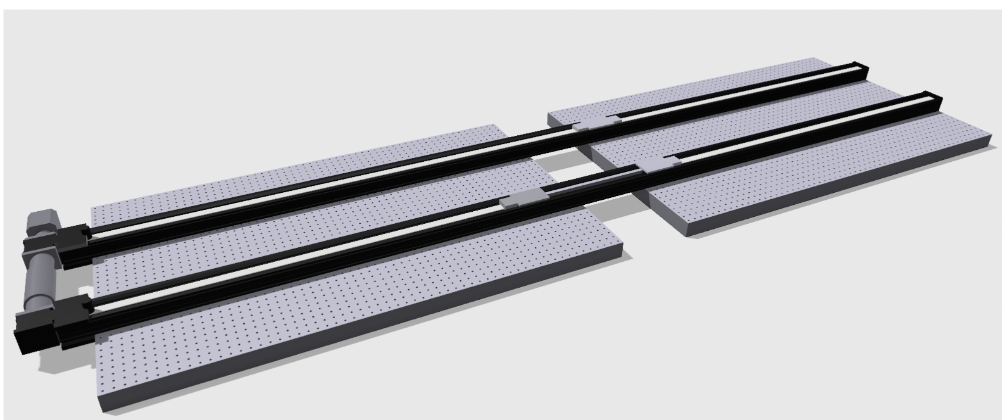

Figure 3.9: x-axis linear positioners mounted on the optical breadboards

Then vertical screw-driven slider is bolted down to the moving plate of the horizontal slider and is supported by two diagonal extrusion large rectangular plates, forming a trirectangular tetrahedron, this geometry provides stability to the moving parts in the y-axis. As was mentioned, this positioner must be aligned to ensure it is as much perpendicular as possible to its base. For this task a line laser level was used. Figure 3.10 shows the vertical positioner being aligned.

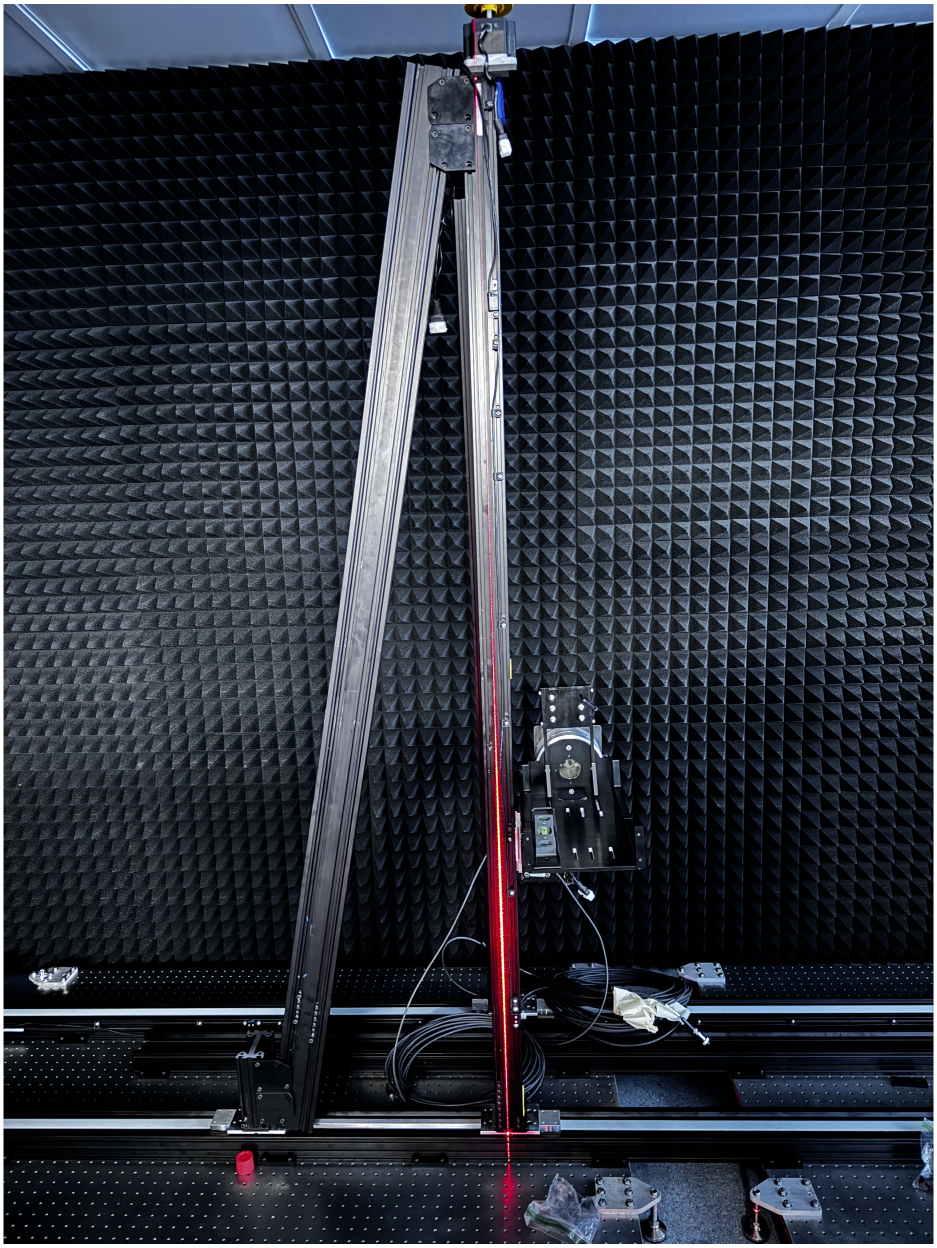

Figure 3.10: y-axis linear positioner alignment (Courtesy: eMWave-tech)

The y screw-driven positioner has a moving plate, which holds the z screw-driven positioner, this is attached by cleats, allowing an easy reconfigurable z-axis origin. Then, a extrusion of 10.5” long is attached to the z-axis positioner by the use of cleats as well. A flat aluminum square is bolted at the top part of the extrusion, which serves as a mounting plate for the rotary table. The extrusion is necessary to elevate the rotary table from the z positioner in order to avoid collisions when the probe is rotating. Figure 3.11 presents a CAD model of the discussed structure section.

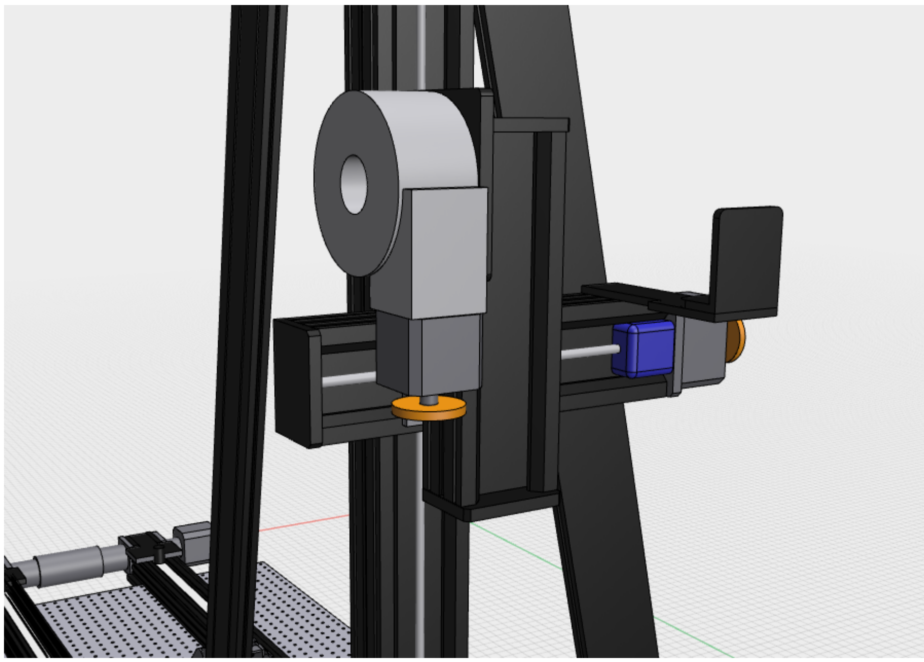

Figure 3.11: Rotary table attachment

The center of the probe should be the exact center of the rotary table to eliminate any misalignment after probe rotation, with that consideration in mind, the hole patterns of the frequency extender bed walls should be design so that the centers align. One of the bed walls is bolted to the rotary table, and the probe is bolted to the opposite bed wall. An exercise was performed to test the correct alignment between probe an rotary table, it consist of marking the probe side center with a laser and then rotate the probe 90^o and check if the laser stills mark the probe side center. As can be seen in Figure 3.12, the probe is still pointing the same position after 90^o rotation.

Another important part of the system are the cable tracks, also known as drag

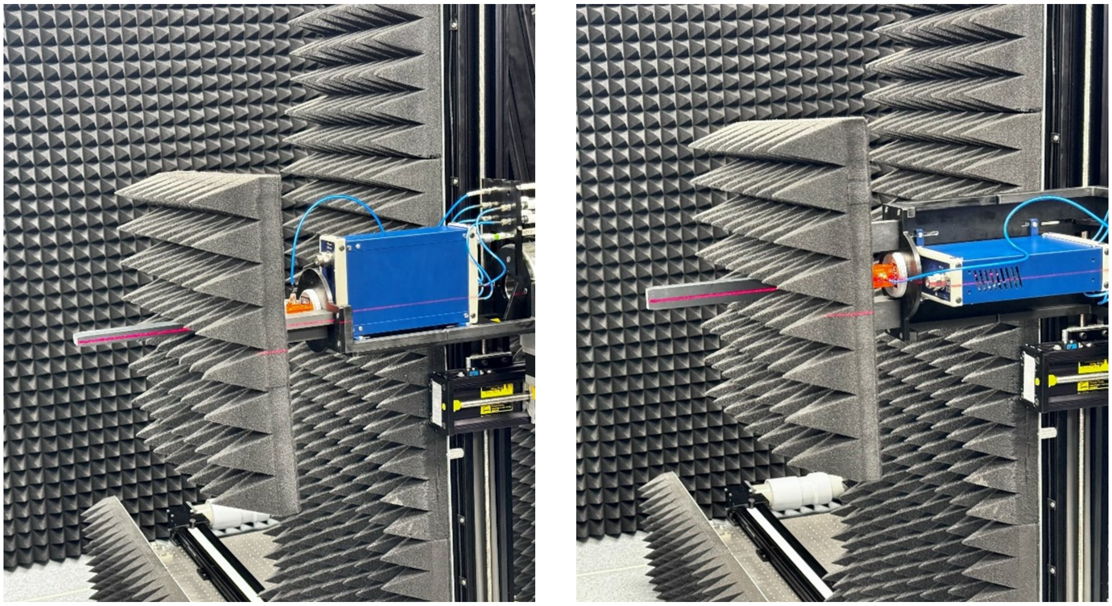

Figure 3.12: Probe side center for both orthogonal polarizations (Courtesy: eMWave-tech)

chains, which organize and protect the cables from dangerous stresses, twists and obstructions, especially when the scanner is in motion, as the tracks enclose the cables, providing a defined and smooth path for them to move and bend. Two cable track chains were installed in the system. One for y-axis motion and one for x-axis motion, for the z-axis no track was required given the short distance motion variation. Figure 3.13 presents the scanner CAD model with the cable tracks included.

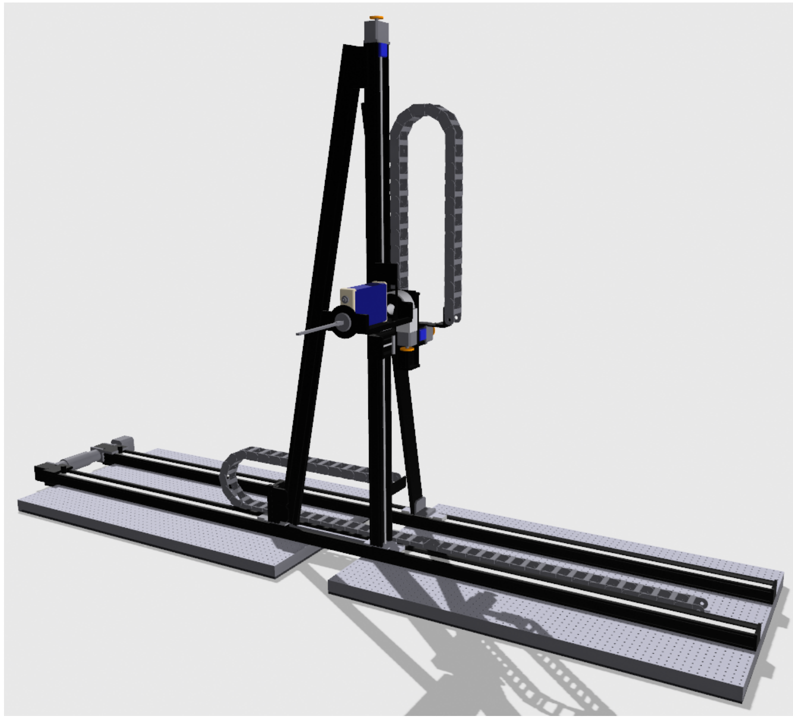

Figure 3.13: Scanner system with cable tracks

Not just cable tracks were used to protect and organize the cables, but loom tubes were also utilized in areas were the installation of cable tracks was difficult or areas where motion was not expected.

RF absorbers are structures that attenuate and absorb electromagnetic waves, they are essential in any antenna measurement system due to their ability to greatly reduce the reflections of electromagnetic waves from unwanted directions. Some of the characteristics to take into account when acquiring absorbers are the absorption level, being able to present reflectivity levels higher than -50 dB [31]; the operating frequencies, and the robustness, in our case, the pyramidal foam absorbers for interiors are optimal.

We have considered tangential fields coming directly from the AUT at the probe tip when performing the mathematical transformations from near-field to far-field; therefore, we must do our best to keep the behavior of the system as close as possible to the approximation to facilitate the calculations, this is why absorbers are so important. The absorbers had to be placed mainly covering the metallic structures facing the AUT and also had to be placed in the areas where diffraction could occur. For this reason pyramidal absorbers were attached to the base of the scanner perpendicular to the ground, thus covering the metal areas of the optical bredboard. Additional absorbers were attached to the vertical linear positioner of the scanner, as this is made of aluminum and must also be covered. Finally, additional absorbers are needed behind the probe to cover all the metal equipment behind it, such as the frequency extender and the z-axis positioner. Figure 3.14 presents a CAD model of the scanner with absorbers included.

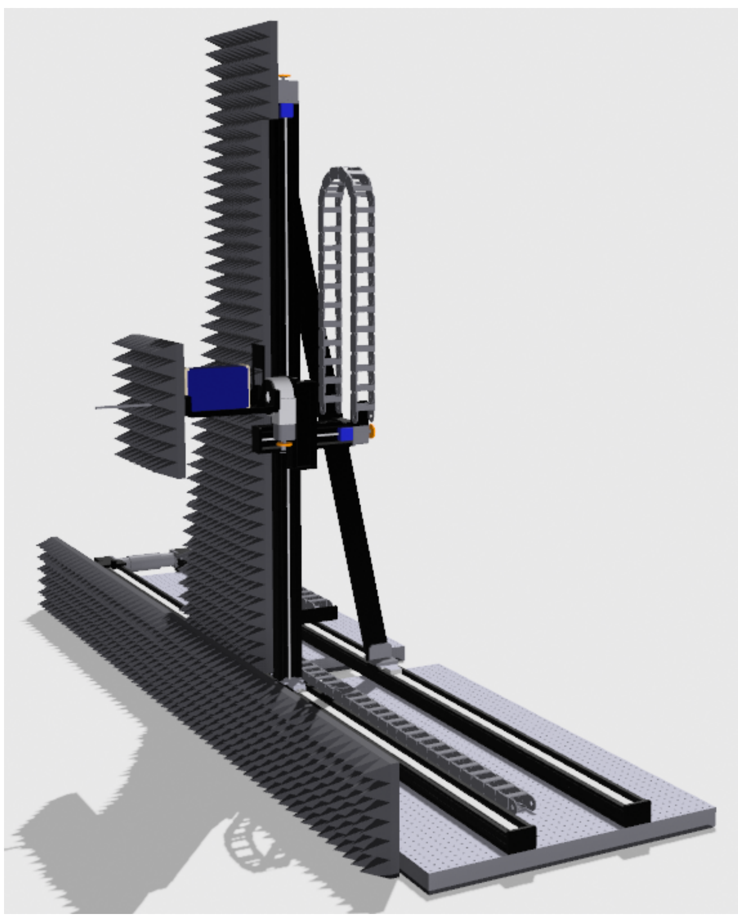

Figure 3.14: Scanner system with absorbers

At this point the scanner structure is built. The next step is mounting the equipment rack. The rack was purchased from *Rack Solutions*, it is a thirty unit high open frame server rack with casters installed. As mentioned in the first chapter, at the bottom of the rack a two unit UPS was installed to keep the center of mass lower, then there is a three unit enclosed empty space, then a three unit drawer, then a one unit enclosed empty space, an extra three drawer at the top, then a one-unit shelf holds the computer tower in a four-unit space, and above that is a retractable shelf that holds the keyboard and mouse. The monitor was installed at one side of the rack with a retractable mounting bracket, so it can be deployed to the one side of the rack. Above the keyboard compartment, another fixed shelf was installed, and our three-unit VNA was bolted on top. Now, since the VNA ports are on the front and all cables must exit out the back of the server, a panel with female to female SMA adapters was placed on top of the VNA in a two-unit space, so we can connect semi-rigid SMA cables from the VNA to the panel and then additional RF cables can be connected from the back. This is the same thing the NSI system does in their equipment racks for the VNA connections. In our case there are four connections per port given that we are using frequency extenders. Finally the last part of the rack is the, six units height, control panel. It is very important because it allows manual operation of the scanner movement, it also shows the exact position of the probe on x, y, and z-axis thanks to the encoder readings and, there is a switch button to turn the system on and off, which is located in the center of the panel. This panel was design but its engraving was made by an external business. Figure 3.15 shows a picture of the equipment rack and the monitor deployed.

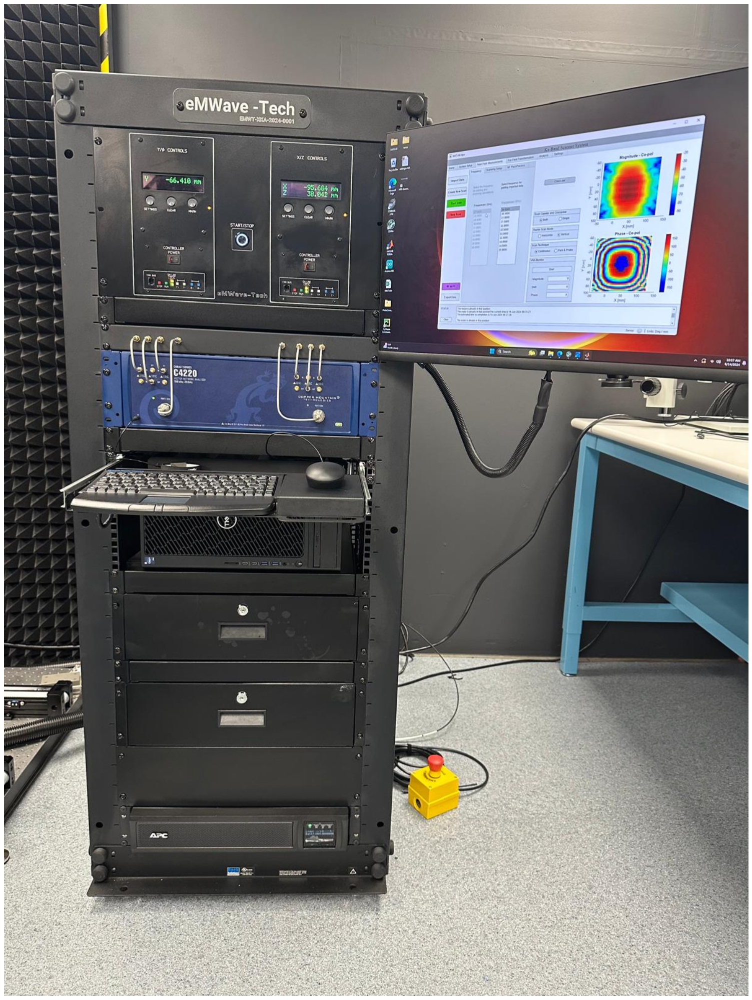

Figure 3.15: Equipment rack (Courtesy: eMWave-tech)

Inside the rack there are three power sources. The first and main one is the UPS. Two power strips are connected to it, one power strip is connected directly to the UPS and is located halfway up the rack, it facilitates the connection of the computer and the VNA. The second power strip is commanded by the start/stop button of the control panel and the emergency stop button. The controllers, encoders and readouts are connected to this strip. Therefore, pressing the emergency stop will turn off everything except the VNA and the computer, the same applies to the start/stop button. The VNA and the computer must be shut down properly, for this purpose they have a separate power strip. To shut down the entire system, the user must turn off the UPS by pressing the power button on the front of the UPS.

The electrical circuit components (contactor, terminal blocks, twelve-volt power supply) were mounted on DIN rail inside the rack. And the cables were enclosed in slotted cable ducts to keep the inside of the rack organized.

All cables are connected to metal male aviation connectors to a rear panel located at the bottom of the rack. This was designed to facilitate installation of the system after shipment, as cables from the scanner system need only be connected to the rear panel, rather than routed inside the rack. It also increases system versatility by facilitating equipment rack relocation. Figure 3.16 shows the rack back view during its assembly process.

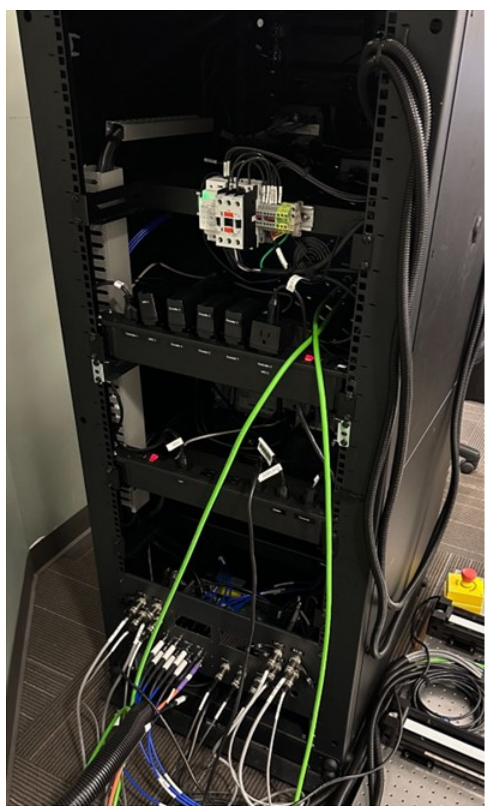

Figure 3.16: Equipment rack back view (Courtesy: eMWave-tech)

Some additional equipment such as joysticks were installed to control the probe movement manually if the front panel of the rack is not used. The joysticks can control the x, y and z-axes, but not the rotary table, this is because there is no encoder for the rotary table and it is not possible for the software to know the movements performed manually. In addition, the rotation is locked in software for angles beyond 90^o, but there is no sensor to physically lock the rotation to 90^o. Therefore, manual control of the rotary table is not allowed.

The system also features an emergency stop button connected to the rack with a long cable, this button can be easily relocated or could be held by the user in any critical scan where a quick stop is necessary. This button can be seen in Figure 3.15 on the floor, at the right side of the rack.

3.3 Software development

3.3.1 Frameworks

MATLAB is a computing environment and programming language, one of its applications is the design of graphical interfaces through the app designer tool. MATLAB app designer was chosen over other programs such as LabVIEW or Python, given the number of existing libraries and scripts for NF antenna scanners, and MATLAB's powerful data processing, plotting capabilities and, most importantly, team experience.

As for TCP/IP communication, Python was used to create the server and the external clients. This is because Python is an open source software whose libraries related to connections using the TCP/IP protocol are free of charge, which is not the case with MATLAB, whose library for creating a server is actually a toolbox that must be purchased in order to use it.

Three libraries were used in Python, sockets, Tkinter and Threading. Sockets are endpoints for sending or receiving data using different protocols such as UDP, ICMP or the one we are using which is TCP. A socket is a combination of an IP address and a port number. It is typically used for communication between local and remote devices. Tkinter is a library that allows to create GUI applications, in the program, it was used to create the command text box, the button to send the command and the history text box, where the user can review previous commands. Threading is a very important library that allows different parts of the program to run at the same time, in this case, it is used to allow multiple user connections to the server.

3.3.2 GUI

This GUI is divided in six tabs, a lower console that displays the GUI messages and a lower panel that informs about the operation mode. The subsequent sections describe each of these areas of the GUI.

Home

In order not to overload the user with different options or functions as soon as the software is launched, the introductory welcome page was designed in a minimalist and concise way. The user finds just two buttons for simplicity, “Start”, clicking it will redirect the user to the next tab; “Documentation”, clicking it will bring up a folder containing manuals, datasheets, list of materials and other useful information. Figure 3.17 presents the Home tab.

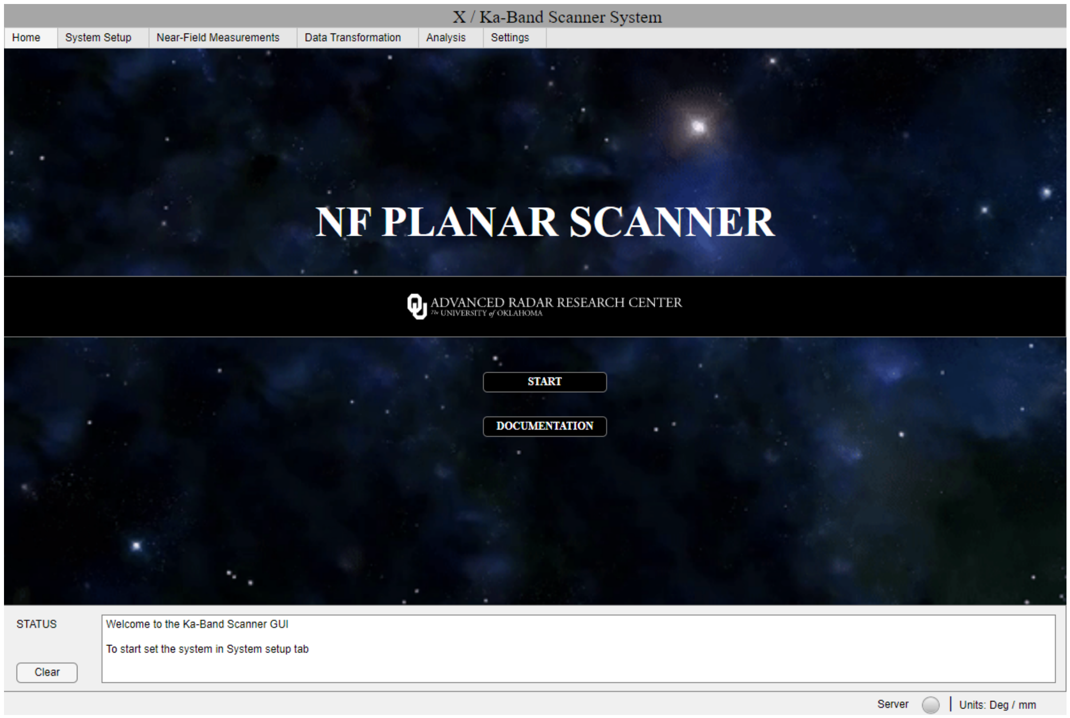

Figure 3.17: Home tab

System Setup

As the name suggests, this second tab allows the user to prepare the scanner system to start a measurement. This preparation basically consist of connecting external devices such as the motor controllers, readouts, VNA, and/or TCP/IP server to the GUI; to center the AUT and probe; and to set the scanner center of coordinates.

Now, we start the detailed explanation of the GUI content for the present tab, please refer to Figure 3.18 for better understanding. The left section contains the controls for external connections (motor controllers, encoder readouts, VNA and other computers through TCP/IP). In the first subtab called "Scanner" There are four drop-downs, designed to help the user to select the associated COM port to the motor controller or encoder readout. Next to them are four indicators, which will turn green if the connection is successful, red if they are disconnected, blue if the motor is moving or yellow if the controller is busy. The default COM ports are those currently associated with the controllers or encoders, but the drop-downs are there in case the system is modified. Below, on the same panel, is a button to activate the joysticks. Activating the joysticks will disconnect the user from the motor controllers, the user may want to click "Connect" after using the joysticks.

In the middle section the user can control the motion of the probe through positive or negative increments by typing the increment in the text box and then clicking one of the buttons at the right side; however, there is a restriction for the motor 4 or rotary table, it does not allow to rotate it more than 90^o or less than 0^o. The user can also find seven predefined functions, these are "Go to limit switches", the probe will move in the negative direction for x, y and z-axis until it reaches the limit switches; "Find center", the probe goes to a limit switch, in the axis selected, and once reached it moves half the maximum distance (This command should be reconfigured if the limit switches are repositioned); "Set zero Position", thanks to this button the user is able to set the origin for each axis; "Set Copol Center" and "Set Crosspol Center" are two buttons that define where is the center for the copol and crosspol measurements, these two buttons are necessary for higher accuracy given the small misalignments between the rotary table center of rotation and the probe center; the "Go to copol center" button, the probe redirects to the previously defined copol center; "STOP SELECTED MOTOR", if this button is clicked and the selected motor was running then it decelerates the motor until a complete stop, bear in mind that this button just stops the selected positioner in the drop-down above the scanner picture. At the bottom of this section the positions of the probe for each axis will be displayed and updated automatically if any movement is done through the GUI, if the movements are executed by an external mean (joysticks, jog buttons or by hand) you can click the "get current positions" button to update the positions.

The right section starts with a drop-down at the top, allowing you to select the linear positioner to set or control in the middle panel. Below there is a picture of the scanner with the coordinate system reference at the top left corner. When a motor is selected the picture gets updated underlining with a red line the axis selected and the positive and negative directions.

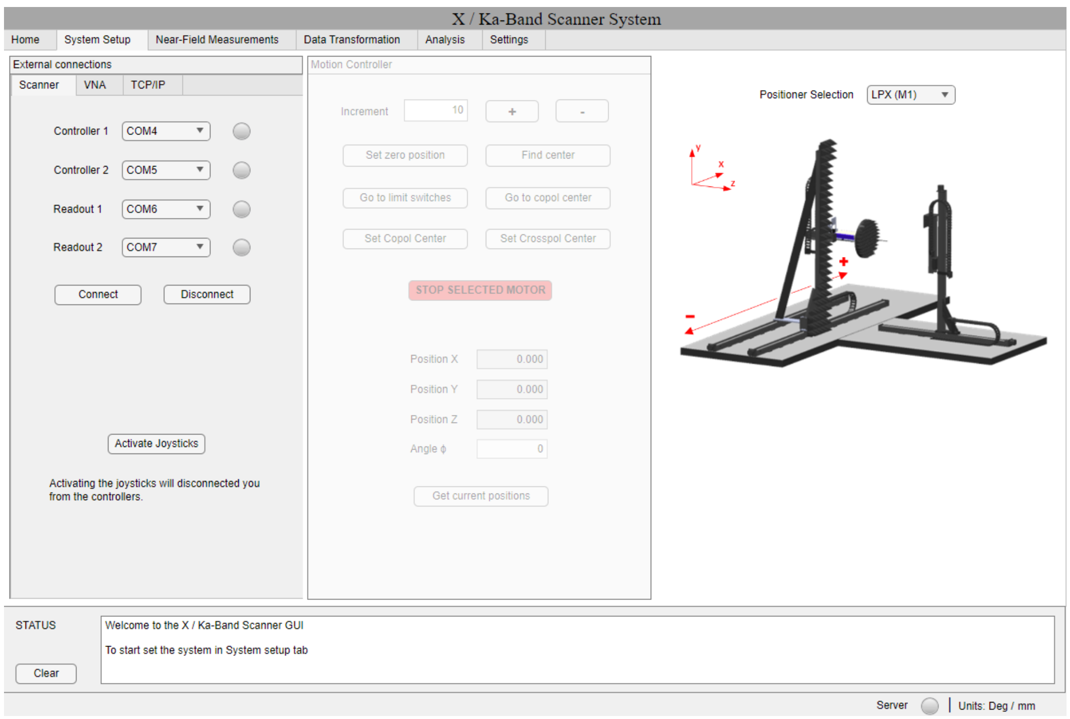

Figure 3.18: System setup tab

The "VNA" subtab (Figure 3.19a) located in the "External connections" panel, has a drop-down to select the parameter to measure (the default is S21 given that the designated port for the AUT is the port 1 and for the probe is port 2). There are a connect and disconnect buttons and three field boxes to define the frequency list. Once the connection is successful, the grey indicator next to the "VNA Status" label turns green. In addition, there is a spinner to configure the average factor, this is the number of samples the VNA average per frequency point before sending the magnitude and phase data to the GUI.

The "TCP/IP" subtab (Figure 3.19b) located in the "External connections" panel has a button for connecting to the server and a button for disconnecting. TCP/IP communication responses are displayed in the status console.

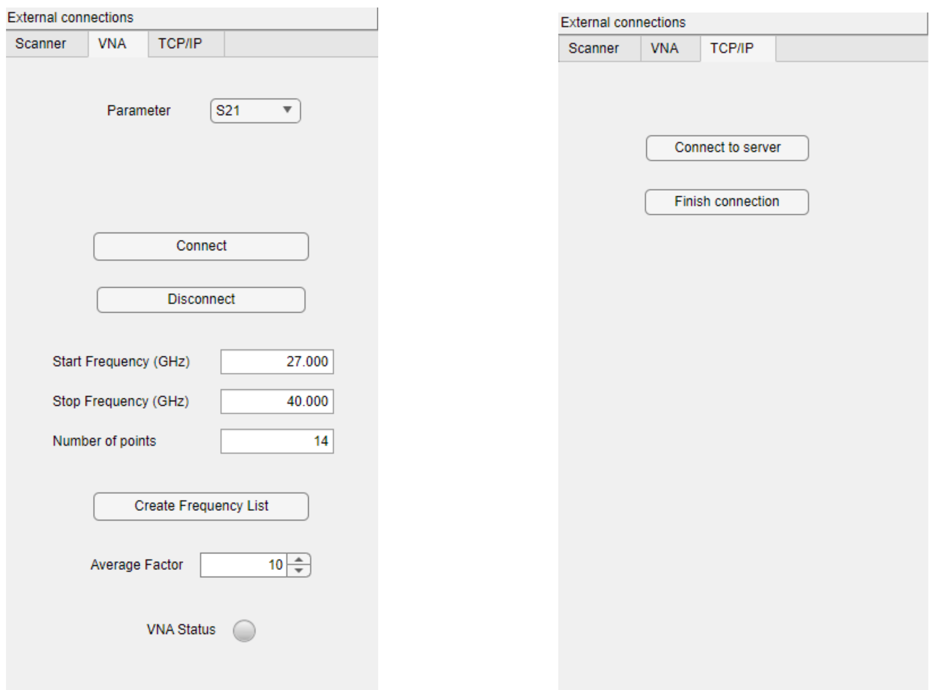

(a) VNA connection subtab (b) TCP/IP connection subtab

Figure 3.19: Subtabs in the "System Setup" tab

Near-Field Measurements

After clicking "Create new scan" button (left menu in Figure 3.20), frequency, AUT dimensions, far field angle, probe dimensions and AUT to probe distance should be selected and defined (refer to Figure 3.21a). By clicking the "Auto Scan Setup" button, the scanning range, delta, and number of points for the scan, are provided.

The scan center is automatically filled when the copol center was defined in the previous tab. At the botton of the same subtab the polarization sense can be defined, this will depend on the antenna polarization orientation, in other words, if the antenna co-polarization orientation is parallel to the x-axis, this can be defined in that drop-down. In this way the scanning will start measuring copol first, this is specially important if hologram projection is needed since the algorithm will take the first set of data (before probe rotation) to calculate hologram projection.

The subsequent subtab (refer to Figure 3.21b) was designed to allow the user to further analyze the near-field data after a scan is finalized. The first feature is the field truncation, basically the user can replace the near-field magnitude values with very small values in x and y-axis independently, this is also called zero-padding an allows an improved resolution of the far-field radiation pattern in terms of resolution. Then, the features behind permit to plot cuts or slices of the 2D near-field magnitude data, this cuts could be either along the x or y-axis.

Going back to Figure 3.20 in the middle there is a series of small panels. Their function is to permit the user to customize the measurements. The first panel, starting from the top, is titled "Scan Copol and Crosspol", and the options are single and both polarizations, there, the user is able to select between a scan of two orthogonal polarizations or just one polarization, either copol or crosspol (this can be configured in the "Polarization Sense" drop-down in the subtab of Figure 3.21a). The following panel is titled as "Raster Scan Mode" the user is able to select between a raster scan with horizontal or vertical retrace. The next panel is titled as "Scan Technique", here the user is able to perform a park and probe scan, where the probe stops at each sample point to take measurements for each defined frequency. The other option is the continuous scan, the system will take the measurements along the continuous probe movement through the scan window. The way how the systems knows where to start the measurements is by a timer. It is important to mention that the continuous scan option is implemented in Python, so the near-field plots are not going to be populated during the scan. Once the scan is finished the user is asked to save the data in a file, then, the user can import this file into the GUI to analyze the continuous scan data. Finally, the last panel titled as “VNA Monitor” is an extra function to check for the SNR in the position where the probe is located. Pressing “Start” again will stop the SNR measurements.

The button above the panels discussed in the last paragraph is to switch between the copol and crosspol plots (plots at the right side of this window). This should be used once the scan is completed or after data was imported.

The “Import Data” button is at the top left corner, and the “Export Data” button is at the bottom left corner.

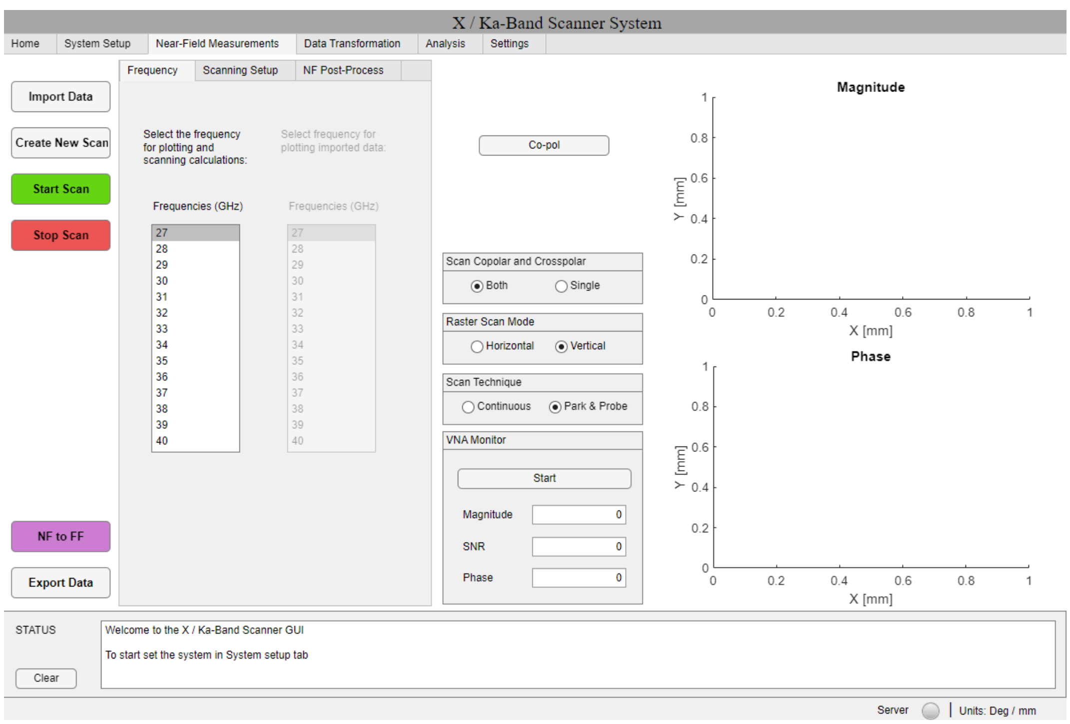

Figure 3.20: Near-Field Measurements tab

On the left menu there is a green button, clicking on it starts the scan and the graphs titled “Magnitude” and “Phase” start populating with the measurement data, once it finishes for one polarization, the graphs go blank and start populating again for the new polarization. To switch to the latest polarization data, the user can click on the button labled as “Copol”, then the button will change its name to “Crosspol”, indicating that clicking it again will change the graphs to contain the measured crosspol data (we assume that copol is measured first).

Additionally, in the left menu there is a red button, clicking on it stops any scanning in progress. This is a safe way to ask the program to stop scanning.

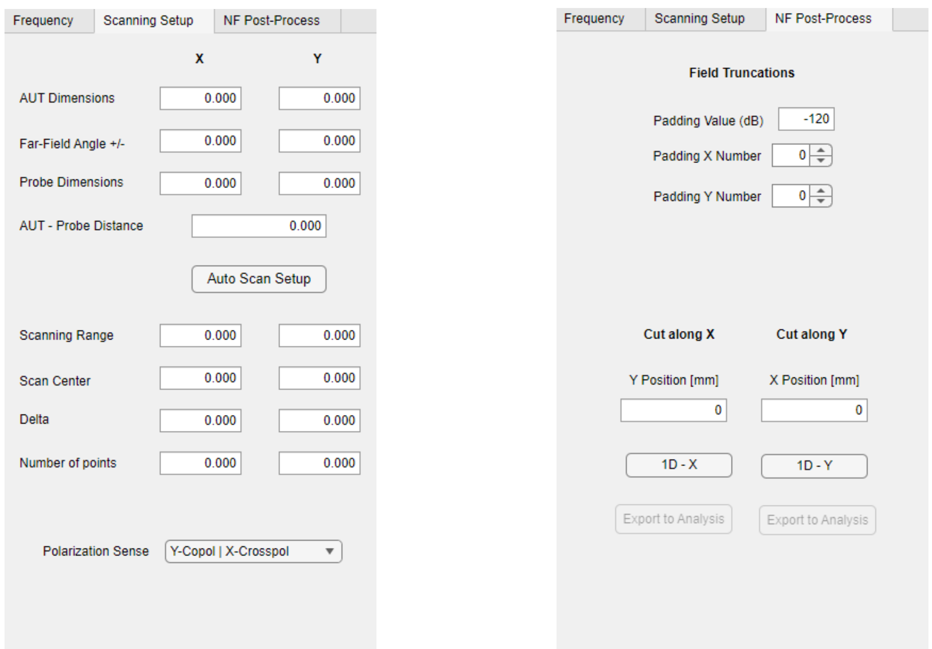

(a) Scanning Setup subtab (b) Polarization subtab

Figure 3.21: Subtabs in the “Near-field Measurements” tab

Data Transformation

After clicking the “NF to FF” button in the “Near-Field Measurements” the program starts the transformation with the measured data and according to the Ludwig definition selected, once finished the GUI automatically opens the “Data

Transformation” tab and presents the three principal cuts for copol and crosspol in the “Radiation Patern” subtab. The user can modify the minimum and maximum magnitude and angle for the radiation on the plot. As can be seen in Figure 3.22, below the plot there are six check boxes that allow the user to hide or show each of the principal cuts. There is also a button to export data to a spreadsheet with the the data shown in the plot.

In the left menu the user can change the Ludwig definition, the options are “Ludwig 3”, “Ludwig 2-1” and “Ludwig 2-2”, and by clicking the button “Re-calculate” The updated pattern will appear in the radiation pattern plot.

In addition, if the user hover the cursor over the radiation pattern plot, five small icons appear at the top right of the plot, allowing the user to pan, zoom in, zoom out, export as an image or return to initial state.

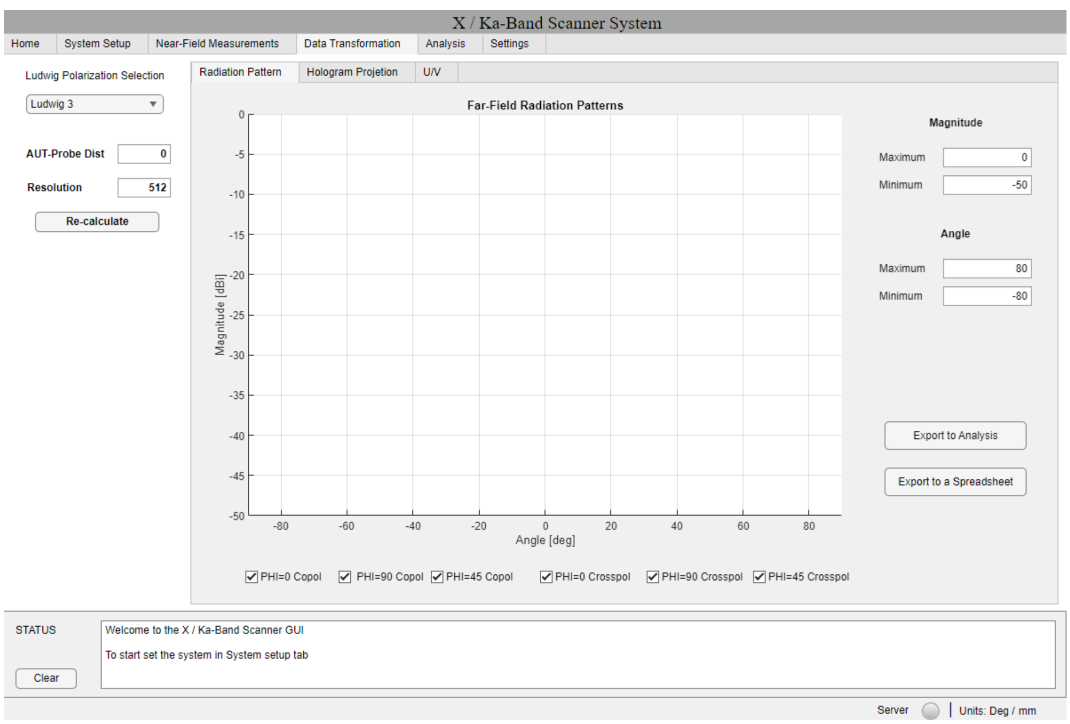

Figure 3.22: “Data Transformation” tab

Regarding the “Hologram Projection tab”. As can be seen in Figure 3.23 there is a plot for magnitude and another for phase. Below them there are drop-downs where the user can select between “Magnitude E”, “Magnitude Ex”, “Magnitude Ey” and “Magnitude Ez” for the magnitude plot, and between “Wrapped Phase Ex”, “Wrapped Phase Ey”, “Unwrapped Phase Ex” and “Unwrapped Phase Ey” for the phase variation plot. It is also possible to present the plotted data in an equal aspect ratio, so the x and y scales coincide in the plot. In addition, below the magnitude graph, there are numeric boxes to configure the magnitude limits. In Chapter four all these plots are presented with real data.

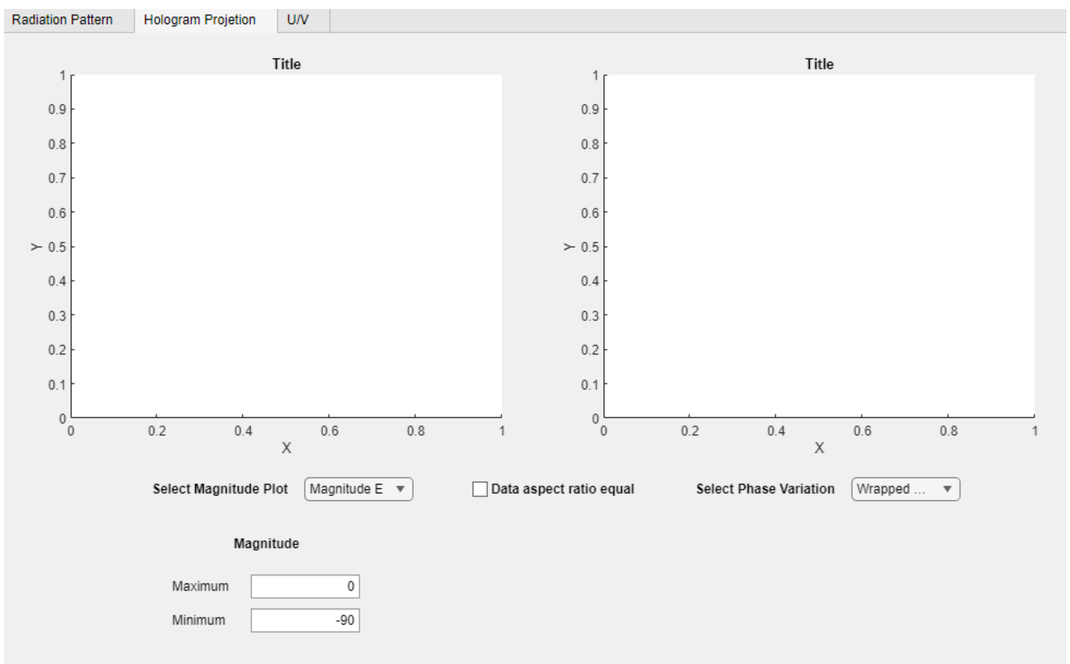

Figure 3.23: Hologram projection subtab

The “U/V” subtab shows by default a 3D view of computed far-field pattern in U and V coordinates. It also allows to rescale the plot by changing the minimum and maximum magnitude. The user can switch between a 3D and 2D view of copol and crosspol, and these three-dimensional data can be exported by clicking on the “Export to a Spreadsheet” button.

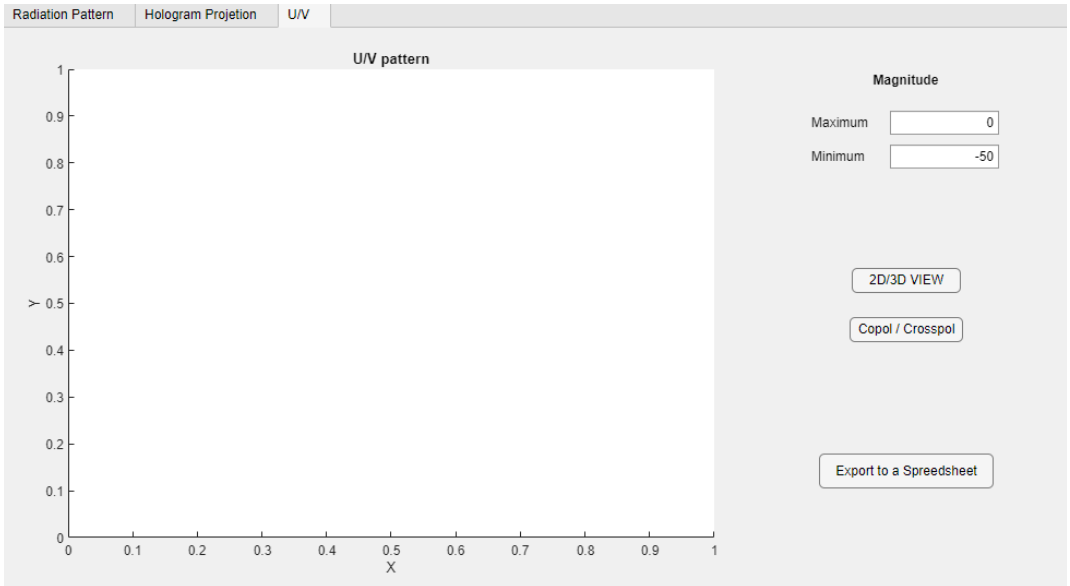

Figure 3.24: U/V subtab

Settings

The "Settings" tab should preferably be used during the measurement setup, but is not entirely necessary if the default values are working. The main panel shows the scanner coordinate system for reference. It is mentioned that the y-axis correspond to scanner vertical axis and the x-axis corresponds to the scanner horizontal axis, for agreement with the planar coordinate system presented by the "IEEE Recommended Practice for Near-Field Antenna Measurements" [3]. On the subtab called "Units" there is a drop-down to select between mm or inches, the lower right corner of the GUI will show the current units selected.

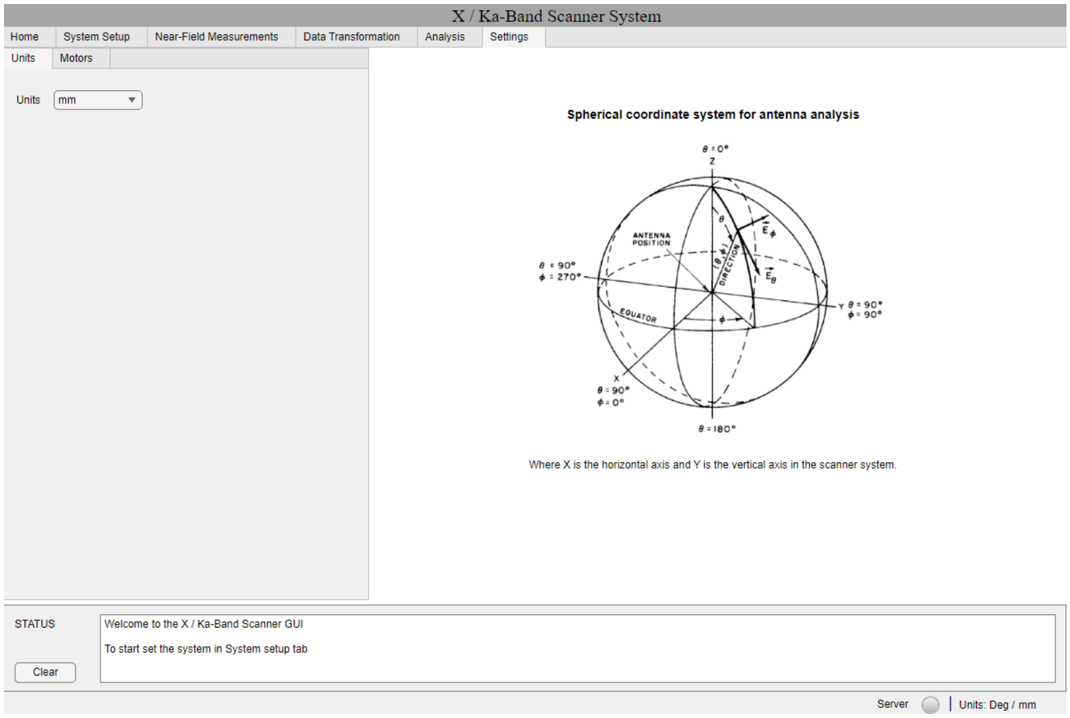

Figure 3.25: Settings tab

The "Motors" subtab (Figure 3.26) allows the user to configure the speed and acceleration of a specific motor that belongs to a specific axis. These settings are automatically saved to an external file. In this way, each time the user opens the GUI the lastest settings are loaded. In order for this tab to work the controllers should be connected.

As for the console, it is located at the bottom of the GUI and is independent of the tabs. It can display different informational or error messages. The user can clear the status console by pressing the "Clear" button located to the left of the text box.

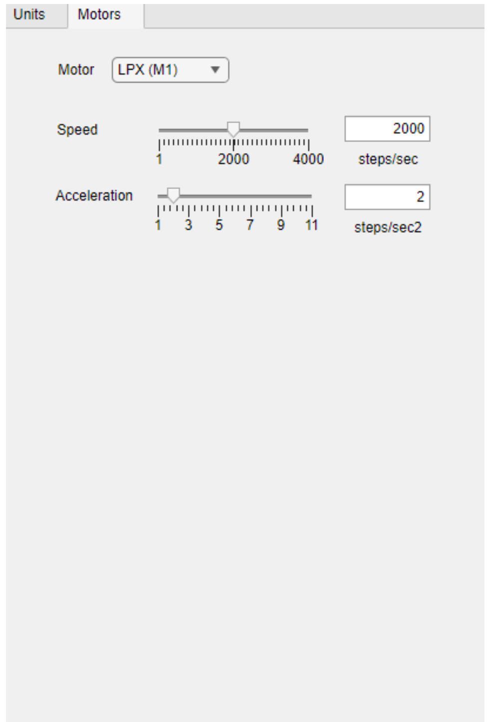

Figure 3.26: Motors subtab

3.3.3 TCP/IP communication

One of the special features of this system is the ability to receive commands to control the scanner from external devices. In other words, control of the scanner is not limited to the computer that has the GUI installed. External devices can request the position of the probe, set the center of coordinates and move the antenna probe.

Figure 3.27 shows a block diagram of the communication topology. As shown the dedicated computer for the scanner assigns the server, this server acts as a broker, what it does is to send each message it receives to all connected clients. The function of this topology can be understood as a group chat where each user is able to see the messages of other clients or users.

The MATLAB GUI works as a client. Once the server is running, the GUI will attempt to obtain a connection to the server. The purpose of the MATLAB GUI client is to receive the messages, process them and execute them. After execution it will send a completion confirmation message, these messages will vary depending on the command requested.

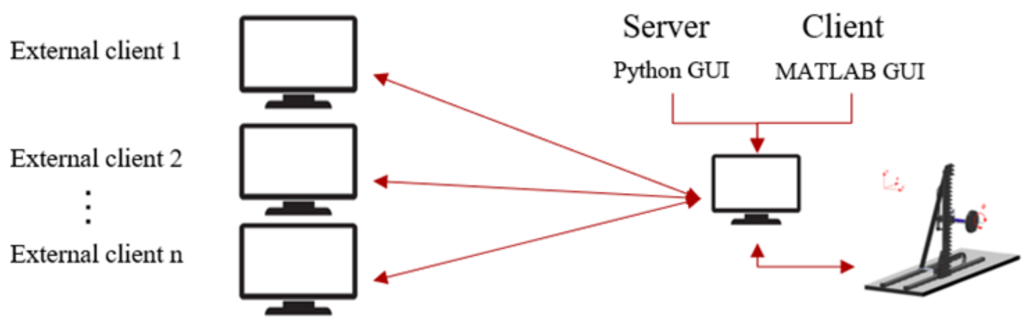

Figure 3.27: TCP/IP communication topology

The following list shows the available TCP/IP commands, it specifies the outputs (information to be sent), the expected input, how to encode the command and an example of encoding.

1. Absolute movement according to where is home located. The input is not distance but a position.
   (a) Output 1: Moving motor.
   (b) Output 2: Desired position.
   (c) Input: "The motor has stopped" confirms that the movement is done, and the motor is stopped. This response comes with a "carriage return" and a "new line" characters.
   (d) Code: AM*x where "*" is the motor number and "x" is the desired position in mm. If you select M4 "x" is in degrees.

(e) Example: **AM12000** the probe will move in the x-axis 2000 mm from home.

2. Relative movement. It is a positive or negative increment in distance.

   (a) Output 1: Moving motor.

   (b) Output 2: Desired increment.

   (c) Input: “The motor has stopped” confirms that the movement is done, and the motor is stopped. This response comes with a “carriage return” and a “new line” characters.

   (d) Code: RM*x where “*” is the motor number and “x” is the desired increment in mm. If you select M4 “x” is in degrees.

   (e) Example: **RM3-400** the probe will go down in the y-axis 400 mm.

3. Retrieve the probe position for an specific axis.

   (a) Output: Desired motor (axis) to get the position.

   (b) Input: Position in mm for the selected motor. It comes as a characters vector.

   (c) Code: PM* where “*” is the motor number.

   (d) Example: **PM4** the angle of the probe for the azimuth will be retrieved in degrees.

4. Reach the limit switch (go home function).

   (a) Output: Desired motor (axis) to go home.

   (b) Input: “The motor has stopped” if the probe reached home, or “Error” if the motor did not reach home.

(c) Code: HM* where "*" is the motor number.

(d) Example: **HM2** the probe will move in z-axis until it reaches home (limit switch).

(e) This command works just for x, y and z-axis, but not for the azimuth (M4).

5. Set Zero

(a) Output: Desired motor (axis) to go home.

(b) Input: "Sent" after the probe position has been set to zero.

(c) Code: ZM* where "*" is the motor number.

(d) Example: **ZM2** the current probe position in the z-axis is set as the new zero position.

Table 3.1 summarizes the motor numbers, their corresponding axis and their model.

Table 3.1: Motor identification

Motor identification	**Axis**	**Model**
M1	x	Vexta PK296-03BA
M2	z	Vexta PK266
M3	y	Vexta PK296-03BA
M4	ϕ	Vexta PK266

3.3.4 Communication procedure

1. Run the python server. This can be done from a terminal in case of Linux or from the cmd console in case of Windows. The server is created by a python file that requires the installation of some libraries. This file is provided in addition to the scanner GUI.

2. Start the Scanner GUI. Go to the “System Setup” tab. In the left panel (“External connection”) go to the “Scanner” tab and then click on the “Connect” button. This will start the connection with the motor controllers and the encoder readouts.

3. In the same “External connection” panel go to the “TCP/IP” tab. Click on the “Connect to server” button. If the connection is successful, the indicator at the bottom bar at the left, labeled as “Server” will turn green.

4. Now, run the “Client” Python program (this can be done from a different computer in the same local area network) in order to send commands to the scanner GUI. The next window will pop up. And you will see the new client connection in the status console in the GUI.

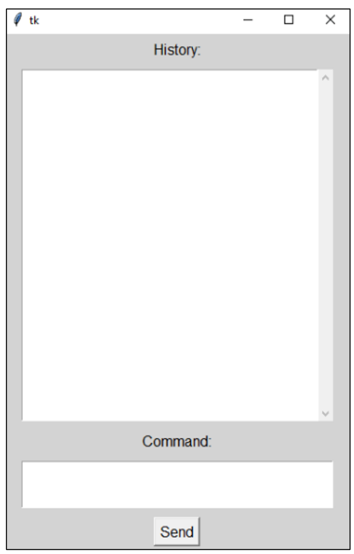

Figure 3.28: Client console

5. Type a command from the above list in the “Command” text box and click the button “Send”. To close the client, just close the window. You will see all the sent commands and responses on the “History” text box.

6. To end the connection, go again to "TCP/IP" tab and click on "Finish connection" button. The indicator will turn grey, and the scanner system will not receive more TCP/IP commands.

7. Finally, stop the Python server program by shutting it down.

3.4 Maintenance

To extend the life of the system, maintain its accuracy and avoid accidents, maintenance is essential. The following sections set out how to care for the system on a regular basis.

Oiling

Oil is necessary to reduce friction and ensure good repeatability. Velmex, inc. recommends lubricating its products with BL-2 lubricant (500 cSt oil). Considerations:

1. Three to four drops of BL-2 should be applied to the lead screw threads and way surfaces. It is also recommended that one to two drops of BL-1 lubricant be added to the lead screw bearing support.

2. Because of the heavy load on the x and y-axis, we recommend weekly lubrication if the system is used continuously. For occasional use, monthly lubrication or when the screw and ways appear to be dry.

3. Before applying new oil, clean out old accumulations of lubricant and debris.

4. Do not over-lubricate, excess oil may spill into areas that are difficult to clean.

Adjustments

After some time of use, the BiSliders will experience problems such as looseness. To avoid this, the white carriage nut (StabilNut II) can be tightened. In addition, it is possible to adjust the carriage adjustment by tightening the bolts on the carriage surface. Figure 3.29 provides a better explanation of the carriage adjustment. BiSliders should be tightened just enough, otherwise wear will increase.

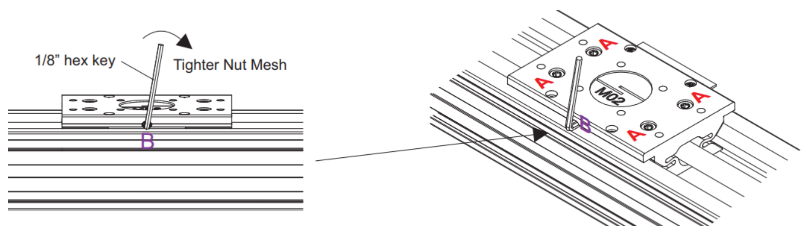

Figure 3.29: Adjustment drawings retrieved from the BiSlide assembly document

The “B” indicates the place where the StabilNut can be tightened. 1/8 of a turn is the maximum recommended. The “A” indicates the bolts that should be tightened to adjust the carriage plate. These bolts should be tightened evenly to guarantee a parallelism and therefore good limit switch functioning.

Cleaning

1. The lead screws and belts should be kept clean of dust and debris or any other contamination from the environment to avoid excessive wear on moving parts.

2. The components in the server rack should be kept clean to prevent buildup of contaminants or damage to sensitive components.

Cabling

All cables in the system should be periodically inspected to ensure that they are in working order and not experiencing unnecessary wear or friction.

Centering/Homing

We recommend Homing before every measurement, this will guarantee maximum accuracy of encoders.

Chapter 4

Measurement process

This chapter is a comprehensive compilation of the steps to perform a measurement with the proposed scanner.

4.1 Pre-measurement

Pre-check

We recommend the user to check the cabling between the rack and scanner for loose or worn cables. The cables to check are:

- Encoder (black cables).
- Motor controller (thick grey cables).
- Limit switch (grey cables).
- Frequency extender control and power (green cables).
- RF SMA Connections (thin blue cables).
- Probe/AUT (silver semi-rigid RF cables).

We also recommend to ensure the maintenance is up to date by checking the lead screws and belts for debris, wear, or damage. And by ensuring the moving parts have sufficient lubrication.

The last thing to check is if the system's range of motion is free of obstructions such as absorbers or any exterior material or tool.

Power on the system

The UPS must be plugged into an at least 13A rated outlet. Then, the UPS power button should be pressed until an audible "beep" is heard, release the button and make sure the green sinewave appears above the display.

At this point the rest of the devices are ready to be powered on. Turn on the PC by pressing in the power button at the from of the PC tower and turn on the monitor. Press the START/STOP button on the front panel, it will get illuminated, then press the "C" button on the encoder readouts (VRO's). Flip the motor controller power switches to the on positions. In case any of these devices does not get powered, check that the power strips at the back of the rack are turned on.

Launch GUI

The user should start here if power has not been lost since last use.

Log on to the computer and on the desktop, there is a GUI shortcut named "NFP-Scanner.mlapp" or in the search bar look for the file named "XKaScanner.mlapp", once found, double click on it and the MATLAB software will open first, then the interface will be displayed. Figure 4.1 illustrates the Home tab. As mentioned in the previous chapter, the user has two options, start using the GUI or review the documentation. To start a measurement, click on the START button and the “System Setup” tab will be automatically displayed.

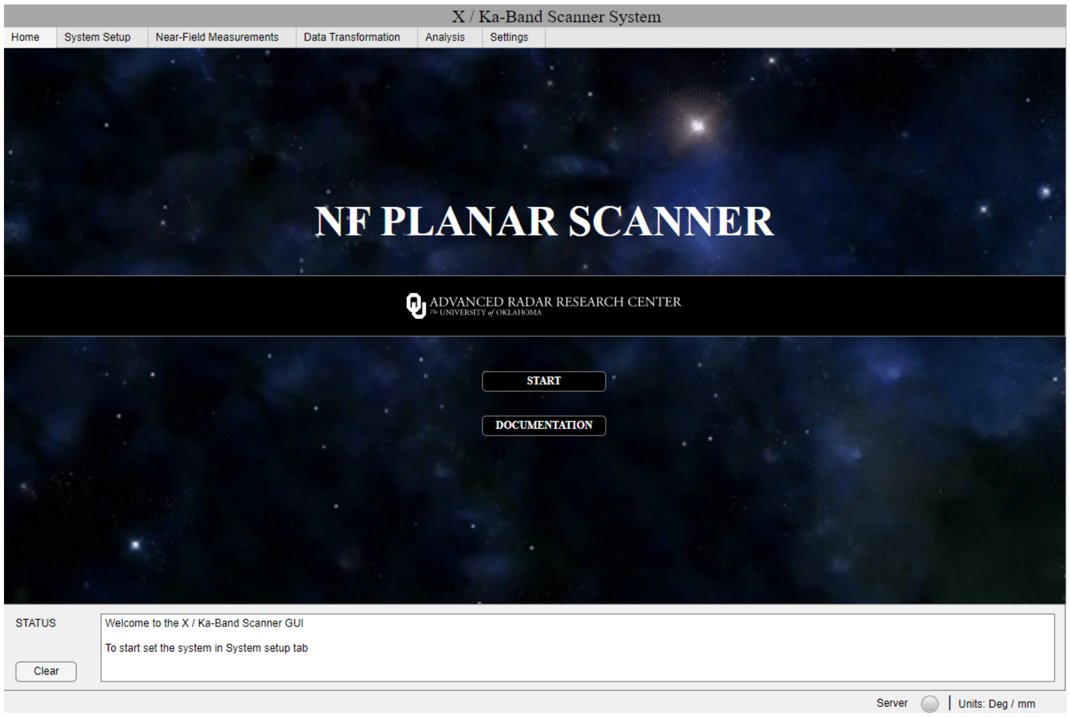

Figure 4.1: Interface home tab

In the “External connections” panel, select the “Scanner” tab. This section allows the user to select the COM ports for each scanner device. Unless the connections for the scanner devices (controllers and readouts) have been altered, the assigned ports by default do not need to be changed, so click on “Connect” to interface the computer with the scanner devices. All the indicators should turn green and the “Motion controller” tab should be enabled. Figure 4.2 shows what the interface should look like after following the mentioned steps.

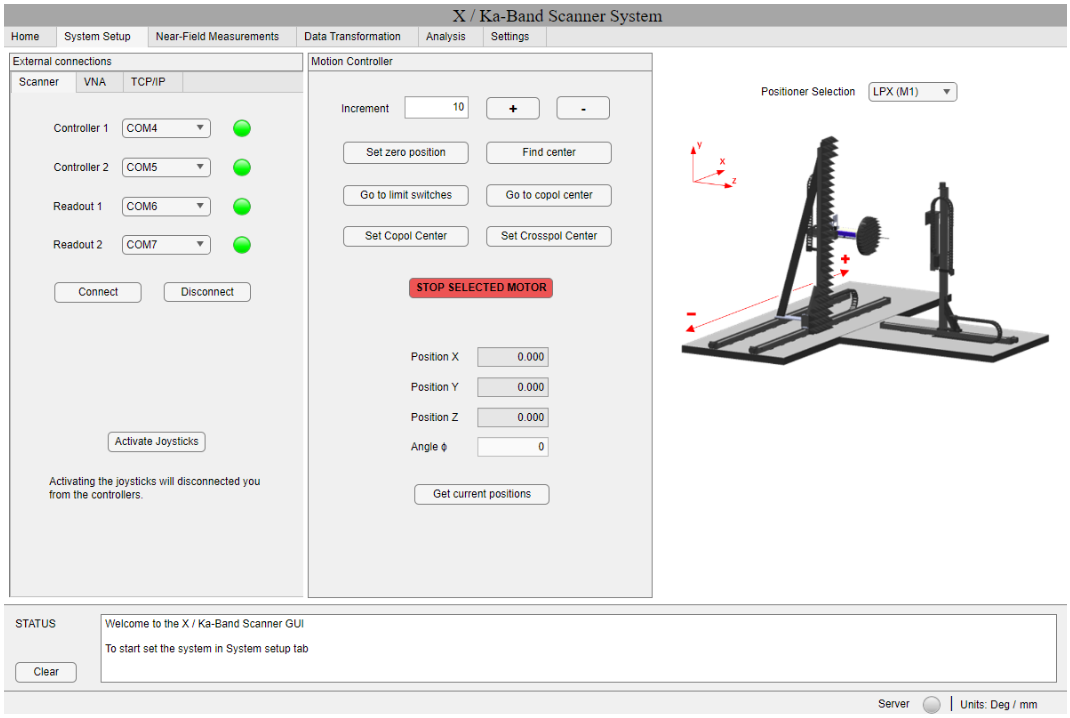

Figure 4.2: System Setup tab

Alignment

Now it is time to place the AUT and align it with the probe. In the "Motion controller" panel at the top there is a numeric field box to enter the desired increment in distance of the probe, the axis for the movement should be selected in the "Positioner selection" drop-down above the picture. Once an axis has been selected, the picture will be updated, underlying the selected axis and specifying where is the positive and negative sense. This increment could be in millimeters or inches, check at the bottom left corner of the GUI for the current units. You can change the unit system in the "Settings" tab.

We recommend using the joysticks for this task. To activate them, in the same "External connections" panel, under the "Scanner" tab click on the "Activate joysticks" button. Move the probe forward (z-axis) until it reaches the limit switch. Then, place the AUT almost touching the tip of the probe. Now, move the probe from edge to edge of the AUT and ensure planarity, do this for x and y-axis. Once planarity is achieved it is time to find the center. It is important to know in advance the center of the AUT, then using an industrial line laser you can align both antennas. The laser will also help to recognize if the probe or AUT is tilted or skewed in certain direction. Now click the button “Set Copol center”. Figure 4.3 presents a real scenario of a horn antenna being aligned with the probe of this scanner in the y-axis orientation. It can be seen that the red line passes exactly through the center of AUT and the probe.

Figure 4.3: Alignment in y-axis (Courtesy: eMWave-tech)

The machined pieces of the scanner are not perfect, like any other system, tolerances are present and accumulation of small imperfections leads to noticeable misalignment. This is the case for the center between copol and crosspol. There is a small deviation (around 1 mm) present when the probe rotates 90^o which means that the center at the tip of the probe does not completely aligns with the center of the rotary table, even when it was designed in that way, and this is due to many factors like the weight and large distance between the rotary table and tip of the probe. There are two possibilities now, to find the deviation and correct the center of the crosspol once the center for copol has been found, or to add a new button so the user can set the crosspol center by his own. The second option was more appealing given that we are not sure further misalignment will occur in the future or if the system will be modified such as replacing the probe or the RF system.

Hence, the next step is to select the rotary table in the drop-down and rotate it $+90^o$, to do this you need to connect the controllers again, given that activating the joysticks deactivates the online connection with the controllers. Now, repeat the process to find the center, once finished click the button "Set Crosspol center". Move the probe back 90^o.

All this time the probe was very close to the AUT, it is time to separate them from three to five lambda distance. Calculate the distance, enter that distance on the increment box, select in the drop-down the z-axis positioner and click on the minus button.

VNA Setting

The next step is to turn on the VNA. Press the power button located in the lower right corner of the VNA, the power icon should turn green, if it does not, check that the switch located on the back of the VNA is in the on position. Then, go to the GUI and in the same "System Setup" tab, navigate to the "VNA" tab in the "External connections" panel.

In a regular scan, the parameter to read is S21, therefore the drop-down does not need to be modified. Click on the "Connect" button and wait until the status indicator turns green. Then, set the start and stop frequency, and the number of points and click on the "Create Frequency List" button. You can also set the number of averages for measurement, decreasing this number will make the scanning faster, but will decrease the quality of the data taken. You can check the frequency list just created by going to “Near-Field Measurements” tab, and then to “Frequency” tab in the middle panel. In the same tab in the lower center area there is a small panel called “VNA Monitor”, clicking on the “Start” button will activate a function that updates the detected magnitude, phase and SNR by the VNA at the probe location. It is important to keep the SNR above 50 dB. This will ensure good quality of data which will not be affected by noise. Press the “Start” button again to stop the monitor. Figure 4.4 shows the “Near-Field Measurements” tab.

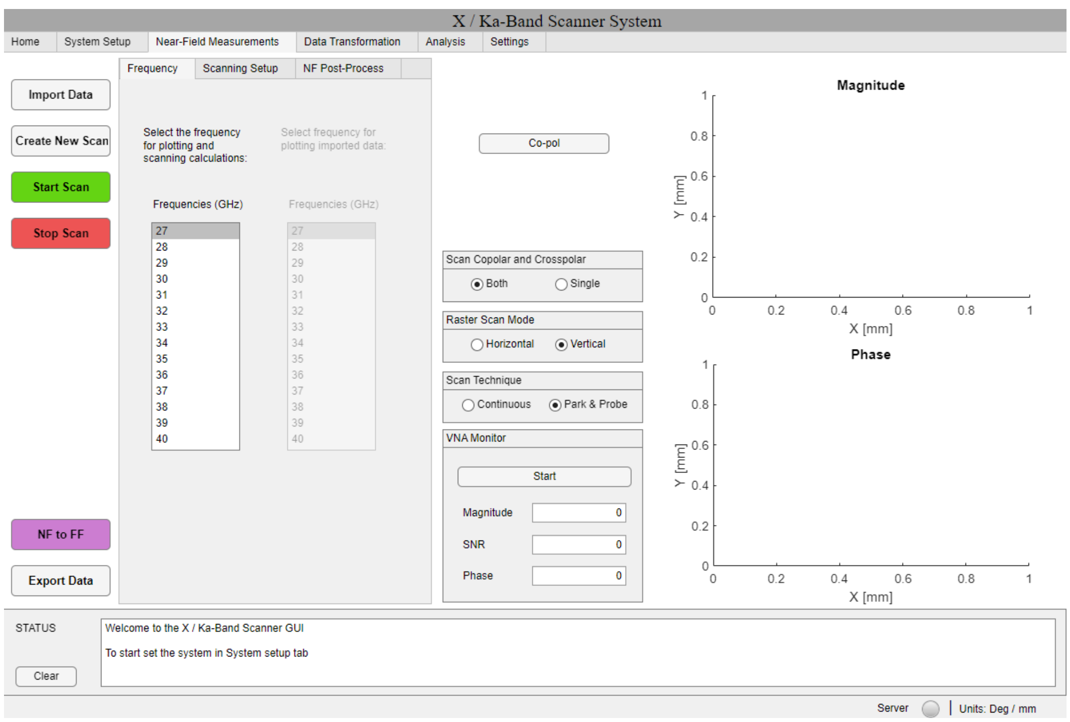

Figure 4.4: Near-Field Measurements tab

Scanning Setup

In the same window, navigate to the “Scanning Setup” tab. All four first parameters need to be defined. These parameters are required to calculate the dimensions of the scanning window and the number and separation of the spacial points to take measurements. Enter the AUT aperture dimensions. The desired far-field angle truncation (remember that the data provided for the far-field angles exceeding the truncation angles, is not reliable). The probe aperture dimensions and the distance between the probe and AUT. Click on the "Auto Scan Setup" button and the text fields below will get populated. The scan center was populated right after defining the copol center.

At the right side there are three small panels to make the scan more customized. The upper panel allows to control the number of orthogonal polarizations to take during the scan, the user is able to select between just measuring a single or both polarizations. The panel below allows to select between the two raster scan modes, vertical or horizontal retrace. And the last panel is to select between the continuous and park and probe scan techniques. These options suppose a trade off between accuracy and time. If accuracy is most important, we recommend to scan with the default options (measuring both orthogonal polarizations, using the vertical retrace mode and defining the scan technique as park and probe).

The continuous scan technique was developed in Pyhton; therefore, when this option is selected, what actually happens is MATLAB calling a python file and executing it, when finished this python file returns the magnitude and phase data for every frequency requested. In addition, given that the scan is not executed in MATLAB, the magnitude and phase plots do not get populated during the scan. In order to see the near-field plots the user has to import the scan file after it was saved.

Now that everything is set up, click on the green "Start Scan" button on the left side of the window. An audio will play saying *starting scan* and then the probe will move to the lower left corner of the scan window and begin measurements. The status console will display the time remaining for the completion of the scan, this time will be updated four times during the scan.

During the scan, the near-field magnitude and phase values are displayed on the near-field plots. These are color plots which means that the values are associated with a range of colors. Is it possible to identify a bad setup from the near-field plots; therefore, we recommend supervision during the scan.

If for some reason, the scan should be stopped, click on the "Stop Scan" red button on the left menu.

4.2 Post-measurement

Post-processing

Once the scan is complete, the probe will return to the initial polarization and another audio will be played, it says *scan completed*. Then a window will show up asking the user to save the recent measured data.

In case you selected a scan with both polarizations, you can switch between copol and cross-pol near-field data by clicking on the upper button labeled "Copol" or "Crosspol" depending on the current polarization displayed.

In addition, there is a tab labeled as "NF Post-Process", inside there are extra functionalities, for instance, the option to truncate the data by replacing the outer values of the near-field magnitude matrix by really small values (the value of truncation could be specified, by default it is -120 dB) the option to plot cuts of the near-field magnitude, it could be a cut along x or y.

To obtain the far-field patterns, first click on "Frequency tab" and select a frequency from the list, then click on the purple button labeled as "NF to FF" and after a couple of seconds you will be redirected to the "Data Transformation" tab, where the far-field patterns of the principal cuts should be plotted. Figure 4.5 presents how the "Data Transformation" tab should look like after clicking the "NF to FF" button, as can be seen, the principal cuts (phi = 90^o, phi = 45^o and phi = 0^o, green, red and blue respectively) for copol and crosspol have been plotted. The plotted far-field pattern cuts or slices correspond to a Ka-band horn antenna.

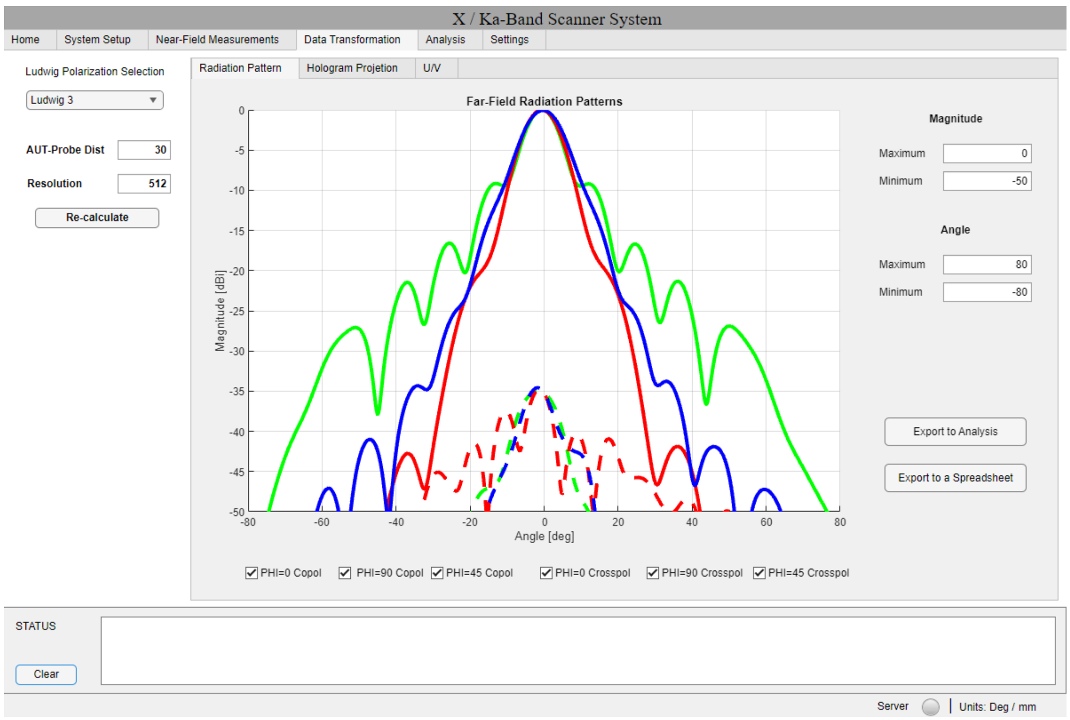

Figure 4.5: Data Transformation tab

By default the magnitude goes from 0 to -50 dB, and the angle from -80 to 80 degrees, but it can be changed using the maximum and minimum boxes at the right side of the plot. Beneath the last options there are two buttons to export the data. The first one allows to export the patterns to the "Analysis" tab. This tab allows to compare up to three different patterns, they could come from different antennas or the same antenna but for different frequencies or different configurations. The second export button is to export the patterns data to a spreadsheet.

Below the graph there are six check boxes to specify the cuts to be plotted.

At the left side of the plot there are extra functionalities. First, there is a drop-down to select the polarization definition, the user has the option to select between Ludwig 3, Ludwig 2-1, and Ludwig 2-2. Beneath there are two options to redefine the AUT to probe distance and the resolution for the discrete Fourier transform. These last two parameters are mainly used to analyze the hologram projection, which could be used for calibration and diagnosis by observing the amplitude and phase distributions on the antenna aperture (specially for arrays) [32]. Figure 4.6 presents the hologram projection for the measured horn antenna. The graph at the left is for magnitude and the phase is the right one. The magnitude limits can be redefined in the two numeric boxes below the magnitude plot.

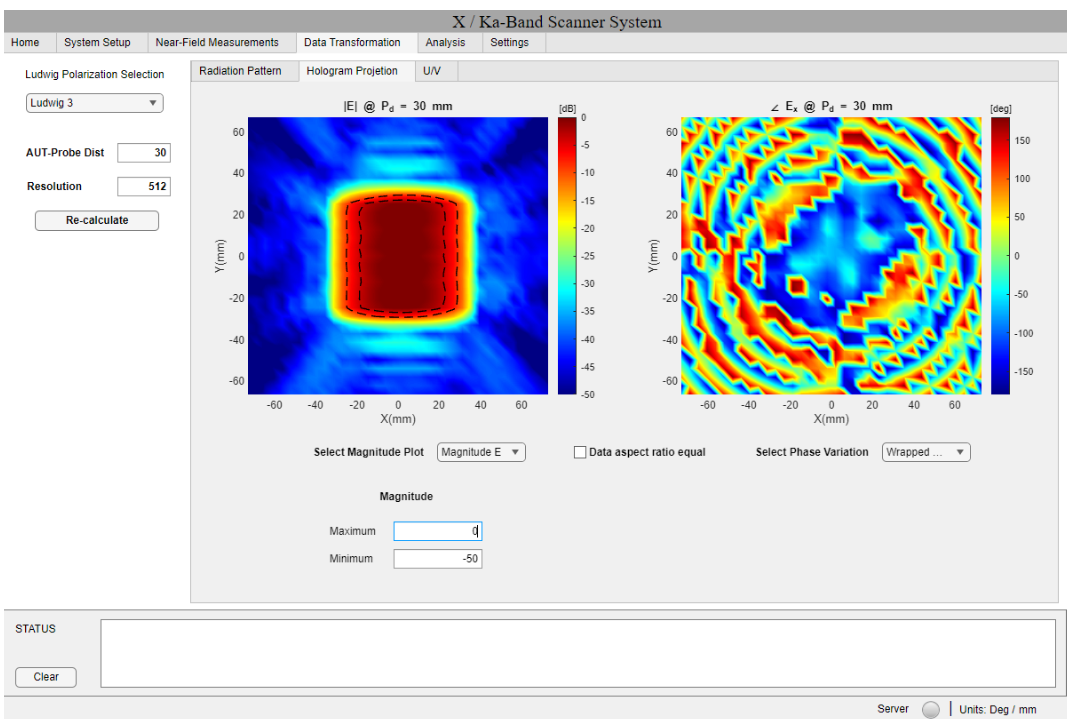

Figure 4.6: Hologram projection tab

The last subtab in this window is "U/V". The importance of this subtab is to visualize copol and crosspol in 3D in “u” and “v” coordinates. In case the user needs further information than the principal cuts, there is an option to export to a spreadsheet the data for one half hemisphere of the radiation pattern, in other words, it is possible to get the data in azimuth from 0^o to 360^o and in elevation from -90^o to 90^o. Figure 4.7 exhibits the UV pattern subtab.

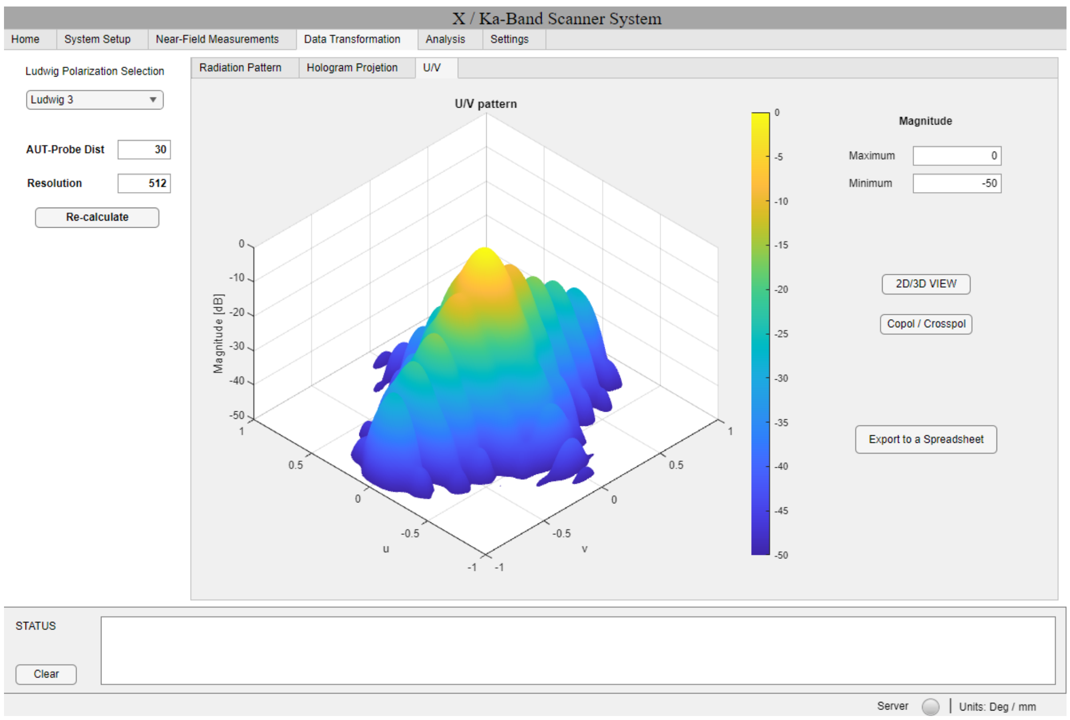

Figure 4.7: U and V coordinates 3D pattern tab

The next main tab is “Analysis” as mentioned, this tab was created to compare up to three sets of patterns. Since each principal cut has a color already assigned to it, the patterns are differentiated by color tone. The lightest set of colors correspond to the first exported cuts, the regular tone color correspond to the second exported set of cuts, and the darkest set of colors correspond to the third set of exported pattern cuts. Figure 4.8 illustrates the above mentioned, in this figure, phi $= 90^o$,and phi $= 0^o$ are plotted for 30, 33 and 35 GHz. We can see how for higher frequencies the patterns are narrower, this is because the aperture is electrically larger. This software will allow the user to keep adding patterns; however, the following ones will have the same color hue order, and this could lead to confusion. If another comparison is needed, click on the button labeled "Clear Graph" in the right side panel. There you can also change the magnitude and angle limits.

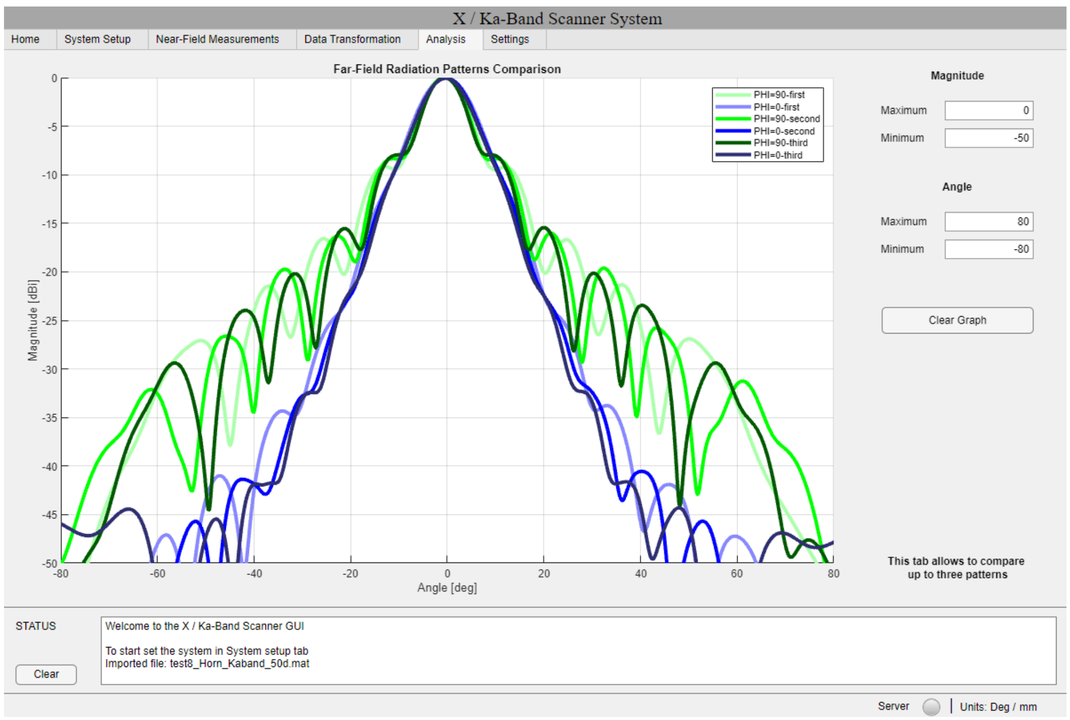

Figure 4.8: Analysis tab

This tab is very useful because it allows the user to easily recognize how the pattern changes when different parameters or settings are applied, even to compare patterns of different antennas, for this the user needs to import the files of the previous measurements, this leads us to the next section.

4.3 Importing measurements

To import past measurements navigate to the “Near-Field Measurements” tab and then click on the button “Import Data” located at the top in the left menu. A regular Windows “select file to open” window will show up, there you can select any saved “.mat” file from previous antenna measurements. Once the data is retrieved, a message will appear in the status console, notifying about the imported file, and the near-field magnitude and phase graphs will be populated with the data from the frequency selected when the data was saved, Figure 4.9 shows an example of data imported. To change the frequency, go to the “Frequency” subtab, you will see that the right side frequency list is enabled while the left list is disabled. Select a frequency and the near-field data will be updated. To obtain the far-field pattern for that frequency click on the purple button labeled as “NF to FF”.

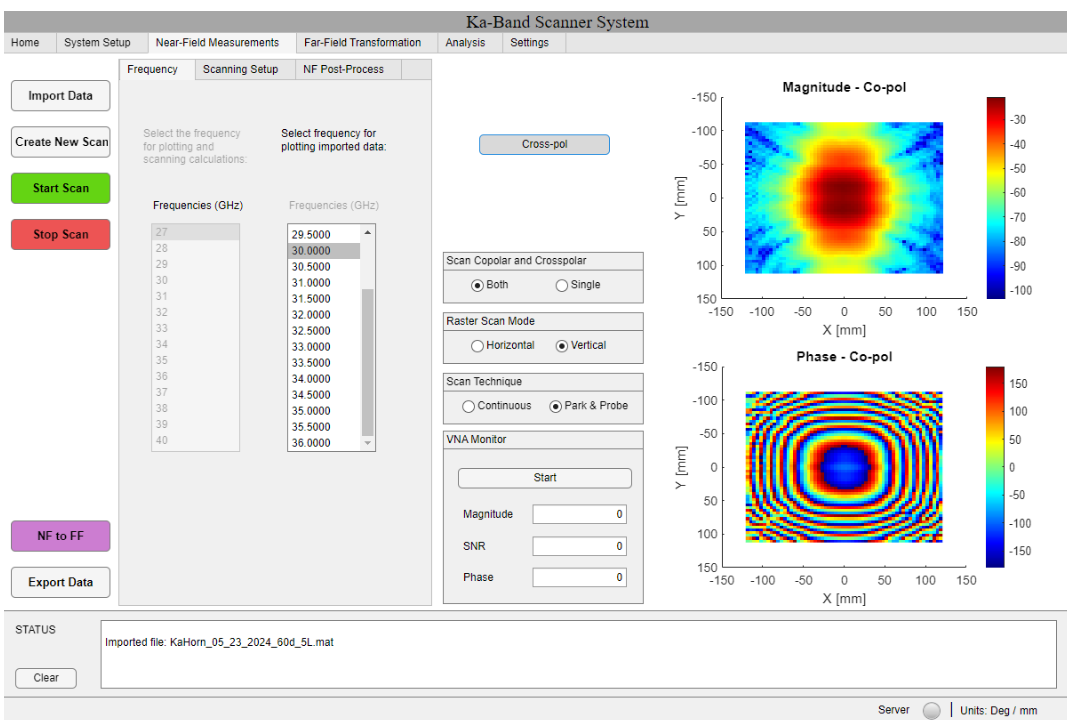

Figure 4.9: GUI after importing data

When any past measurement is imported, not just the magnitude and phase for a list of frequencies is retrieved, but also information like the AUT dimensions, the far-field truncation angles, the probe dimensions, the AUT to probe distance, the spatial coordinates for every sample point, and the state of a flag that indicates if the scan was performed for a single or both orthogonal polarizations. Most of these data can be look at the “Scanning Setup” subtab, once the file was imported.

4.4 Settings

The “Settings” tab was included for some functionalities that are not strictly necessary to perform a measurement. It also was included to provide additional information. The user can check or modify the speed and acceleration of each scanner motor. In addition, the user can switch between the metric system and the imperial unit systems (millimeters or inches). When the GUI is configured to use inches, all distance-related inputs will assume the inputs are inches; however, all calculations in the back-end of the interface work in mm. In addition, the axes of the near-field plots will remain in mm.

Part of the additional information provided in this tab is the coordinate system used in the scanner. Figure 4.10

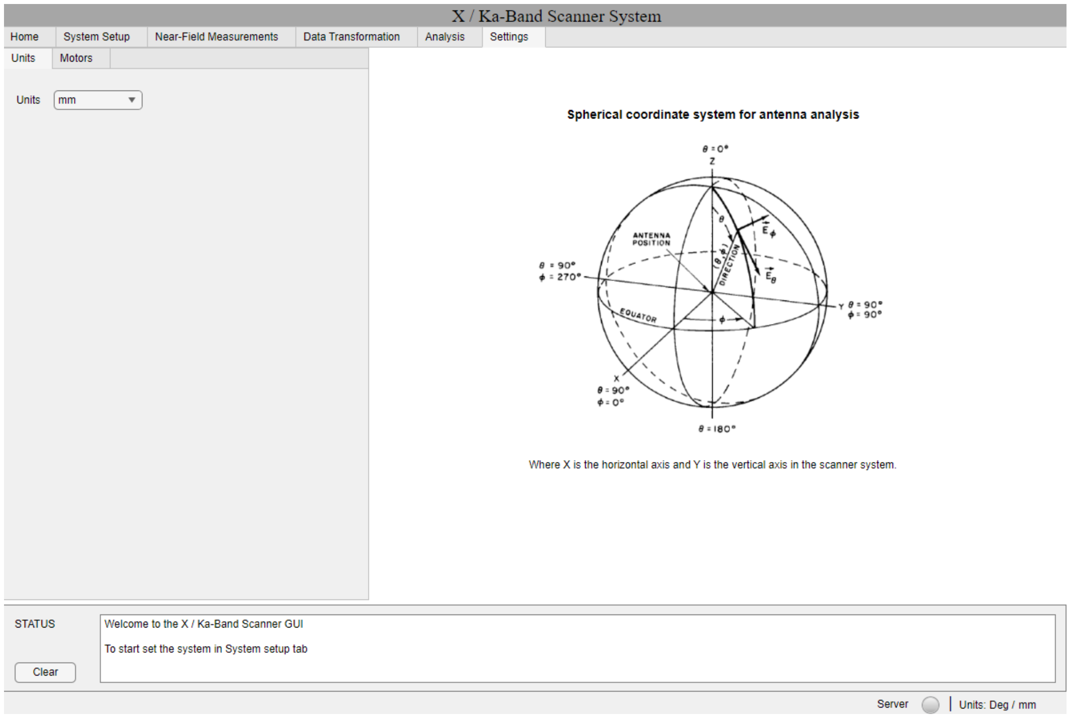

Figure 4.10: Settings tab

Chapter 5

Validation

As the system is now finished and working, the next step is to test the level of accuracy that this system has and validate the results with data provided by legitimate external sources or justifiable experiments.

5.1 Results

5.1.1 Far-field patterns

The first antenna selected for validation of the results is a standard gain horn antenna, model SGH2650, manufactured by Microwave Vision Group (MVG). This antenna operates between 26.5 GHz and 40 GHz. Figure 5.1 presents the horn antenna.

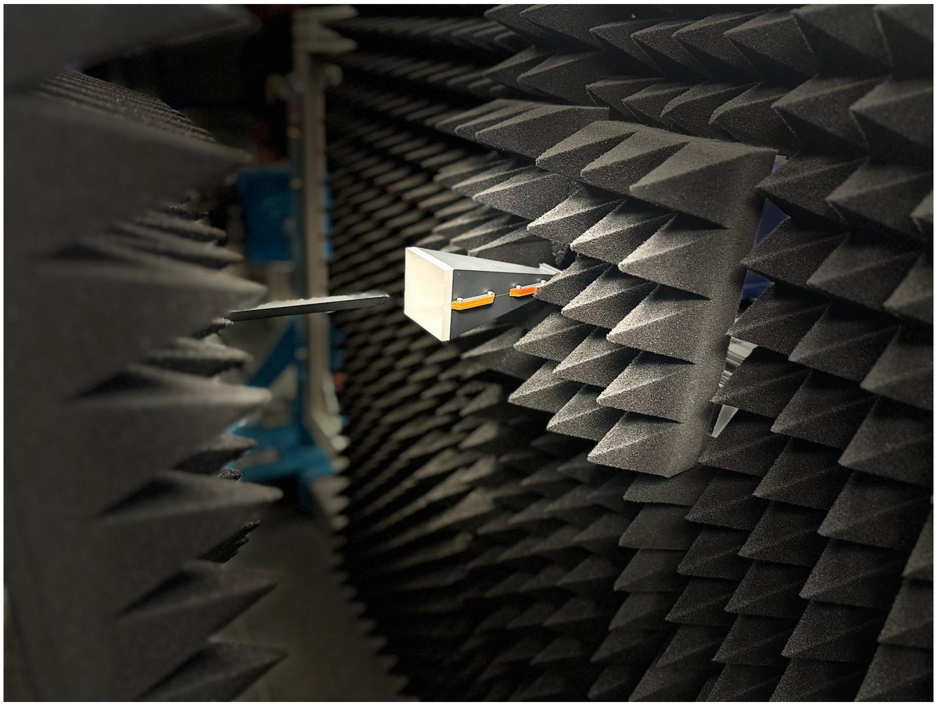

Figure 5.1: Near-field measurement setup with the SGH2650 horn antenna (Courtesy: eMWave-tech)

The manufacturer provided the far-field pattern data for 33.3 GHz and 35.3 GHz for the phi=0^o, phi=45^o and phi=90^o principal cuts for copol. The idea is to perform a scan considering the same frequencies and then compare the results expecting good agreement.

Table 5.1 summarizes some important details of the scan setup.

Table 5.1: Scan setup parameters for Ka-band standard gain horn

Parameters	**Value**	**Unit**
Scan technique	Park and probe	-
AUT dimensions	70-x, 58-y	mm
Far-field angles	$\pm$ 50	Deg
AUT - Probe distance	30	mm
Probe dimensions	9-x, 4-y	mm
Scanning window	150-x, 131.3-y	mm
Delta	3.75	mm
Number of points	41-x, 36-y	-

The near-field data obtained from this scan, for both frequencies, is presented in figure 5.2.

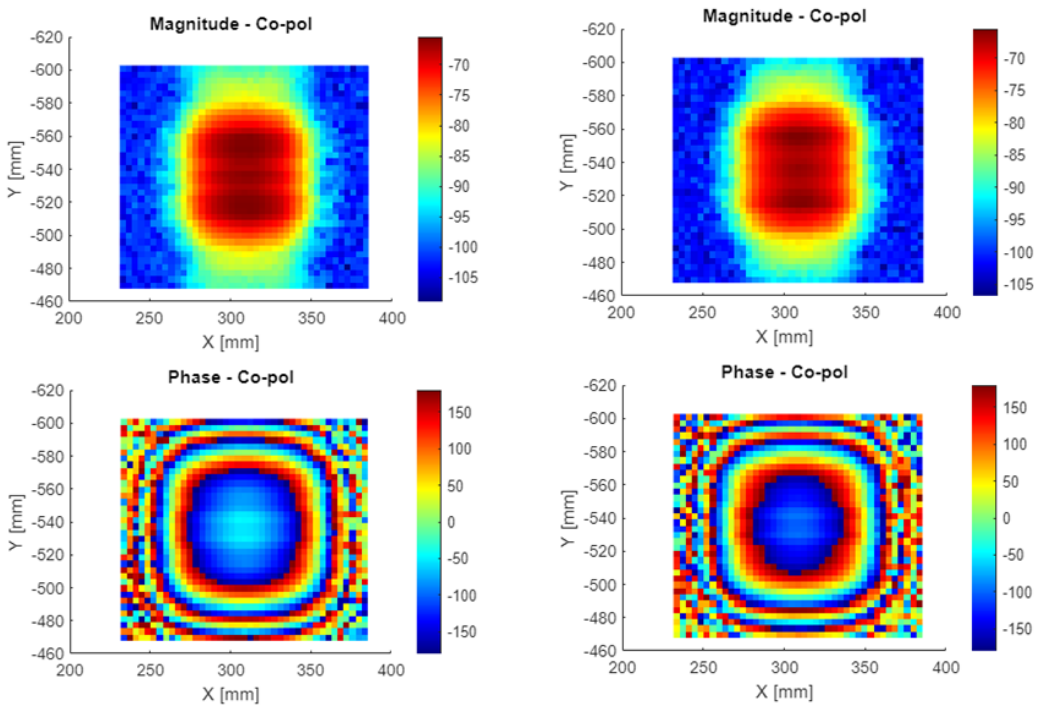

(a) 33.3 GHz

(b) 35.3 GHz

Figure 5.2: Near-field magnitude and phase data for both measured frequencies

The near-field data is important in the sense that it indicates whether the scan setup has been performed correctly. For example, if the first column of the magnitude plots does not maintain a constant color, it could mean that the VNA or frequency extender is not working properly or that there is a misconnected cable. In this case, for the phase plots in the above figures, we can see that the outer values are mostly random, this could be a sign that the SNR is not large enough for the selected scan window size. Also, odd color pixels that do not follow the pattern in magnitude as in phase could be a case of reflections in that area.

The far-field patterns obtained for each frequency are showed in the next figures. Figure 5.3 presents the far-field principal cuts for copol and crosspol (dashed line) for the measurements at 33.3 GHz, where the green line represents the E-cut or phi=90^o, the blue line represents the H-cut or phi=0^o, and the red line represents the D-cut or phi=45^o.

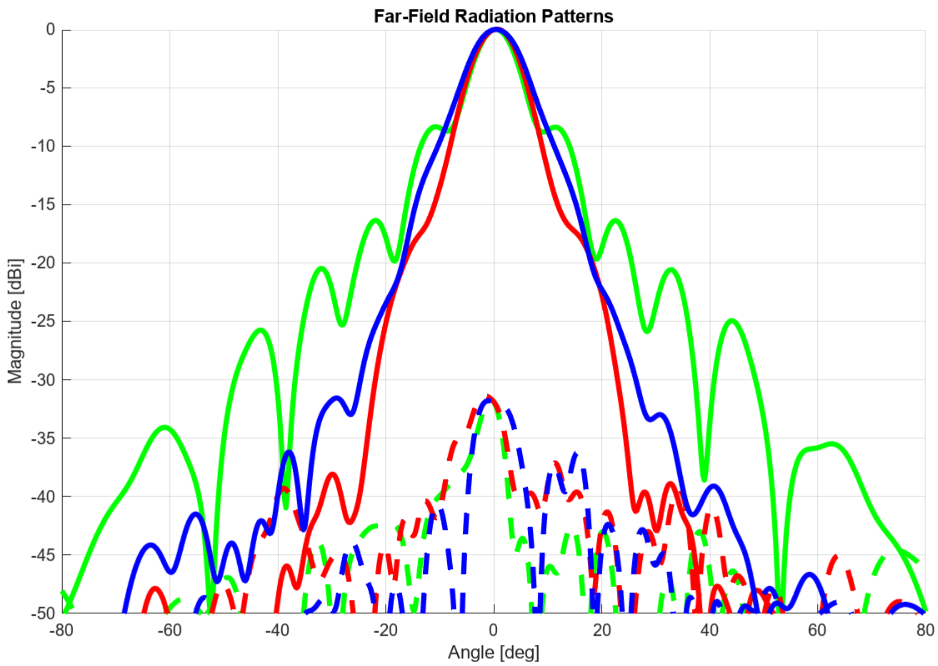

Figure 5.3: 33.3 GHz - Far-field principal cuts for co and crosspol

Looking at the far-field patterns we could say that we obtained a fairly decent measurement; nonetheless, crosspol is a bit high and does not behave as it should, the reason for this could most probably be the fact that these measurements were not performed in a anechoic chamber. In addition, we can see that the blue line (H-cut) is not really symmetric for angles beyond 30 degrees from boresight. This may be related to insufficient SNR.

Figure 5.4 presents the far-field principal cuts for copol and crosspol (dashed line) for the measurements at 35.3 GHz.

Once the results were obtained, a comparison between the manufacturer radiation patterns and our own measurements is presented next for each principal cut. The data from the manufacturer (MVG) is dashed and the continuous line corresponds to our own data.

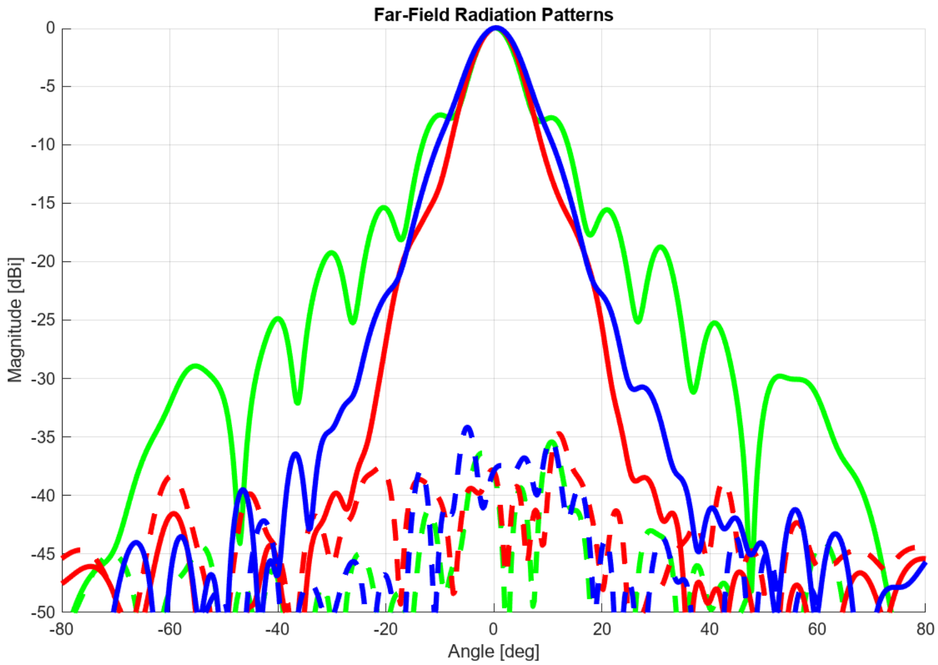

Figure 5.4: 35.3 GHz - Far-field principal cuts for co and crosspol

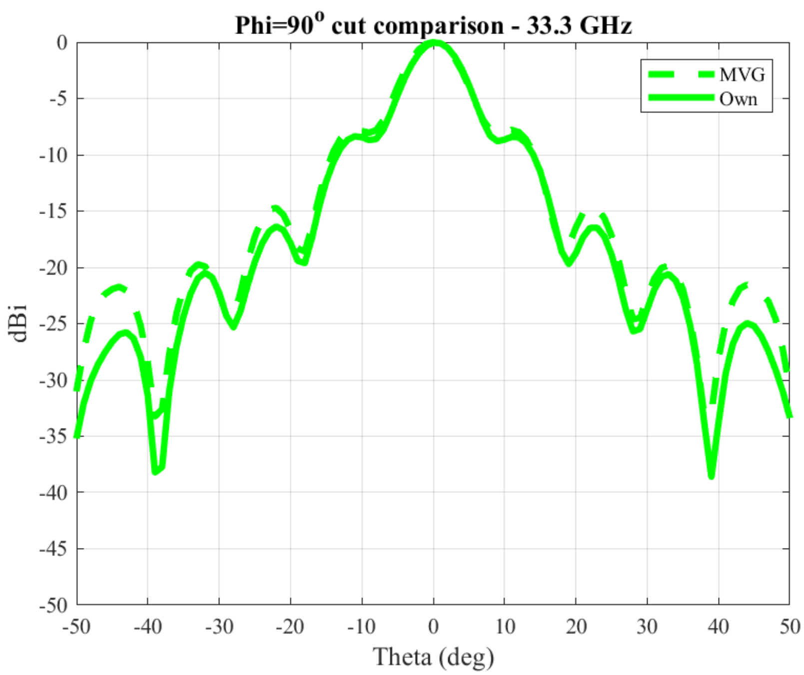

Figure 5.5: 33.3 GHz - E-cut comparison

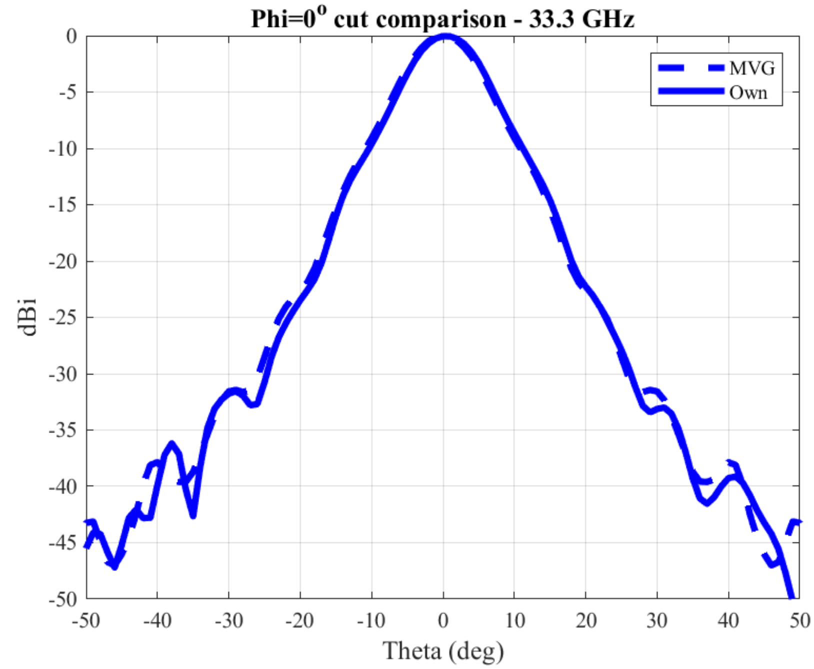

Figure 5.6: 33.3 GHz - H-cut comparison

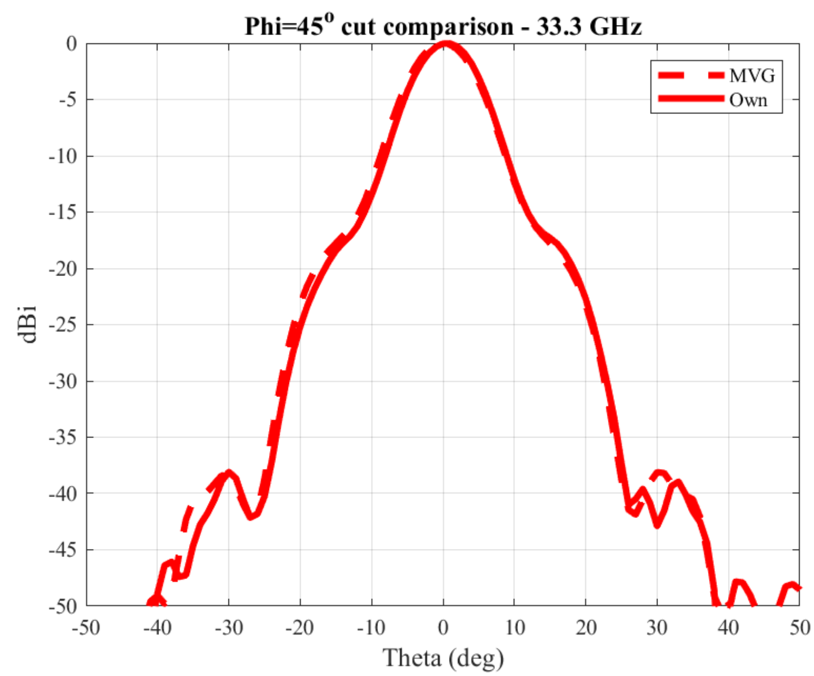

Figure 5.7: 33.3 GHz - D-cut comparison

As we can see in the last three figures, the agreement is acceptable for phi=0^o

and phi=45^o, but there is a considerable disagreement for the phi=90^o cut for angles 20^o beyond the boresight axis, the explanation for this offset is due to the fact that the probe correction has not yet been applied. However, the question that now arises is, then why phi=0^o and phi=45^o do not exhibit the same disagreement at the same angles? well, this is because the effect of the probe on considerably high directive AUT's is not significant [33]. And as we can see, the pattern for D and H-cut is substantially more directive than the E-cut.

Let us apply probe correction to these three cuts and analyze the results. MVG kindly provided the probe patterns for the principal cuts, for 26.5, 33.3 and 40 GHz. These patterns were obtained after CST simulation and they do not consider the absorber collar. Figure 5.8 presents the probe's (OEW2650) principal cuts.

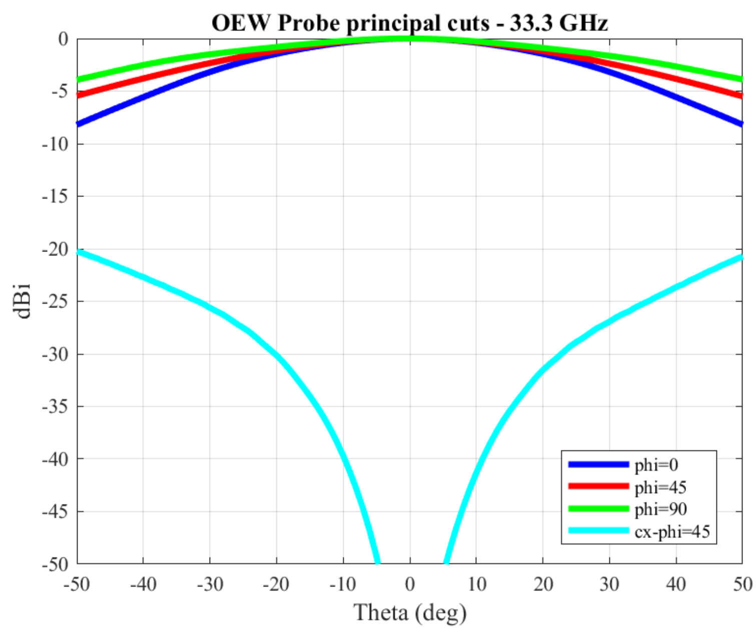

Figure 5.8: OEW Probe principal cuts for 33.3 GHz

According to Masters [29], the true AUT response would be given by:

$$\boldsymbol{E}_p = \frac{\boldsymbol{E}_{pp2}\boldsymbol{E}_{pu} - \boldsymbol{E}_{cp1}\boldsymbol{E}_{cu}}{\boldsymbol{E}_{pp1}\boldsymbol{E}_{pp2} - \boldsymbol{E}_{cp1}\boldsymbol{E}_{cp2}} \tag{5.1}$$

Where:

- $\boldsymbol{E}_p$ = True principle AUT response.
- $\boldsymbol{E}_c$ = True principle AUT response.
- $\boldsymbol{E}_{pu}$ = Uncompensated principle AUT response.
- $\boldsymbol{E}_{cu}$ = Uncompensated cross-pol AUT response.
- $\boldsymbol{E}_{pp1}$ = Probe-1,2 principle response.
- $\boldsymbol{E}_{pp2}$ = Probe-1,2 cross-pol response.

If we do not consider the AUT and probe cross-pol, then we can simplify Equation 5.1, the result is:

$$\boldsymbol{E}_p = \frac{\boldsymbol{E}_p u}{\boldsymbol{E}_p p1} \tag{5.2}$$

Then, converted to dB.

$$\boldsymbol{E}_p[dB] = \boldsymbol{E}_{pu}[dB] - \boldsymbol{E}_{pp1}[dB] \tag{5.3}$$

This means that the measured pattern in dB minus the probe pattern (for the same cut at the same frequency). Then, applying the simplified probe correction equation we obtain the results in Figures 5.9, 5.10 and 5.11. We can see an improvement for the phi=90^o, but an slight deterioration for phi=0^o and phi=45^o.

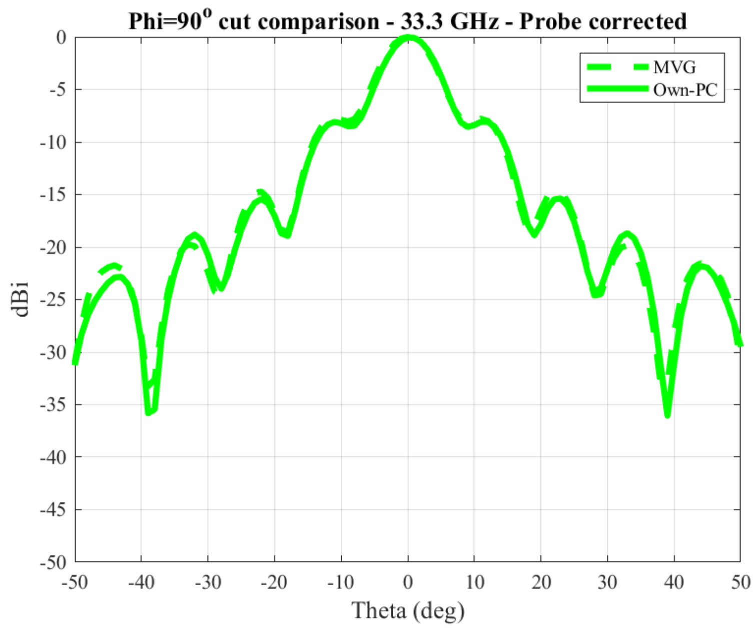

Figure 5.9: 33.3 GHz - E-cut comparison - PC included

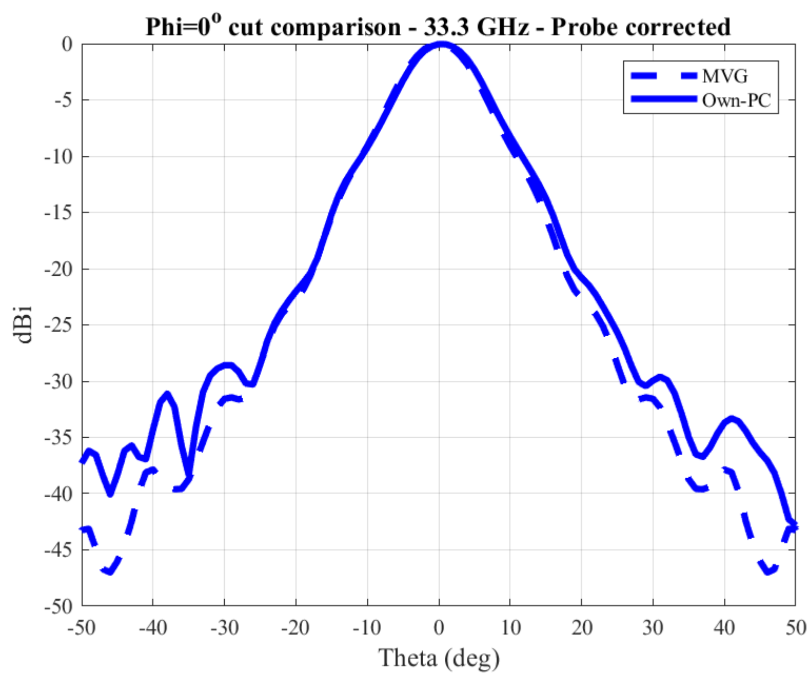

Figure 5.10: 33.3 GHz - H-cut comparison - PC included

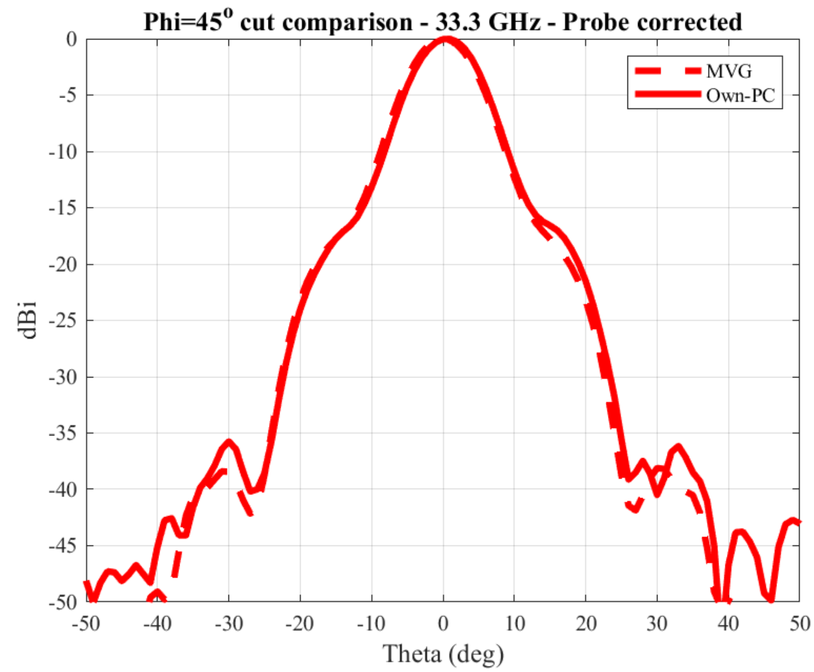

Figure 5.11: 33.3 GHz - D-cut comparison - PC included

The deterioration of the D and H cuts can be explained in the next way. If we do consider the AUT and probe cross-pol, but we assume that the multiplication of probe cross-pol ($\boldsymbol{E}_{cp1}\boldsymbol{E}_{cp2}$) ends up in a negligible amount. Then we can simplify Equation 5.1 to:

$$\boldsymbol{E}_p = \frac{\boldsymbol{E}_{pu}}{\boldsymbol{E}_{pp1}} - \frac{\boldsymbol{E}_{cp1}\boldsymbol{E}_{cu}}{\boldsymbol{E}_{pp1}\boldsymbol{E}_{pp2}} \tag{5.4}$$

As we can see, the biggest contribution to the true response comes from the measured AUT pattern ($\boldsymbol{E}_{pu}$), if this value is large, then the subtraction will have small effect on the tru response during the conversion to dB. However, if the measured AUT pattern has small values, then the subtraction will have a more considerable effect on the true response. In summary, we need to consider the AUT cross-pol and at least one probe cross-pol for accurate correction for small response values, which are the ones farther away from the boresight angle or 0^o

angle.

Following with the validation analysis, the next three patterns correspond to a comparison between the MVG patterns and our own measurements at a different frequency (35.3 GHz). Figures 5.12, 5.13 and 5.14 present the comparison results. We can notice an slight improvement in all these three cuts, one reason to explain this change is the fact that the aperture is electrically bigger at this higher frequency, and larger aperture is correlated with higher directivity, and as it was explained, the more directive the pattern, the less correction it needs.

Unfortunately, the probe correction analysis cannot be done at this frequency and this is because we do not posses the probe's pattern cuts. However, the agreement is still acceptable.

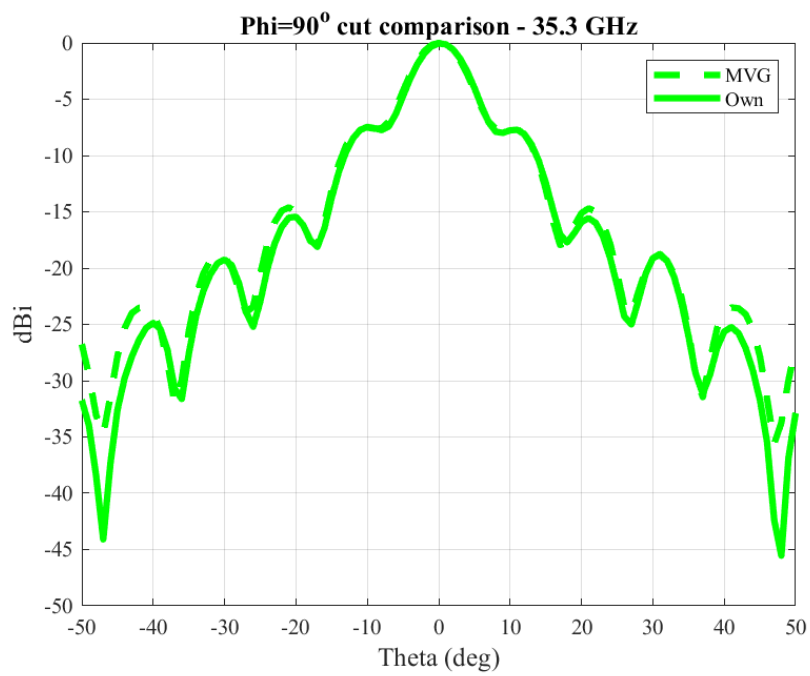

Figure 5.12: 35.3 GHz - E-cut comparison

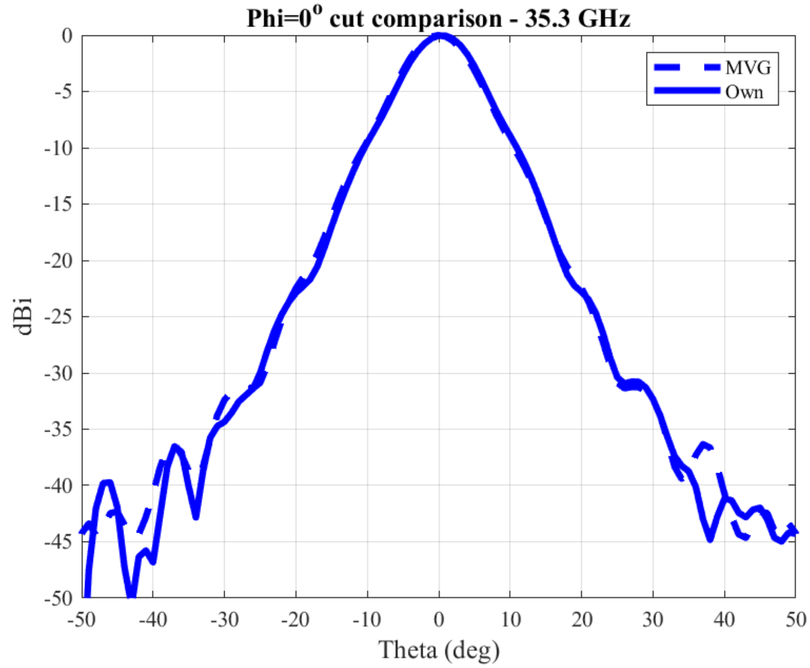

Figure 5.13: 35.3 GHz - H-cut comparison

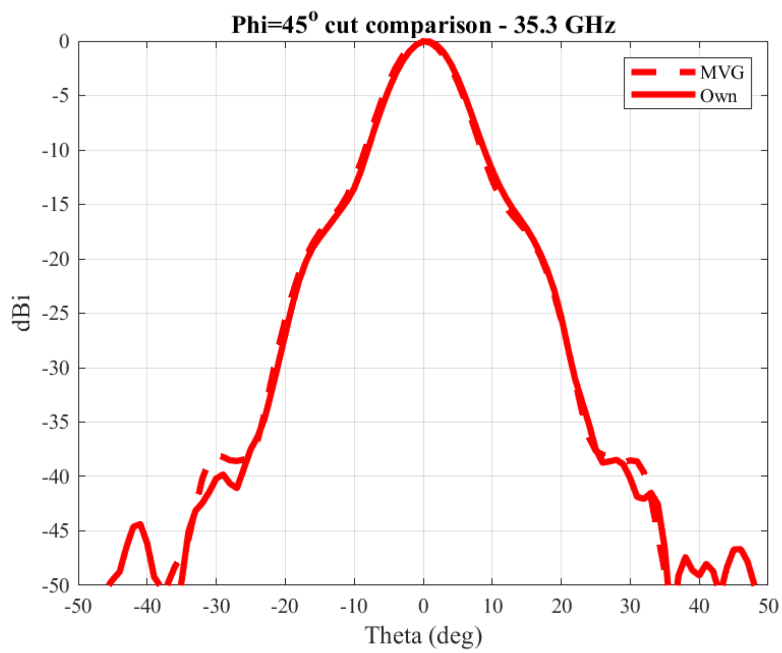

Figure 5.14: 35.3 GHz - D-cut comparison

The second antenna selected for results validation is a scalar feed horn antenna model SAF-2633031728-28-S1, manufactured by ERAVANT. This antenna works from 26 to 30 GHz. Figure 5.15 presents this horn antenna.

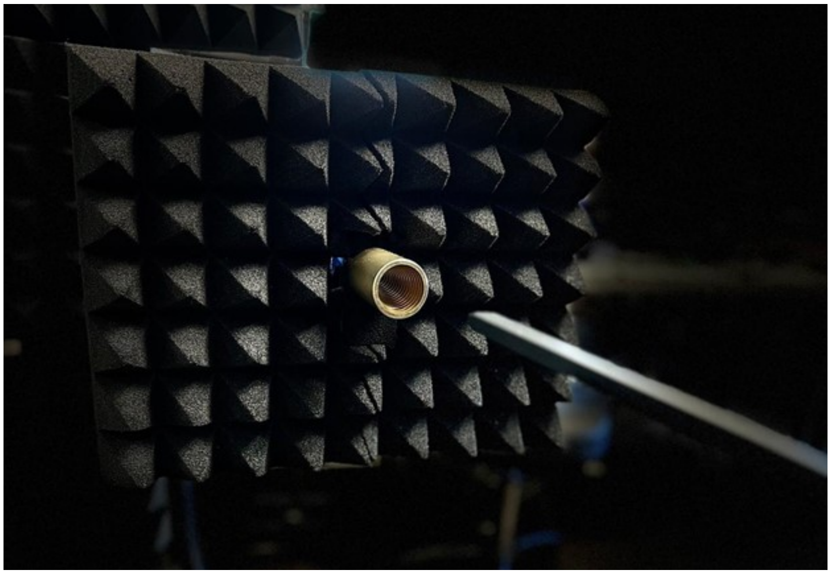

Figure 5.15: Near-field measurement setup with the scalar feed horn antenna (Courtesy: eMWave-tech)

The manufacturer provided the far-field pattern data for 28 GHz and 30 GHz for the phi=0^o and phi=90^o principal cuts for copol. The idea is the same, to perform a scan considering the same frequencies and then compare the results expecting good agreement.

Table 5.2 summarizes some important details of the scan setup.

Table 5.2: Scan setup parameters for Ka-band scalar feed horn antenna

Parameters	**Value**	**Unit**
Scan technique	Park and probe	-
AUT dimensions	37.65-x, 37.65-y	mm
Far-field angles	$\pm$ 70	Deg
AUT - Probe distance	51.5	mm
Probe dimensions	9-x, 4-y	mm
Scanning window	325-x, 320-y	mm
Delta	5	mm
Number of points	66-x, 65-y	-

The near-field data obtained from this scan, for both frequencies, is presented in figure 5.16.

These near-field plots are a good example of a clean measurement. There is good symmetry for the selected scan window and no outer random data, no odd spots. The setup for this scan was performed properly.

The far-field patterns obtained for each frequency are showed in figures 5.17 and 5.18. Figure 5.17 presents the far-field principal cuts for copol and crosspol (dashed line) for the measurements at 28 GHz, where the green line represents the E-cut or phi=90^o, the blue line represents the H-cut or phi=0^o, and the red line represents the D-cut or phi=45^o.

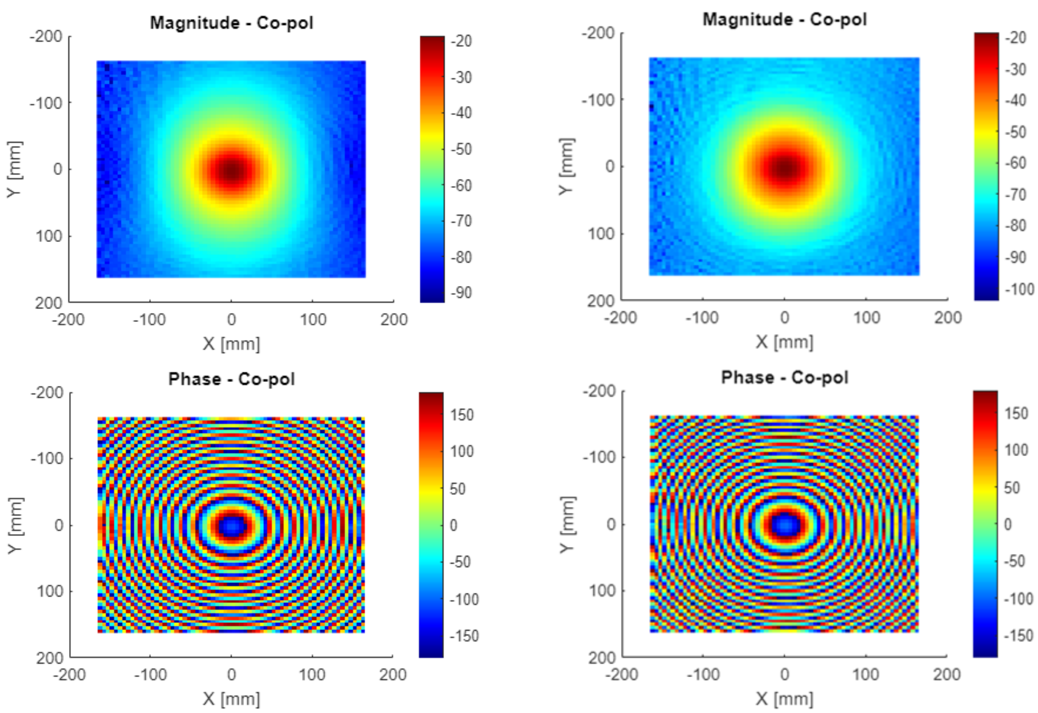

(a) 28 GHz (b) 30 GHz

Figure 5.16: Near-field magnitude and phase data for both measured frequencies

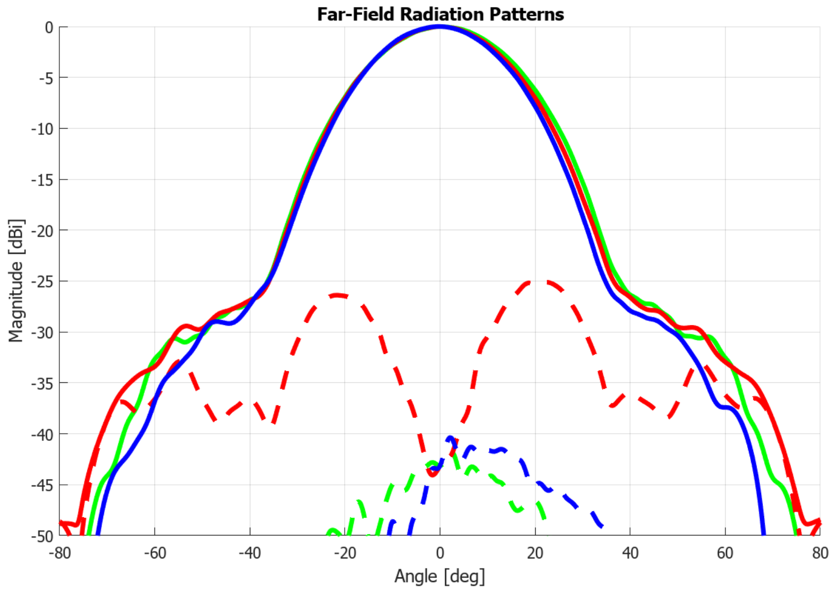

Figure 5.17: 28 GHz - Far-field principal cuts for co and crosspol

Figure 5.18 presents the far-field principal cuts for copol and crosspol (dashed line) for the measurements at 30 GHz.

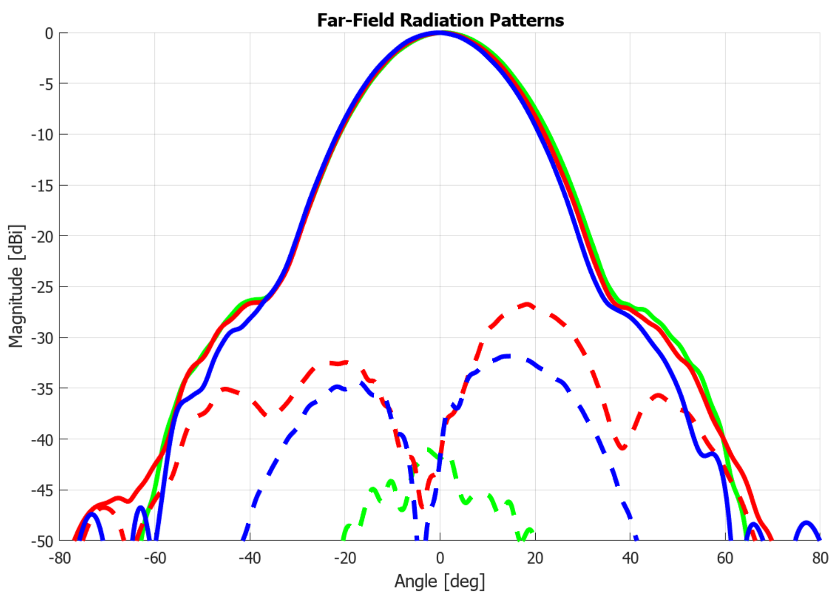

Figure 5.18: 30 GHz - Far-field principal cuts for co and crosspol

Once the results were obtained, a comparison between the manufacturer radiation patterns and our own measurements is presented next for each principal cut. The data from the manufacturer (ERAVANT) is dashed, and the continuous line corresponds to our own data.

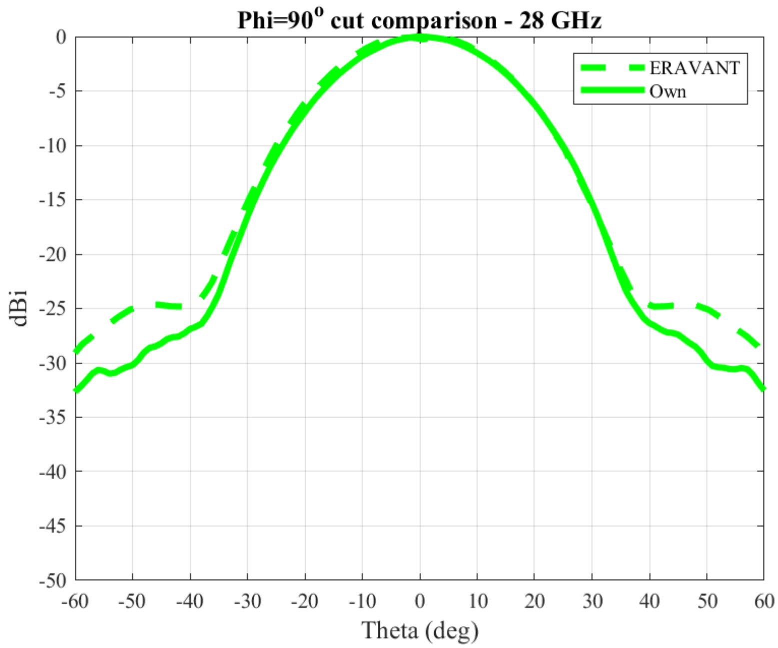

Figure 5.19: 28 GHz - E-cut comparison

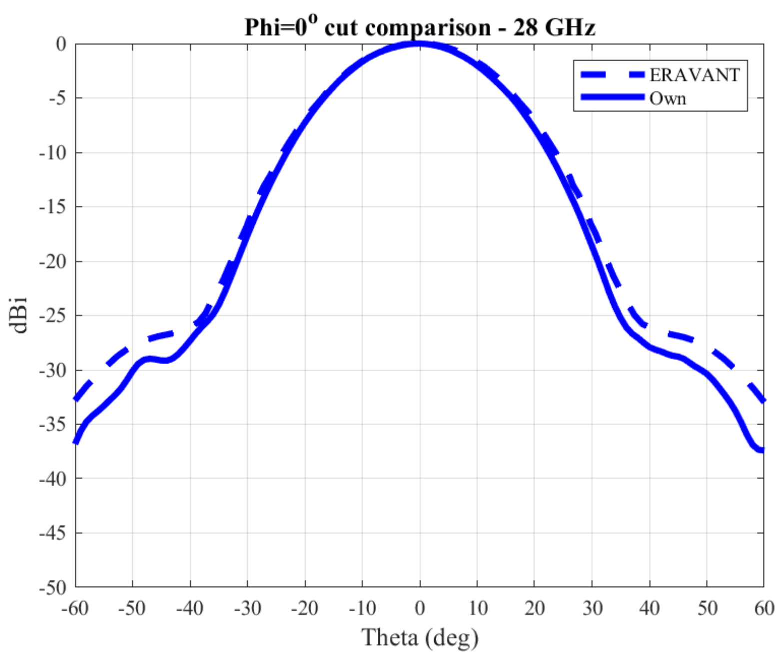

Figure 5.20: 28 GHz - H-cut comparison

As we can see in figures 5.19 and 5.20, the agreement is acceptable between $\pm 35^o$ for both cuts, but beyond that range the disagreement is considerable. For these patterns probe correction is needed. Let us present the patterns of this antenna at 30 GHz.

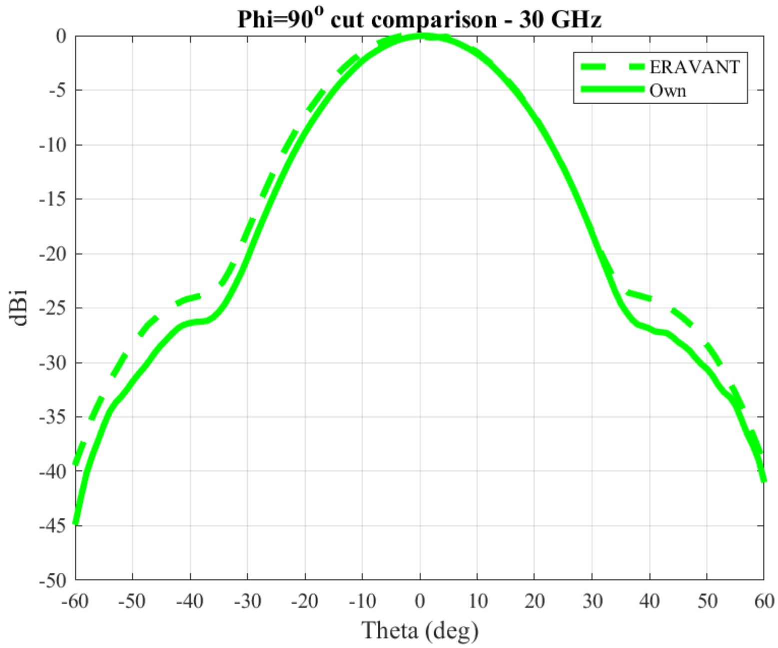

Figure 5.21: 30 GHz - E-cut comparison

It is clear that these cuts do not match perfectly, and probe correction is needed, but still there is a level of agreement, we should consider that the data provided from ERAVANT is simulated data. In addition, these measurements have not been performed in an anechoic chamber.

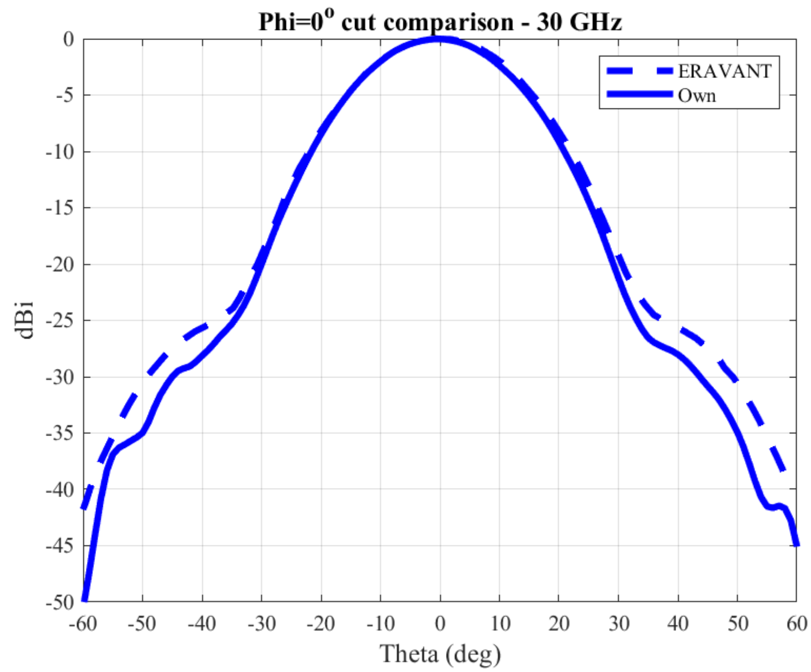

Figure 5.22: 30 GHz - H-cut comparison

Ideally, we would like to apply the probe correction; however, we do not have the probe patterns for all these measured frequencies and the ARRC does not have capabilities to measure far-field at Ka-band. In this sense, we are limited. One solution is to simulate the probe in HFSS or CST. This task is left as future work.

5.1.2 Hologram projection

For the hologram projection demonstration, it was decided to utilize a linear patch antenna array as an AUT. This is a 20 element liner array which works at X-band. Figure 5.23 shows the discussed array. This section not only presents the capabilities of hologram projection but also the system capabilities to measure at X-band. In order to switch the system operational frequency some changes need to be done, a RF amplifier is required, the frequency extenders are removed and the probe is switched by a X-band open-ended waveguide.

Figure 5.23: X-band linear patch antenna array (Courtesy: eMWave-tech)

Table 5.3 summarizes some important details of the scan setup.

Table 5.3: Scan setup parameters for X-band patch antenna array

Parameters	**Value**	**Unit**
Scan technique	Park and probe	-
AUT dimensions	450-x, 100-y	mm
Far-field angles	$\pm$ 55	Deg
AUT - Probe distance	150	mm
Probe dimensions	22.8-x, 9.8-y	mm
Scanning window	900-x, 525-y	mm
Delta	15	mm
Number of points	61-x, 36-y	-
Number of polarizations	2	-

The near-field data obtained from this scan is presented in figure 5.24.

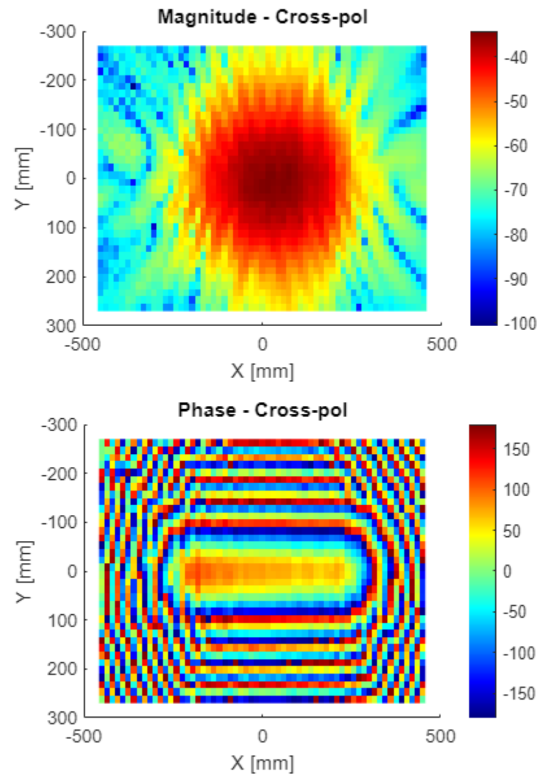

Figure 5.24: Near-field magnitude and phase data for the array measured at 9.5 GHz

The far-field pattern obtained at the 9.5 GHz frequency is presented in figure 5.24, where, once again, the green line represents the E-cut, the red line represents the D-cut, and the blue line represents the H-cut. Crosspol is represented by the dashed line. We can see that the H-cut narrow beam is very well defined, the E-field is a bit distorted and the crosspol is extremely high. Let us see how the hologram projection results for this array.

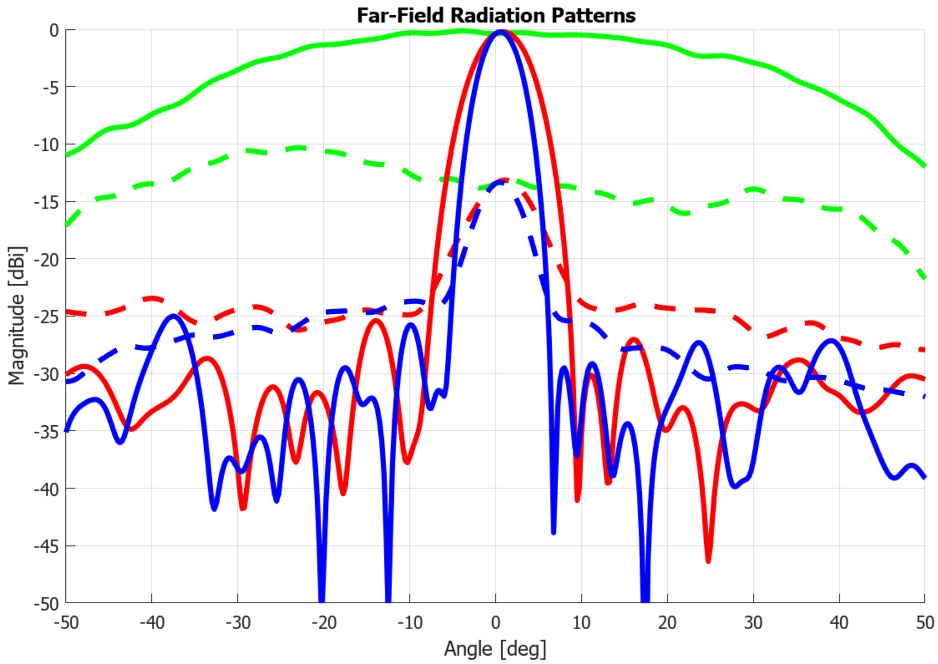

Figure 5.25: 9.5 GHz - Patch antenna linear array - Far-field principal cuts for co and crosspol

The exercise to test the antenna hologram projection is as follows. First, we will do a small scan window measurement and obtain the hologram projection, then the idea is to cancel one of the array antenna elements, to do this, a piece of copper tape larger than the patch antenna area is placed on top of one element. Finally, there is a comparison of results.

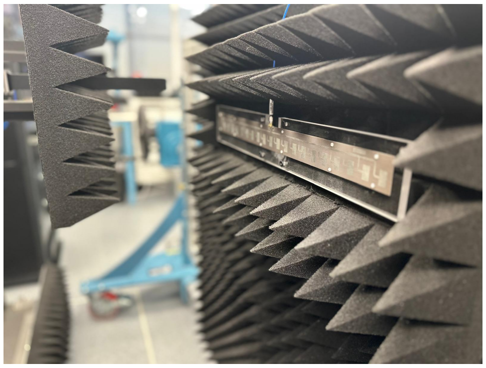

(a) Non modified array

(b) Copper taped array

Figure 5.26: Setup comparison between taped and non-taped array (Courtesy: eMWave-tech)

Figure 5.26 shows the array in the two stages of this experiment. A small square of copper tape was placed on the fifth element starting from the right side.

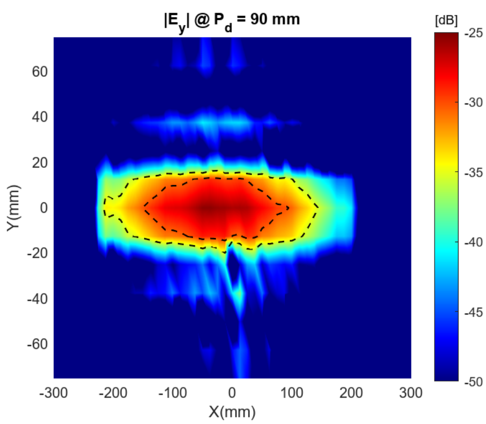

(a) Magnitude projection

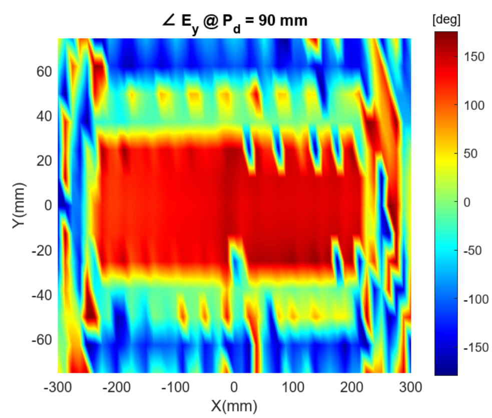

(b) Phase projection

Figure 5.27: Hologram projection plots for the non-taped array measurement

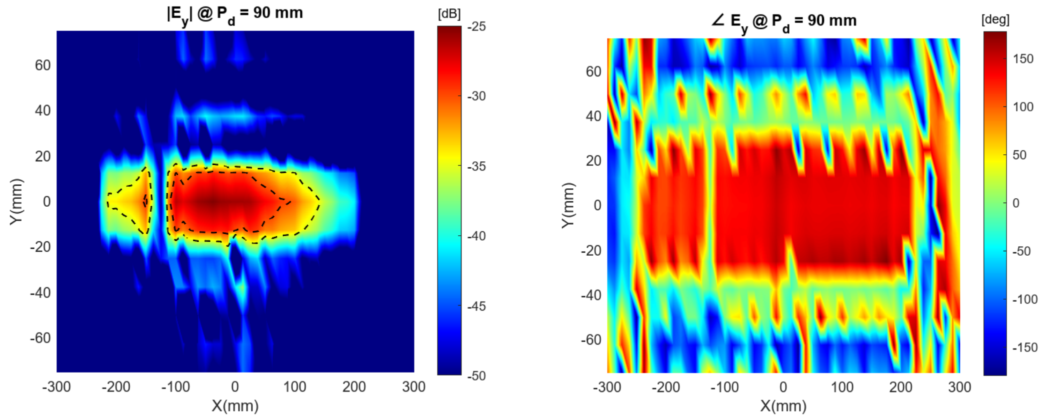

(a) Magnitude projection (b) Phase projection

Figure 5.28: Hologram projection plots for the copper taped array measurement

Hologram projection plots in figures 5.27 and 5.28 represent the magnitude of the fields in the y-axis direction at the plane of the AUT aperture.

Looking at figure 5.27 for the magnitude plot, the array shape can be distinguished, we also can see that the strongest magnitude is in the middle, this is because the phase is close to be uniform along the array as can be notice in 5.27b, where the center area is mostly red, it means that the relative phase is between 100^o and 150^o along the array.

Now, if we look at the figure 5.28a we will notice a considerable gap at about -120 mm on the x-axis. This is the effect of the copper tape on the array. Basically, the fields are very low at that location. Similar behavior for the phase, we can see that the phase of the electric fields is around 40 degrees.

Hologram projection is essential as it helps to detect malfunctioning elements in an array by showing spots with a magnitude color that does not correspond to a properly working array. It also helps with phase calibration, as we observe in figure 5.27b, the phase is not completely uniform across the array, the right and left sides appear to have slightly different phases, then, this can be corrected.

As the reader may have already picked up, the taped array gap in the hologram projection plots is on the left side; however, the copper tape was placed on the right side of the array. We should understand that these figures are the same as looking at the AUT from behind, in this manner, the plots make sense.

Chapter 6

Conclusions and Future Work

6.1 Conclusions

This thesis has been a summary of the development, from the ground up, of a low budget, customized and open source planar near-field scanner aimed to work primarily at Ka-band, with the capability to switch to X-band. This scanner is intended to measure digital phase array radars of about 2 by 1 m aperture, hence the concern in providing a reliable versatile system that allows modifications in hardware and software without compromising the level of accuracy.

This system offers a number of advantages that are not common to near-field systems, such as control via TCP/IP communication, near-field analysis, 3D far-field patterns in U/V coordinates, operational frequency from 100KHz to 54 GHz if the correct probe antennas are used, control of positioner speed and acceleration, and the design for versatility so that hardware and software can be modified.

The present thesis covered in the introduction an explanation of the benefits of rectangular planar near-field system over other approaches to obtain far-field patterns. It also discusses the state of the art and the direction of research on this field. The second chapter provides all the mathematical equations and theoretical foundations of a planar near-field scanner. The third chapter is a comprehensive explanation of the hardware and software design. Chapter four discusses the process of using the present scanner to perform a measurement taking advantage of the full capabilities of the system. And chapter five presents a validation of the results by comparing our measured data with the data provided by the antennas manufacturers.

The results in chapter five show that the designed scanner performs as expected, meeting all requirements, allowing users to measure X-band and Ka-band antennas with decent results that can be improved with proper use of probe correction techniques. The ability of the system to perform hologram projection was also demonstrated.

This system has been installed in two laboratories in the US showing great performance and showing at the same time the trust from other institutions on our design. Figure 6.1 shows the entire scanner installed and ready for operation.

Figure 6.1: Finalized version of the near-field planar scanner (Courtesy: eMWave-tech)

6.2 Future work

Part of the future work is to implement an option in the GUI that allows the user to apply the probe correction, including cross-polarization, for a range of frequencies and for both probe antennas (X-band and Ka-band). To apply this correction, both probe far-field patterns are required and, if the correction is to be applied to data from the entire 3D hemisphere, the required probe patterns must also be from an entire hemisphere.

Probe antennas are usually open-ended waveguides whose pattern is really broad, not directive, so a planar near-field system cannot be used to measure it.

The alternative and part of future work is to simulate these probes including the absorbing collars and obtain the far-field patterns from its simulation.

For future designs we plan to use electromagnetic positioners, these offer higher accuracy, higher speed and reduced noise, in fact, there is no audible noise in these systems.

Finally, an evolved version of this scanner would be a multi-probe scanner that includes an RF board for probe switching. In the first chapter it was mentioned that multi-probe scanners can consistently reduce scanning time, providing accurate results from the park and probe technique, but in a fraction of the time.

References

[1] R. Johnson, H. Ecker, and J. Hollis, "Determination of far-field antenna patterns from near-field measurements," *Proceedings of the IEEE*, vol. 61, no. 12, pp. 1668–1694, 1973. DOI: 10.1109/PROC.1973.9358.

[2] A. Yaghjian, "An overview of near-field antenna measurements," *IEEE Transactions on Antennas and Propagation*, vol. 34, no. 1, pp. 30–45, 1986. DOI: 10.1109/TAP.1986.1143727.

[3] "Ieee recommended practice for near-field antenna measurements," *IEEE Std 1720-2012*, pp. 1–102, 2012. DOI: 10.1109/IEEESTD.2012.6375745.

[4] G. Sinclair, E. Jordan, and E. Vaughan, "Measurement of aircraft-antenna patterns using models," *Proceedings of the IRE*, vol. 35, no. 12, pp. 1451–1462, 1947. DOI: 10.1109/JRPROC.1947.234570.

[5] "Ieee recommended practice for antenna measurements," *IEEE Std 149-2021 (Revision of IEEE Std 149-1977)*, pp. 1–207, 2022. DOI: 10.1109/IEEESTD.2022.9714428.

[6] C. Balanis, *Antenna Theory: Analysis and Design*. Wiley, 2015, ISBN: 9781119178996. [Online]. Available: https://books.google.com/books?id=u-xbCwAAQBAJ.

[7] L. Williams, Y. Rahmat-Samii, and R. Yaccarino, "The bi-polar planar near-field measurement technique, part i: Implementation and measurement comparisons," *IEEE Transactions on Antennas and Propagation*, vol. 42, no. 2, pp. 184–195, 1994. DOI: 10.1109/8.277212.

[8] J. Ala-Laurinaho, S. K. Karki, V. Viikari, *et al.*, "Design of a multiprobe planar near-field scanner for ku-band," in *2023 Antenna Measurement Techniques Association Symposium (AMTA)*, 2023, pp. 1–6. DOI: 10.23919/AMTA58553.2023.10293503.

[9] A. Newell, "Error analysis techniques for planar near-field measurements," *IEEE Transactions on Antennas and Propagation*, vol. 36, no. 6, pp. 754–768, 1988. DOI: 10.1109/8.1177.

[10] S. K. Karki, J. Ala-Laurinaho, V. Viikari, A. Alanne, P. Moseley, and M. Simeoni, "Positioning of orthogonally-polarized waveguide probes for near-field antenna measurement," in *2021 15th European Conference on Antennas and Propagation (EuCAP)*, 2021, pp. 1–5. DOI: 10.23919/EuCAP51087.2021.9411114.

[11] F. Saccardi, N. Gross, P. Iversen, *et al.*, "Fast multi-probe planar near field measurements with full probe compensation," in *2021 15th European Conference on Antennas and Propagation (EuCAP)*, 2021, pp. 1–5. DOI: 10.23919/EuCAP51087.2021.9411444.

[12] F. Saccardi, A. Giacomini, L. J. Foged, *et al.*, "Experimental validation of linear multiprobe arrays for fast and accurate pnf antenna characteriza-

tions," in *2023 Antenna Measurement Techniques Association Symposium (AMTA)*, 2023, pp. 1–5. DOI: 10.23919/AMTA58553.2023.10293720.

[13] L. Durand, L. Duchesne, T. Blin, *et al.*, "Fast testing technique for multibeam antennas," in *2011 IEEE Applied Electromagnetics Conference (AEMC)*, 2011, pp. 1–4. DOI: 10.1109/AEMC.2011.6256820.

[14] F. R. Varela, M. S. Castañer, F. Saccardi, L. Scialacqua, and L. Foged, "Planar wide mesh scanning using multi-probe systems," in *2023 Antenna Measurement Techniques Association Symposium (AMTA)*, 2023, pp. 1–5. DOI: 10.23919/AMTA58553.2023.10293361.

[15] R. Rafiee Alavi, R. Mirzavand, A. Kiaee, and P. Mousavi, "An adaptive data acquisition technique to enhance the speed of near-field antenna measurement," *IEEE Transactions on Antennas and Propagation*, vol. 70, no. 7, pp. 5873–5883, 2022. DOI: 10.1109/TAP.2022.3145452.

[16] A. Ivanov, K. Lemberg, S. Polenga, R. Krylov, and Y. Salomatov, "Implementation of antenna near-field scanning without using probe position sensors," in *2015 International Siberian Conference on Control and Communications (SIBCON)*, 2015, pp. 1–3. DOI: 10.1109/SIBCON.2015.7147334.

[17] M. V. Snastin and E. M. Dobychina, "Calibration of a planar scanner for near-field antenna measurements," in *2020 Systems of Signals Generating and Processing in the Field of on Board Communications*, 2020, pp. 1–4. DOI: 10.1109/IEEECONF48371.2020.9078605.

[18] D. Kremer, "Alignment procedures for planar near-field positioners," *IEEE Antennas and Propagation Magazine*, vol. 41, no. 4, pp. 86–89, 1999. DOI: 10.1109/74.789739.

[19] D. J. van Rensburg and G. Hindman, "An overview of near-field sub-millimeter wave antenna test applications," in *2008 14th Conference on Microwave Techniques*, 2008, pp. 1–4. DOI: 10.1109/COMITE.2008.4569882.

[20] D. J. van Rensburg and G. Hindman, "Sub-millimeter wave planar near-field antenna testing," in *2009 3rd European Conference on Antennas and Propagation*, 2009, pp. 1988–1992.

[21] J. L. Salazar-Cerreno, Z. Qamar, and N. Aboserwal, "A multipurpose and reconfigurable mm-wave scanner system for accurate measurements of passive/active antenna array, array calibration, radome and material characterization," in *2021 IEEE Conference on Antenna Measurements & Applications (CAMA)*, 2021, pp. 555–559. DOI: 10.1109/CAMA49227.2021.9703579.

[22] M. Nesterova and S. Nicol, "Analytical study of 5g beamforming in the reactive near-field zone," in *12th European Conference on Antennas and Propagation (EuCAP 2018)*, 2018, pp. 1–5. DOI: 10.1049/cp.2018.1086.

[23] H. G. Booker and P. C. Clemmow, "The concept of an angular spectrum of plane waves and its relation to that of polar diagram and aperture distribution," *Journal of the Institution of Electrical Engineers*, vol. 97, pp. 11–17, 1950. [Online]. Available: https://api.semanticscholar.org/CorpusID:11276126.

[24] G. Masters, *NSI 2000 Operating Manual*. NSI Nearfield Systems Inc, 2011.

[25] A. Ludwig, "The definition of cross polarization," *IEEE Transactions on Antennas and Propagation*, vol. 21, no. 1, pp. 116–119, 1973. DOI: 10.1109/TAP.1973.1140406.

[26] N. A. Aboserwal, J. L. Salazar, J. A. Ortiz, J. D. Díaz, C. Fulton, and R. D. Palmer, "Source current polarization impact on the cross-polarization definition of practical antenna elements: Theory and applications," *IEEE Transactions on Antennas and Propagation*, vol. 66, no. 9, pp. 4391–4406, 2018. DOI: 10.1109/TAP.2018.2845945.

[27] D. Paris, W. Leach, and E. Joy, "Basic theory of probe-compensated near-field measurements," *IEEE Transactions on Antennas and Propagation*, vol. 26, no. 3, pp. 373–379, 1978. DOI: 10.1109/TAP.1978.1141855.

[28] C. Taybi, M. A. Moutaouekkil, K. Rodrigues, B. Elmagroud, and A. Ziyyat, "Probes correction for planar near field antennas measurements," in *2015 IEEE 15th Mediterranean Microwave Symposium (MMS)*, 2015, pp. 1–4. DOI: 10.1109/MMS.2015.7375494.

[29] G. Masters, "Probe-correction coefficients derived from near-field measurements," *IEEE Transactions on Antennas and Propagation*, 1991. [Online]. Available: https://api.semanticscholar.org/CorpusID:201823424.

[30] A. Newell and S. Gregson, "The effect of the absorber collar on open ended waveguide probes," 2009.

[31] P. Dixon, *Theory and application of rf/microwave absorbers*, Available at https://www.laird.com/resources/white-papers/laird-tech-notes-theory-and-application-rf-microwave (05/14/2024).

[32] J. T. Logan, D. S. Reinhard, and K. E. Hauck, "Phased array calibration and diagnostics utilizing a student-built planar near-field system," in *2010 IEEE International Symposium on Phased Array Systems and Technology*, 2010, pp. 279–286. DOI: 10.1109/ARRAY.2010.5613358.

[33] G. E. Hindman, D. S. Fooshe, and Nearfield, "Probe correction effects on planar , cylindrical and spherical near-field measurements," 2005. [Online]. Available: https://api.semanticscholar.org/CorpusID:201824600.

Appendix A

List of Acronyms and Abbreviations

AUT	Antenna under test
FE	Frequency extender
GUI	Graphical user interface
IP	Internet protocol
RF	Radio frequency
SMA	SubMiniature version A
TCP	Transmission control protocol
UPS	Uninterruptible power supply
VNA	Vector network analyzer